RATIONAL DESIGN OF FUNCTIONAL HEME COPPER OXIDASES IN MYOGLOBIN

BY

KYLE DAVID MINER

DISSERTATION

Submitted in partial fulfillment of the requirements
for the degree of Doctor of Philosophy in Biochemistry
in the Graduate College of the
University of Illinois at Urbana-Champaign, 2011

Urbana, Illinois

Doctorial Committee:

Professor Yi Lu, Chair and Director of Research
Professor John Cronan
Professor Robert Gennis
Professor Chad Rienstra

ABSTRACT

Proteins are involved in nearly every process that occurs in living systems, either as a main participant in the process or preforming a supporting role. It is estimated that approximately half of proteins in living systems are associated with a metal in some fashion. With such a high percentage of proteins interacting with metals, it may not be a surprise that most cellular pathways that have at least one metalloprotein performing one or more steps. Many, if not all, of the most important and complex processes that occur in living systems are performed by a metalloprotein. These processes include photosynthesis, cellular respiration, and nucleic acid repair. The metals in these proteins expand the potential chemistry beyond what can be done with only the 20 naturally occurring amino acids. However, nature uses relatively few metal complexes, such as heme cofactors or iron sulfur clusters or metal ions, considering the number of functions that metalloproteins perform. Also, nature uses a surprisingly small number of protein domains and folds compared the number of possible folds. In metalloproteins, both the metal and protein environment surrounding it play an important role in determining the chemistry that is performed. The protein adjusts the properties of the metal, such as the redox potential or the number of open coordination sites. Many metal ions found in metalloproteins are less reactive outside of a protein environment. Despite many years of study, we are only beginning to understand the functioning of large complex metalloproteins, such as heme copper oxidases (HCOs) in respiration or the oxygen evolving complex in photosystems. Large complex proteins pose two problems with respect to studying function. Large complexes are relatively difficult to isolate in a biologically relevant form and the multiple metal sites can either interfere with spectroscopic analysis or require the use of relatively sophisticated methodology.

As an alternative to studying these complex proteins, we have chosen instead to redesign an existing well-studied heme protein, myoglobin, to mimic the bimetallic, heme-Cu_B site of HCOs. This is the site where molecular oxygen is converted to water as part of cellular respiration. The conversion of oxygen to water is highly difficult as there are many highly reactive intermediates that must stabilized so that the reaction can result in water formation. Such a redesign can be thought of as going from the "bottom up" with respect to the desired function. In the process of building up such a model, we are producing minimalistic versions in order to see what the function of each of the structural features is and how it affects chemistry.

This thesis describes the improvement of an existing myoglobin based model system of HCOs, named Cu_BMb, where an non-native copper site was previously engineered into myoglobin by adding two histidine residues. Along with the native histidine, the resulting site resembles the Cu_B site found in HCOs. This model protein is purified without metal in the Cu_B site and therefore it is possible to determine the role of the bound metal and the effect of using other metals. Previous studies of this model have not observed the desired chemistry, production of water from oxygen. However, HCOs have a novel feature found in no other proteins, namely a covalently attached histidine and tyrosine moiety that is critical for function of HCOs *in vivo*. To roughly mimic this novel feature, a tyrosine was introduced into Cu_BMb at various locations in the designed heme-Cu_B site. To guide the selection of the positions to place our tyrosine we used both the amino acid sequence information of HCOs and computer based protein models of myoglobin with a tyrosine. The computer models were compared to reported crystal structures of HCOs. The most similar mutants were made and characterized. The resulting tyrosine containing Cu_BMbs displayed the ability to produce water from oxygen, despite the absence of the covalent bond between tyrosine and one of the hisitidines used to bind the copper, as in HCOs. Even more

unexpectedly the desired activity was observed without the copper in the Cu_B site.. This result is both interesting and unexpected. To futher improve the observed rate, more features of HCOs such as proton delivery channels and non-natural heme cofactors with similar features compared to heme cofactors found in HCOs were introduced into myoglobin. The proton channels had positive effects on the observed activity. In addition to these interesting results, attempts were made to try and react the tyrosine containing Cu_BMbs under various conditions to induce formation of a covalent bond analogous to the crosslinked histidine and tyrosine found in HCOs. In the process, a crystal structure of a novel species, where an oxygen species is bound "side-on" to the metal of the heme cofactor instead of the expected "end-on" mode that to our knowledge has never been observed in a heme protein.

In summary, to better understand the functioning complex proteins like HCOs, a model protein was previously constructed. Introduction of new structural features, into the model protein (Cu_BMb), with the purpose of mimicking features similar to those found in found in HCOs caused the model system to become competent to perform the desired chemistry with less features than what is thought to be required in HCOs. As more features were attempted we discovered an interesting oxygen species bound to our protein. These type of results show the advantage of trying to build upto a minimal model. It is possible with such a system to obtain unique proteins and intermediates in addition to what information one is attempting elucidate. One is also able to perform experiments that would be impossible in the native system and obtain useful information. The insights gained by this modeling work will help the designers of the next version of Cu_BMb overcome the limitations of this version and gain insight into how to generally build and design metalloproteins.

To my parents, Kathy and Jim, who have always supported and encouraged me in my pursuits and taught me the value of an education. Also to my younger brother Greg who has provided me with someone to set a good example for.

ACKNOWLEDGEMENTS

First, I wish to thank my advisor Prof. Yi Lu. Thank you for your patience, understanding, and sound advice. To my committee members for useful questions and feedback on my research and for the use for equipment, without which large portions of this thesis may not have happened.

Thank you to all the past and current Lu lab members who created an enjoyable and enriching lab environment to come to everyday. Thank you Dewain Garner, Tom Pfister, Xuan Zhao, and Natasha Yeung for the help in those first years and continued friendship since. To Nathan Sieracki, Eric Null, Nick Marshall, Tiffany Hopper, and Igor Petrik for being good friends and for all the good times in and out of lab. To Arnab Mukherjee and Igor Petrik for all the help, useful discussions, and insightful questions.

TABLE OF CONTENTS

CHAPTER 1

INTRODUCTION

1.1 A brief introduction to metalloproteins

Proteins are the catalysts of choice for effectively all of the critical processes in living systems ranging from signal transduction to energy conversion and utilization. In a recent report, it was shown that greater than half of the proteins expressed in living systems contain some form of metal cofactor, or are otherwise associated with a metal[1]. The function of these metal cofactors can range from being merely structural[2,3], to transferring electrons[4], to directly interacting with and chemically modifying bound substrates[5]. While metals are vital to the functioning of metalloproteins, the surrounding protein environment is also critical in determining and facilitating function. For example, in zinc fingers[3], and metal sensing proteins[2] the metal plays a structural role but the resulting difference in protein conformation can alter interactions with other macromolecules and effect processes like gene transcription. When removed from the protein environment, the cofactors no longer function effectively in most cases. Furthermore, changes to the ligand set within the protein and even changes to the surrounding, long-range, hydrogen bonding, hydrophobic or ionic interactions can be altered in order to alter or introduce new functionality into a protein scaffold.

1.2 CcO/HCO activity and function and structural features

Living systems must produce large quantities of high energy molecules, like adenosine triphosphate (ATP), in order to store and transfer chemical energy and facilitate the production of molecules vital for life. In aerobic organisms, the reduction of oxygen to water is coupled to

translocation of protons across the inner mitochondrial membrane to create a proton gradient[6,7], which is then used to drive the production ATP. The class of enzymes responsible for the conversion of oxygen to water is the heme copper oxidases (HCOs)[5]. These enzymes bind oxygen at a heme site with a nearby secondary metal site, known to contain a copper atom. The oxygen is then efficiently reduced to water, with little to no production of partially reduced, reactive oxygen species, with electrons that are transferred through two alternate metal sites. The electron transfer events are then coupled to proton transfer through the protein and across the inter-mitochondrial membrane.

While HCOs have been extensively studied[8-13], detailed studies of the inner workings of these proteins are difficult [14]. All of the proteins in this class are large transmembrane proteins, the mass of bovine CcO is ~200,000 Da, [14,15](see figure 1.1), which make these proteins difficult to express and purify in large yield. The other metal based electron transfer sites also have similar electron absorption spectra as compared to the catalytic site, which convolutes the spectroscopy. Modeling the metal sites of HCO proteins individually in smaller systems is, therefore, critical to understanding the intricacies of these proteins.

In order to effectively model features of HCO proteins, an understanding of the important features in native HCOs is critical. In native HCOs, subunit I contains the heme-Cu_B site[5], where oxygen binds, which consists of a His ligated heme cofactor and Cu atom ligated by 3 His residues, known as the Cu_B site. The role of the copper in the site is to transfer the second electron to bound oxygen[14]. Mutations that affect copper binding inhibit activity of HCOs. One of the His ligands of the Cu_B site is covalently attached to a nearby tyrosine residue by a novel His-Tyr cross-link, which has only been observed in HCOs. In many HCOs, the a-type and b-type HCOs[5,12], the covalently attached His and Tyr residues are separated by 4 residues in the

protein sequence. However, in c-type HCOs, the His and Tyr are on separate helices[16]. Subunit I also contains a 6 coordinate low spin heme cofactor that is the intermediate step in the transfer of electrons from a dicopper site, Cu_A, in Subunit II, to the heme cofactor in the heme-Cu_B site. The Heme-Cu_B[12] site is located deep within the lipid bilayer, which requires that a proton channel exist for efficient transfer of protons to the site for oxygen reduction.

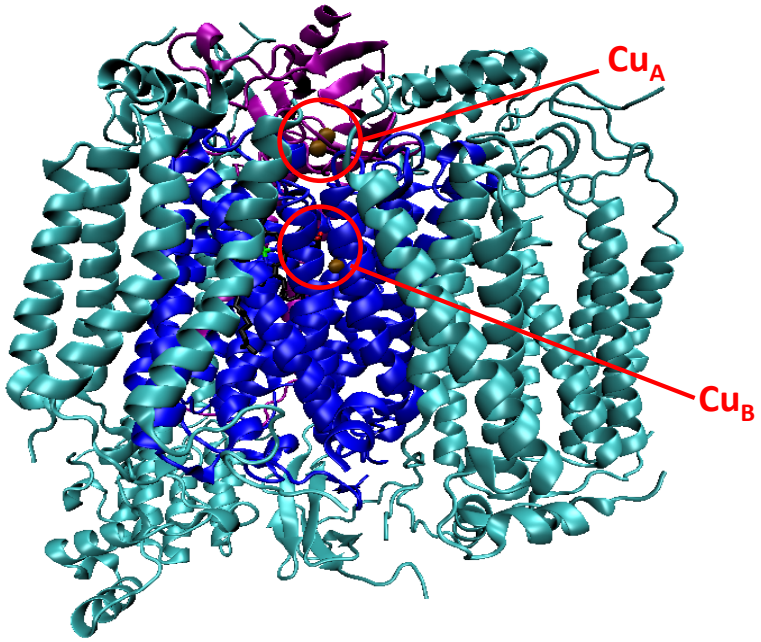

Figure 1.1 Crystal structure of Bovine CcO (PDB 1V54). Subunit I containing the heme Cu_B site is colored blue. Subunit II containing the Cu_A site is in purple. Locations of metal sites are indicated by red circles. All other subunits are in cyan. Coppers are represented as brown spheres

1.3 Synthetic model systems for studying HCOs

As mentioned above, the HCOs are large transmembrane proteins that are integral to the production of ATP in aerobic organisms. Study of these proteins is also complicated by the fact that HCOs have multiple metal containing sites and contain at least 2 heme cofactors. The heme-Cu_B site, where the reduction of oxygen to water occurs[12], has been the extensively studied, but the fine details of the intermediates involved in HCOs are often difficult to elucidate due the

complexity of the enzyme[14]. The multiple heme cofactors, in particular, are problematic as subtle changes at one site can be masked by an overlapping signal from the other site. As an alternative to studying the native HCOs, synthetic models of only the heme-Cu_B site have been constructed. Recently, some of these model systems have been shown to perform oxygen reduction[17,18]. These model systems typically consist of Fe containing porphyrin molecules, mimicking the heme of the heme-Cu_B site[19], with either covalently attached linkers connecting His analogs[18] (commonly pyridine or methyl histidine) or non-covalently attached with pyridine complexes that bind tridentate to the copper serving as a Cu_B site analog[20,21]. The non-covalent Cu_B analogs use the oxygen binding affinity of the heme and copper sites to ensure proximity[20]. Some of the more sophisticated versions of these synthetic systems contain an analog of the novel His-Tyr linkage seen in HCOs[18,22-24]. These systems represent the bare minimum that is required for HCO like oxygen reduction, with the hydrophobic protein environment mimicked with organic solvent. Work by Collman and coworkers[18,22] reported the first active HCO model and characterized their model system with and without copper and with and without a cross-linked His-Tyr analog but not with the Tyr present, but unattached to the His.

However, these large synthetic model complexes, are not well suited to physiological conditions, making them less relevant to the biological system. In addition, study of the roles of other features, such as the proton channels is impossible to reproduce in such systems as each variation would potentially require a different synthetic approach for each version and the insolubility of such complexes in water makes delivery of protons in a biologically relevant way impossible. Furthermore, longer-range interactions, like hydrogen bonding from nearby residues, which are known to be critical for fine-tuning protein function, cannot be studied in such systems because synthetic molecules are typically limited in size and the number of functional groups

that may be incorporated. As such, a semi-synthetic approach using small scaffold proteins, outlined below, to accommodate the important feature of the heme-Cu_B site in an environment where such properties can be investigated was employed here.

1.4 Protein design methodology

Protein design and engineering offers the potential to create proteins unseen in nature with functions not seen in nature[25], or proteins with the same function but better suited for either study or practical application. While the ultimate goal of protein design would be to design a protein from the primary amino acid sequence[26,27], i.e. de novo protein design, where a protein could be designed from scratch and contain all the functional features of the protein of interest. The ability to design proteins in such a way is limited, however, by current knowledge of protein folding[28].

As an alternative to completely de novo protein design, the use of native proteins as scaffolds[28-33], into which the functional elements of another protein can be incorporated. This method is aided by the fact that there are several thousand different scaffold types currently known. With the development of methodologies such as site directed mutagenesis the alteration of existing proteins sequences has become relatively simple. Therefore, the rational alteration of a known protein function should be achievable given a clear target activity and a protein having the desired function to emulate. It should be noted that more information that is known about the effects of mutagenesis on given "scaffold protein" particularly point mutations in a given region or position the more effective methodologies of this nature will be. Computer based protein design methodologies, using programs such as Visual Molecular Dynamics[34] (VMD) and Scalable Molecular Dynamics (NAMD)[35] or the Rosetta software package[36], provides guidance

in the selection of given the point mutations to introduce proteins. Studies where computer aided rational redesign of native proteins has been employed have been successful, such as in the engineering of myoglobin into a structural and functional mimic of NOR[31] (described below in section 1.1.5.3). Another prominent example computer based design work comes from the work of David Baker's lab where they successfully made proteins with functions not seen in any known natural protein[25]. The advantage of such methodologies is that with proper parameters the equivalent of saturation mutagenesis at multiple sites can be performed and analyzed *in silico*. However, with any computer based protein design method confirmation by experimental work is highly important. With these tools, the rational design of proteins that mimic or model more complex protein from the "bottom up" is achievable. The advantage of such methodologies is that functions assigned by other models or by top down methodologies, i.e., classical biochemistry where something functional is altered to infer function, can be tested and confirmed or reassigned. The bottom up methodology tests if what is thought to impart function truly does.

1.5 Selected protein engineering studies in myoglobin and previous work on Cu_BMb

1.5.1 Selection of a proper protein scaffold for modeling HCOs

Engineering functionality into a protein that does not natively exhibit the desired functionality is highly complex and requires that an appropriate scaffold protein first be chosen from the thousands of choices available[28]. Any scaffold must satisfy many criteria to be considered for protein engineering. In the case of modeling the heme-Cu_B site of HCO proteins, the scaffold protein must be readily isolated in high yield and not have multiple interfering chromophores that will overlap in spectroscopic studies. The scaffold protein must also be highly stable and able to withstand the many mutations required to introduce new activity. The scaffold

protein must also be, in this case, a heme protein capable of binding oxygen, as oxygen is the substrate. For modeling of the HCO heme-Cu_B site, the small heme protein myoglobin (Mb) was chosen as a scaffold.

Myoglobin is a very well-characterized small heme protein[37], ~17 kDa, whose natural function is oxygen storage. Mb is a highly stable protein and has been extensively mutated[38-40]. Such a vast library of studied mutations and their effects also provides an excellent knowledge base from which to draw from when considering further mutations to construct. In addition, Mb is relatively easy to crystalize[41], which allows for easy structural characterization of variants, and its spectroscopic features have been thoroughly investigated making characterization of reactive intermediates easier[37]. Furthermore, Mb has been previously used as a scaffold[32,42], into which various functions have been designed. Described below are previous studies where myoglobin's oxygen based chemistry has been altered by point mutations and replacement of the native heme cofactor to gain insight into the function of other heme proteins or introduce new function.

1.5.2 Conversion of myoglobin into a peroxidase and peroxygenase

Work by Watanabe and coworkers focused on the enhancement of Mb based peroxidase[43] activity. Mutations showed that naturally occurring peroxidase activity of sperm whale Mb (swMb) can be enhanced by site directed mutagenesis. The mutations were chosen based on comparisions between oxygen bound structures of swMb and cytochrome c peroxidase (CcP). The distal histidine, His64, of Mb was mutated to Leu and a His residue was introduced at either residue 29 (L29H) or residue 43 (F43H). A nearby His in CcP is known to be critical in peroxidase functionality by aiding in cleavage of the oxygen-oxygen bond of hydrogen peroxide through hydrogen bonding, while the Leu mutation increased the lifetime of cpd I by preventing

radical formation at His64[43]. His29 in Mb was found to be too far away to enhance peroxidase activity, but His43 did enhance activity, as it has a similar distance to the bound oxygen as the His in CcP. This F43H/H64L myoglobin displays increased peroxidase activity[44] and oxidizes Guaiacol and ABTS.

Additional work by Watanabe and coworkers in myoglobin include the engineering of p450 like chemistry by rational design. The first mutations performed involved mutation of His 64 as part of an attempt to mimic the activity of chloroperoxidase from *Caldariomyces fumago* in Mb, which is known to have an Asp residue near the active site that is important for activity. The incorporation of H64D[45] into myoglobin resulted in increased peroxidase and peroxygenase activity by 78- and 580- fold respectively. This study is a good example of how one point mutation carefully selected point mutation can substantially change activity. A series of mutations were then tested to fine-tune the H64D mutant[46,47] based on observations that position 68 can affect binding properties of ligands in myoglobin[48]. Mutation of Val 68 to Ile was found to give the best increase in activity even compared to the Leu mutation. This study highlights that even subtle differences in animo acid side chains affect reactivity. The incorporation of the F43W mutation also resulted in increased peroxidase and peroxygenase activity in Mb[49] of 3- and 20- fold respectively over both wild type and H64L Mb background. The Trp43 in F43W/H64L Mb oxidized was during reaction to 2,6-dihydro-2,6-dioxoindole[50] based on NMR spectroscopy. The F43W/H64D/V68I mutant (WDI Mb) was made by incorporation of F43W into the above mentioned H64D/V68I background[32]. The Trp43 of WDI Mb was shown to be stoichiometrically oxidized by hydrogen peroxide. This observation allowed for isolation and characterization of the +16 Da product, unable to isolated in the previous study. This study was

the first to demonstrate preferential hydroxylation of the 6 position of Trp. The WDI Mb study confirmed the proposal of mechanism of 2,6-dihydro-2,6-dioxoindole[50] proposed previously.

1.5.3. Study of NORs by altering Cu_BMb

There is a high level of similarity between HCOs and bacterial nitric oxide reductases (NORs).[51] Differences, however, based on modeling and sequence homology are the presence of additional glutamic acid residues near the heme cofactor and non-heme iron site, i.e. the Fe_B site[52-54] and the absence of the His-Tyr cross-link of HCOs. Cu_BMb is a myoglobin based model of HCOs described below in section 1.1.5.4. Lu and coworkers [31] modeled bacterial NORs based on the similarities between NORs and HCOs. A glutamate residue was therefore added to Cu_BMb at position 68 in the place of valine, and the resulting protein was called Fe_BMb. As there was no crystal structure of bacterial NORs at the time for overlay and comparison, an energy minimized computer model of Fe_BMb was made, using Zn in the model as a Fe analog. A crystal structure of Fe bound Fe_BMb was also obtained that confirmed the computer modeling. Fe_BMb displays the activity of NORs, ie the conversion of two NO to N_2O and H_2O. Making Fe_BMb the first model of NORs that is both structurally and functionally consistent with NORs. This study shows that the chemistry of large complex transmembrane proteins such as NORs and HCOs can be successfully reproduced in a much smaller Mb based system. In fact, the a high degree of structural similarities between Fe_BMb and c type NORs (cNORs) was later confirmed[51] when the crystal structure of the NOR from *Pseudomonas aeruginosa* was crystalized in complex with antibodies.

As a futher extension of cNOR modeling an additional Glu residue[55] was added into the heme pocket to see how NOR activity was affected as previous studies of NORs suggested

multiple Glu residues may be present in the heme-Fe_B site of NOR[52-54]. The main difference between the Glu residue at position 68 and the additional Glu at position 107 is that the new Glu residue is not a ligand to the metal site. The effect of the mutation however is substantial in that it doubles the rate of NOR activity compared to the original Fe_BMb. As the I107E mutant does not significantly alter the redox potential to protein it is likely involved in proton transfer via a hydrogen bonding network. This additional work on top of Fe_BMb shows that features such as hydrogen bonding networks and other secondary coordination sphere features can be rationally designed with careful selection of point mutations.

1.5.4 Design and previously reported work on Cu_BMb

The work described above showed that engineered His residues in the distal pocket of Mb can have a dramatic effect on the function of the protein. Similar in nature to the work described above, Sigman et al.[56] engineered multiple His residues into the heme pocket of myoglobin, in order to build a heme-Cu_B site similar to that in HCOs. The mutations made were chosen based on overlays of crystal structures of WTswMb and bovine cytochrome c oxidase. Two mutations of amino acid sidechains to His , L29H and F43H, were introduced into the Mb scaffold to form a tris-His metal binding site along with the native distal His in Mb, His64 (Figure 1.2). Because this site is similar to the Cu_B site of HCOs, this Mb variant with the tris-His site will be referred to as Cu_BMb[56], although the secondary metal site should be regarded as free of metal, unless otherwise noted.

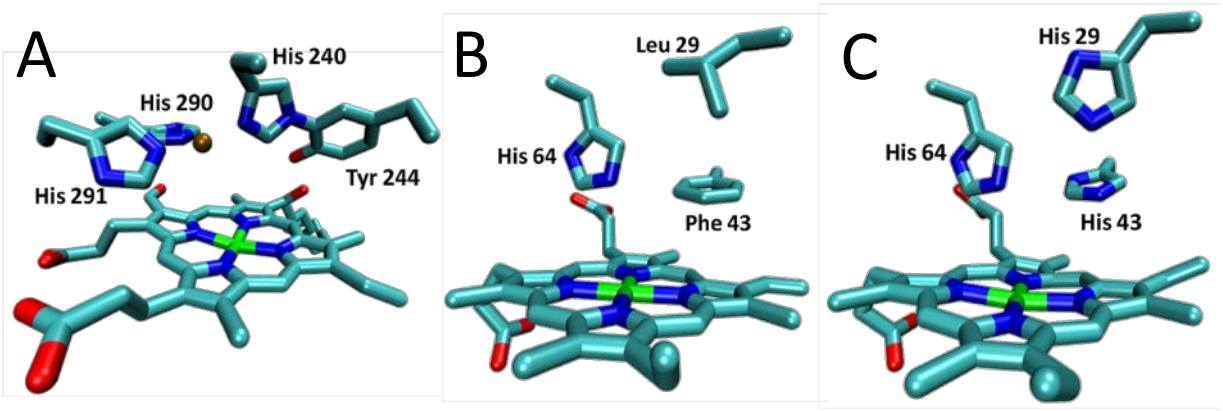

Figure1.2 Comparison of (A) the heme-CuB site of bovine CcO (PDB 1V54), (B) Heme pocket of WT swMb (PDB 1JP6) and (C) heme pocket of Cu_BMb

As mentioned above, the copper in the site Cu_B of HCOs has been shown to provide a second electron to the bound oxygen in the reduction of oxygen to water, and is critical for native HCO function. This engineered site is similar to the Cu_B site in HCOs, in that the positioning of bound copper binding site is ~5Å from the heme iron[56]. The engineered protein does display weaker oxygen binding compared to wild type myoglobin, but binds copper with a K_d ~ 9 µM . An major advantage of studying Cu_BMb as opposed to native HCOs is that it Cu_BMb is not purified with a metal in the Cu_B site. This feature allows for the placement of any metal in the Cu_B site, which cannot be done in native HCOs. Positioning of copper in the engineered site was confirmed using EPR to demonstrate antiferromagnetic coupling between cyanide bound heme iron and added Cu[56].

When myoglobin is reduced by ascorbate in the presence of TMPD as a mediator it binds oxygen and forms oxyMb in tris-HCl at pH 8 similarly to WTswMb. However, Cu_BMb also displays copper dependent oxygen chemistry that WTswMb does not[57]. In the absence of catalase, OxyMb reacts with hydrogen peroxide to form verdoheme[58,59]. In the presence of catalase the hydrogen peroxide is degraded and OxyMb is stable. Cu_BMb mutations did not

prevent oxygen binding, however the oxygen affinity Cu_BMb as demonstrated by a small deoxyMb shoulder in the soret band[57]. The addition of Ag(I) can restore wild type like oxygen binding as evidenced by the 418nm soret band with little or no deoxy shoulder. In the presence of Cu, heme oxygenase chemistry is observed as evidenced by a decrease in the intensity of the soret band and an increase in absorbance at 622 nm and 678 nm.

This copper dependent chemistry is interesting, not only because wild type myoglobin doesn't display this, but also because heme oxygenase chemistry[60,61] shares a ferric hydroperoxo intermediate, also known as cpd 0, with HCO chemistry[57]. If this intermediate remains unprotonated it will cause degradation of the heme cofactor forming verdoheme and bilverdin via heme oxygenase chemistry. If protonated, the dioxygen bond would likely cleave heterolytically forming cpd I, i.e. ferryl heme with a cation radical and proceed toward HCO like chemistry. The formation of such an intermediate from oxygen bound myoglobin would require an electron and a proton transferred to OxyMb[57]. Based on studies of wild type myoglobin, the protonation of the bound oxygen typically causes release of superoxide[62]. However, for reduction of oxygen to water protonation of the bound species must occur. Therefore the protein must coordinate electron and proton delivery carefully to avoid undesired chemistry. In the initial generation of the Cu_BMb catalyst, the chemistry seen indicated that while electron transfer occurred, introduction of protons was problematic. The inability of transfer protons as needed leads away from HCO activity and towards heme oxygenase chemistry[61]. Building other functional pieces of HCO proteins into the Cu_BMb scaffold, therefore, became a large priority.

1.5.5 Replacement of heme b with a mimic of o type heme

One element that was missing from the original Cu_BMb system was a hydrogen bonding network to deliver protons to the catalytic site from bulk solvent. In an effort to create a more complete hydrogen bonding network in Cu_BMb and avoid heme oxygenase chemistry by increasing the likelihood of protonation of Cpd 0, the native heme b of myoglobin was replaced with an unnatural heme[63], having a hydroxyethyl in the place of a vinyl group n heme b. The inspiration for this study was taken from the fact that different HCOs natively vary in the type of heme located in the Heme-Cu_B site[5]. The a/o type hemes of aa_3, ba_3, and bo_3 oxidases contain a hydroxyfarnesyl group that is within hydrogen bonding distance of both the novel cross-linked His-Tyr and positioned at the end of the K-channel[12,64], which has been implicated in the delivery of protons into the heme-Cu_B site[65,66]. Proposed catalytic mechanisms of HCO proteins suggest a hydrogen bonding network with the hydroxyfarnesyl hydroxyl and water molecules bridging the bound oxygen and the tyrosine hydroxyl. Other HCOs, such as bb3 types[8], contain a b type heme, like myoglobin does, that lacks the hyrdroxyfarnesyl group. These HCOs compensate by having a nearby Tyr residue supply the hydroxyl group needed.

Another attractive feature of the Cu_BMb system is that the heme cofactor in myoglobin can be replaced by unnatural hemes to study the effects different cofactors have on oxygen chemistry[67,68]. Lu and coworkers[63] took advantage of this feature of myoglobin by replacing the b type heme of myoglobin with a mimic of o type heme o (Fe(III)-2,4 (4,2) hydroxyethyl vinyl deuterioporphyrin IX) that replaces a vinyl group of heme b with a hydroxyethyl group to analogous that of the hydroxyl of the o type heme. Cu_BMb containing heme o mimic, denoted as $Cu_BMb(o)$ slowed the copper dependent heme oxygenase chemistry of by approximately 19-

fold. Suggesting that the hydrogen bonding network was altered in Cu_BMb(o) by the unnatural cofactor and that this network regulates activity in HCOs.

1.6 Thesis goals and outlook

While several interesting features were observed in the Cu_BMb system, it still failed to meet the goal of performing as a viable mimic of HCO proteins. The goal of the work described in the following chapters is, therefore, to improve upon the Cu_BMb model system described above, thus making a functional and more accurate model of HCOs. Chapter 2 describes work aimed at introducing a tyrosine positioned similarly to the His-Tyr crosslinked amino acids observed in HCO and observing the effect of introduced tyrosine on the activity of Cu_BMb. It was seen that the tyrosine containing variants of Cu_BMb display the ability to consume oxygen and convert it to water, mimicking HCO activity. Presumably by affecting the hydrogen bonding network. It was also observed that the rate of activity is dependent upon the location of the tyrosine introduced. Chapter 3 describes work towards improving the activity observed in Chapter 2 by further expanding the hydrogen bonding network in the distal pocket of myoglobin by two methods. The first is by replacing heme b with the mimic of the o type heme described above. The second involves making additional point mutations to create a hydrophilic channel from the bulk solution to heme pocket to deliver protons to the heme Cu_B site. Chapter 4 is a summary of progress toward the formation of a His-Tyr crosslink, analogous to the one found in HCOs into Cu_BMb with the ultimate purpose of studying the effects on activity in comparison to the results of work in the preceding chapters. Chapter 5 describes the observation, via crystallography, of a side-on bound oxygen species bound to heme iron, this is the first direct observation of such a feature in a heme protein, although such features have been proposed in

some heme proteins. The chapter also discusses initial spectroscopic characterization of this novel species.

1.7 References

1 Andreini, C., Bertini, I., Cavallaro, G., Holliday, G. L. & Thornton, J. M. Metal ions in biological catalysis: from enzyme databases to general principles. *JBIC, Journal of Biological Inorganic Chemistry* **13**, 1205 (2008).

2 Waldron, K. J., Rutherford, J. C., Ford, D. & Robinson, N. J. Metalloproteins and metal sensing. *Nature* **460**, 823 (2009).

3 Klug, A. The discovery of zinc fingers and their applications in gene regulation and genome manipulation. *Annu. Rev. Biochem.* **79**, 213 (2010).

4 Marshall, N. M. *et al.* Rationally tuning the reduction potential of a single cupredoxin beyond the natural range. *Nature* **462**, 113 (2009).

5 Kaila, V. R. I., Verkhovsky, M. I. & Wikstrom, M. Proton-Coupled Electron Transfer in Cytochrome Oxidase. *Chem. Rev.* **110**, 7062 (2010).

6 Babcock, G. T. How oxygen is activated and reduced in respiration. *Proc. Natl. Acad. Sci. U.S.A.* **96**, 12971 (1999).

7 Babcock, G. T. & Wikstrom, M. Oxygen Activation and the Conservation Of Energy In Cell Respiration. *Nature* **356**, 301 (1992).

8 Buschmann, S. *et al.* The structure of cbb3 cytochrome oxidase provides insights into proton pumping. *Science* **329**, 327 (2010).

9 Egawa, T., Lee, H. J., Gennis, R. B., Yeh, S.-R. & Rousseau, D. L. Critical structural role of R481 in cytochrome c oxidase from Rhodobacter sphaeroides. *Biochim. Biophys. Acta* **1787**, 1272 (2009).

10 Chang, H.-Y., Hemp, J., Chen, Y., Fee, J. A. & Gennis, R. B. The cytochrome ba3 oxygen reductase from Thermus thermophilus uses a single input channel for proton delivery to the active site and for proton pumping. *Proc. Natl. Acad. Sci. U.S.A.* **106**, 16169 (2009).

11 Aoyama, H. *et al.* A peroxide bridge between Fe and Cu ions in the O2 reduction site of fully oxidized cytochrome c oxidase could suppress the proton pump. *Proc. Natl. Acad. Sci. U.S.A.* **106**, 2165 (2009).

12 Namslauer, A. & Brzezinski, P. Structural elements involved in electron-coupled proton transfer in cytochrome c oxidase. *FEBS Lett.* **567**, 103 (2004).

13 Pawate, A. S. *et al.* A Mutation in Subunit I of Cytochrome Oxidase from Rhodobacter sphaeroides Results in an Increase in Steady-State Activity but Completely Eliminates Proton Pumping. *Biochemistry* **41**, 13417 (2002).

14 Brzezinski, P. & Gennis, R. B. Cytochrome c oxidase: exciting progress and remaining mysteries. *J. Bioenerg. Biomembr.* **40**, 521 (2008).

15 Tsukihara, T. *et al.* The whole structure of the 13-subunit oxidized cytochrome c oxidase at 2.8 Angstrom. *Science* **272**, 1136 (1996).

16 Hemp, J. *et al.* Evolutionary Migration of a Post-Translationally Modified Active-Site Residue in the Proton-Pumping Heme-Copper Oxygen Reductases. *Biochemistry* **45**, 15405, doi:10.1021/bi062026u [doi] (2006).

17 Collman, J. P. *et al.* A Cytochrome c Oxidase Model Catalyzes Oxygen to Water Reduction Under Rate-Limiting Electron Flux. *Science* **315**, 1565 (2007).

18 Collman, J. P. & Decreau, R. A. Functional biomimetic models for the active site in the respiratory enzyme cytochrome c oxidase. *Chem. Commun.*, 5065 (2008).

19 Chufan, E. E., Puiu, S. C. & Karlin, K. D. Heme-Copper/Dioxygen Adduct Formation, Properties, and Reactivity. *Acc. Chem. Res.* **40**, 563 (2007).

20 Chishiro, T. *et al.* Isolation and crystal structure of a peroxo-bridged heme-copper complex. *Angew. Chem. Int. Ed.* **42**, 2788 (2003).

21 Kim, E., Chufan, E. E., Kamaraj, K. & Karlin, K. D. Synthetic Models for Heme-Copper Oxidases. *Chem. Rev.* **104**, 1077 (2004).

22 Collman, J. P., Yang, Y. & Decreau, R. A. Synthesis of Nitric Oxide Reductase Active Site Models Bearing Key Components at Both Distal and Proximal Sites. *Org. Lett.* **9**, 2855, doi:10.1021/ol071007p [doi] (2007).

23 Liu, J.-G., Naruta, Y. & Tani, F. Synthetic models of the active site of cytochrome c oxidase: influence of tridentate or tetradentate copper chelates bearing a His-Tyr linkage mimic on dioxygen adduct formation by heme/Cu complexes. *Chem. Eur. J.* **13**, 6365 (2007).

24 Liu, J.-G., Naruta, Y. & Tani, F. A functional model of the cytochrome c oxidase active site: Unique conversion of a heme-m-peroxo-CuII intermediate into heme-superoxo/CuI. *Angew. Chem. Int. Ed.* **44**, 1836 (2005).

25 Roethlisberger, D. *et al.* Kemp elimination catalysts by computational enzyme design. *Nature* **453**, 190 (2008).

26 Calhoun, J. R. *et al.* Artificial diiron proteins: From structure to function. *Biopolymers* **80**, 264 (2005).

27 Korendovych, I. V. *et al.* De Novo Design and Molecular Assembly of a Transmembrane Diporphyrin-Binding Protein Complex. *J. Am. Chem. Soc.* **132**, 15516 (2010).

28 Lu, Y., Yeung, N., Sieracki, N. & Marshall, N. M. Design of functional metalloproteins. *Nature* **460**, 855 (2009).

29 Lu, Y., Berry, S. M. & Pfister, T. D. Engineering novel metalloproteins: Design of metal-binding sites into native protein scaffolds. *Chem. Rev.* **101**, 3047 (2001).

30 Gengenbach, A., Syn, S., Wang, X. & Lu, Y. Redesign of Cytochrome c Peroxidase into a Manganese Peroxidase: Role of Tryptophans in Peroxidase Activity. *Biochemistry* **38**, 11425 (1999).

31 Yeung, N. *et al.* Rational design of a structural and functional nitric oxide reductase. *Nature* **462**, 1079 (2009).

32 Pfister, T. D. *et al.* Monooxygenation of an Aromatic Ring by F43W/H64D/V68I Myoglobin Mutant and Hydrogen Peroxide: Myoglobin Mutants as a Model for P450 Hydroxylation Chemistry. *J. Biol. Chem.* **280**, 12858 (2005).

33 Watanabe, Y. & Hayashi, T. Functionalization of myoglobin. *Prog. Inorg. Chem.* **54**, 449 (2005).

34 Humphrey, W., Dalke, A. & Schulten, K. VMD: Visual molecular dynamics. *J. Mol. Graphics* **14**, 33 (1996).

35 Phillips, J. C. *et al.* Scalable molecular dynamics with NAMD. *J. Comput. Chem.* **26**, 1781 (2005).

36 Das, R. & Baker, D. Macromolecular modeling with Rosetta. *Annu. Rev. Biochem.* **77**, 363 (2008).

37 Antonini, E., Brunori, M., Neuberger, A. & Tatum, E. L. *Hemoglobin and Myoglobin in their Reactions with Ligands*. Vol. 21 (Elsevier New York N. Y, 1971).

38 Smerdon, S. J. *et al.* Interactions among residues CD3, E7, E10, and E11 in myoglobins: Attempts to simulate the ligand-binding properties of Aplysia myoglobin. *Biochemistry* **34**, 8715 (1995).

39 Matsui, T., Nagano, S., Ishimori, K., Watanabe, Y. & Morishima, I. Preparation and Reactions of Myoglobin Mutants Bearing both Proximal Cysteine Ligand and Hydrophobic Distal Cavity: Protein Models for the Active Site of P-450. *Biochemistry* **35**, 13118 (1996).

40 Peterson, E. S., Friedman, J. M., Chien, E. Y. T. & Sligar, S. G. Functional Implications of the Proximal Hydrogen-Bonding Network in Myoglobin: A Resonance Raman and Kinetic Study of Leu89, Ser92, His97, and F-Helix Swap Mutants. *Biochemistry* **37**, 12301 (1998).

41 Phillips, S. E. V. Structure and refinement of oxymyoglobin at 1.6 .ANG. resolution. *J. Mol. Biol.* **142**, 531 (1980).

42 Ozaki, S.-i., Matsui, T. & Watanabe, Y. Conversion of Myoglobin into a Peroxygenase: A Catalytic Intermediate of Sulfoxidation and Epoxidation by the F43H/H64L Mutant. *J. Am. Chem. Soc.* **119**, 6666 (1997).

43 Matsui, T., Ozaki, S.-i. & Watanabe, Y. On the formation and reactivity of compound I of the His-64 myoglobin mutants. *J. Biol. Chem.* **272**, 32735 (1997).

44 Matsui, T., Ozaki, S.-I., Liong, E., Phillips, G. N., Jr. & Watanabe, Y. Effects of the location of distal histidine in the reaction of myoglobin with hydrogen peroxide. *J. Biol. Chem.* **274**, 2838 (1999).

45 Matsui, T., Ozaki, S.-i. & Watanabe, Y. Formation and Catalytic Roles of Compound I in the Hydrogen Peroxide-Dependent Oxidations by His64 Myoglobin Mutants. *J. Am. Chem. Soc.* **121**, 9952 (1999).

46 Yang, H.-J. *et al.* Molecular Engineering of Myoglobin: Influence of Residue 68 on the Rate and the Enantioselectivity of Oxidation Reactions Catalyzed by H64D/V68X Myoglobin. *Biochemistry* **42**, 10174 (2003).

47 Kato, S. *et al.* Asymmetric Sulfoxidation and Amine Binding by H64D/V68A and H64D/V68S Mb: Mechanistic Insight into the Chiral Discrimination Step. *J. Am. Chem. Soc.* **124**, 8506 (2002).

48 Quillin, M. L. *et al.* Structural and functional effects of apolar mutations of the distal valine in myoglobin. *J. Mol. Biol.* **245**, 416 (1995).

49 Ozaki, S.-i., Hara, I., Matsui, T. & Watanabe, Y. Molecular Engineering of Myoglobin: The Improvement of Oxidation Activity by Replacing Phe-43 with Tryptophan. *Biochemistry* **40**, 1044 (2001).

50 Hara, I. *et al.* Oxidative modification of tryptophan 43 in the heme vicinity of the F43W/H64L myoglobin mutant. *J. Biol. Chem.* **276**, 36067 (2001).

51 Hino, T. *et al.* Structural Basis of Biological N2O Generation by Bacterial Nitric Oxide Reductase. *Science* **330**, 1666 (2010).

52 Butland, G., Spiro, S., Watmough, N. J. & Richardson, D. J. Two conserved glutamates in the bacterial nitric oxide reductase are essential for activity but not assembly of the enzyme. *J.Bacteriol.* **183**, 189 (2001).

53 Flock, U. *et al.* Defining the proton entry point in the bacterial respiratory nitric-oxide reductase. *J. Biol. Chem.* **283**, 3839 (2008).

54 Flock, U., Lachmann, P., Reimann, J., Watmough, N. J. & Aedelroth, P. Exploring the terminal region of the proton pathway in the bacterial nitric oxide reductase. *J. Inorg. Biochem.* **103**, 845 (2009).

55 Lin, Y.-W. *et al.* Roles of glutamates and metal ions in a rationally designed nitric oxide reductase based on myoglobin. *Proc. Natl. Acad. Sci. U.S.A.* **107**, 8581 (2010).

56 Sigman, J. A., Kwok, B. C. & Lu, Y. From Myoglobin to Heme-Copper Oxidase: Design and Engineering of a CuB Center into Sperm Whale Myoglobin. *J. Am. Chem. Soc.* **122**, 8192 (2000).

57 Sigman, J. A., Kim, H. K., Zhao, X., Carey, J. R. & Lu, Y. The role of copper and protons in heme-copper oxidases: Kinetic study of an engineered heme-copper center in myoglobin. *Proc. Natl. Acad. Sci. U.S.A.* **100**, 3629 (2003).

58 Sigman, J. A., Wang, X. & Lu, Y. Coupled Oxidation of Heme by Myoglobin Is Mediated by Exogenous Peroxide. *J. Am. Chem. Soc.* **123**, 6945 (2001).

59 Murakami, T., Morishima, I., Matsui, T., Ozaki, S.-i. & Watanabe, Y. Effects of the arrangement of a distal histidine on regioselectivity of the coupled oxidation of sperm whale myoglobin mutants. *Chem.Commun.*, 773 (1998).

60 Ortiz de Montellano, P. R. Heme Oxygenase Mechanism: Evidence for an Electrophilic, Ferric Peroxide Species. *Acc. Chem. Res.* **31**, 543 (1998).

61 Ortiz de Montellano, P. R. & Wilks, A. Heme oxygenase structure and mechanism. *Adv.Inorg.Chem.* **51**, 359 (2001).

62 Brantley, R. E., Jr., Smerdon, S. J., Wilkinson, A. J., Singleton, E. W. & Olson, J. S. The mechanism of autooxidation of myoglobin. *J. Biol. Chem.* **268**, 6995 (1993).

63 Wang, N., Zhao, X. & Lu, Y. Role of Heme Types in Heme-Copper Oxidases: Effects of Replacing a Heme b with a Heme o Mimic in an Engineered Heme-Copper Center in Myoglobin. *J. Am. Chem. Soc.* **127**, 16541 (2005).

64 Das, T. K., Pecoraro, C., Tomson, F. L., Gennis, R. B. & Rousseau, D. L. The Post-Translational Modification in Cytochrome c Oxidase Is Required To Establish a Functional Environment of the Catalytic Site. *Biochemistry* **37**, 14471 (1998).

65 Blomberg, M. R. A., Siegbahn, P. E. M. & Wikstroem, M. Metal-Bridging Mechanism for O-O Bond Cleavage in Cytochrome c Oxidase. *Inorg. Chem.* **42**, 5231 (2003).

66 Cukier, R. I. A molecular dynamics study of water chain formation in the proton-conducting K channel of cytochrome c oxidase. *Biochim.Biophys.Acta* **1706**, 134 (2005).

67 Zahran, Z. N., Chooback, L., Copeland, D. M., West, A. H. & Richter-Addo, G. B. Crystal structures of manganese- and cobalt-substituted myoglobin in complex with NO and nitrite reveal unusual ligand conformations. *J. Inorg. Biochem.* **102**, 216 (2008).

68 Che, C. M., Chiang, H. J., Margalit, R. & Gray, H. B. Preparation and properties of osmoglobins. Oxidation-reduction catalytic activity of ruthenated osmoglobin. *Catal. Lett.* **1**, 51 (1988).

CHAPTER 2

OXYGEN CHEMISTRY OF CU_BMB AND THE EFFECT OF INTRODUCING TYROSINE RESIDUES INTO THE CU_BMB SITE

Portions of this chapter a taken from the final draft of a manuscript submitted to Proc Natl Acad Sci USA as "A Designed Functional Metalloenzyme that Reduces O_2 to H_2O with over a Thousand Turnovers" (Miner,K. D., Mukherjee, A., Gao, Y.-G., Null, E. L., Petrik I. D., Zhao, X., Yeung, N., , Robinson, H., and Lu, Y.)

2.1 Introduction

2.1.1 Rationale for protein design

Protein enzymes drive nearly all biological functions, catalyzing a wide range of reactions with high efficiency. Many of the enzymes involved in the most important and interesting processes for life, such as photosynthesis and respiration, are quite complex, making the fine details of their function difficult to study, understand, and mimic in artificial systems. Therefore, it is a grand challenge to rationally design smaller and more robust artificial enzymes with catalytic sites and activities similar to those native enzymes. To meet this challenge, we must test and expand our current knowledge of the working of enzymes to design enzymes capable of use in biotechnological applications. Toward this goal, great progress has been made in designing proteins with structures similar to native enzymes[1-7] and advances in computational biology have allowed for rational design of function as well[8-14]. Despite these achievements, most designed enzymes have relatively simple active site structures and low activities with limited turnovers. Designing artificial enzymes with more complexity and higher turnovers will advance this field and decrease the likelihood that background reactivity or experimental artifacts would be mistaken for enzymatic reactivity. Building enzymes from the ground up will reveal structural features responsible for tuning enzymes and facilitate incorporation of artificial enzymes into practical applications. Here, we report the rational design of a functional model of

heme-copper oxidase (HCO), a metalloenzyme with a heterogeneous binuclear metal center that catalyzes the reduction of oxygen to water. Our model enzyme can actively reduce oxygen to water with over 1000 turnovers. By constructing this model enzyme from the bottom up we have gained insight into some of the critical structural features involved in native HCO respiration activity. Insights gained from further studies of such a designed enzyme may lead to alternatives to precious metal catalysts in fuel cells.

Heme-copper oxidases represent an ultimate test of our ability to design complex proteins with important functions. As the terminal oxidases in aerobic respiration, HCOs catalyze the reduction of oxygen to water while transferring the free energy of this reduction into a proton gradient for the production of ATP, a universal energy source for most biological processes[15-17]. This reduction reaction is a difficult part of the aerobic respiration process and is also crucial to alternative energy production via fuel cells. While many catalysts that reduce oxygen to water have been reported[18-21], a long-standing challenge is to carry out the reaction without the production of reactive oxygen species (ROS), such as superoxide and peroxide. ROS not only damage biomolecules in cells and components in fuel cells, but also decrease energy efficiency as ROS are a result of incomplete catalysis. In addition, efficient catalysts using non-precious metal ions such as iron or copper will greatly decrease costs in practical applications[22,23].

The active site of HCO responsible for such an important reaction is a complex heterogeneous bimetallic center containing a His-ligated heme center coupled to a copper center (called Cu_B) that is coordinated by three His residues, one of which is cross-linked to a Tyr residue (Figure 1A). Despite numerous studies, the exact structural features of HCO responsible for efficient oxygen reduction, such as the role of the metal ion in the Cu_B site and that of the tyrosine next to the copper coordinating His, are not well understood[24-27]. The gap in the

understanding of this enzyme is a direct result of HCOs being large membrane proteins, with molecular weights of ~200,000 Da., making it difficult to prepare homogeneous protein in large amounts. In addition, HCOs contain multiple metal-binding sites, making it difficult to study a single site without interference from the other sites. These complications prevent the use of HCOs in practical applications, despite being highly efficient catalysts under mild conditions. While much effort has been devoted to preparing synthetic models to overcome these limitations[18,19], very few model systems are capable of actively reducing oxygen to water with multiple turnovers and without releasing ROS[20,28]. Furthermore, because synthetic models are prepared using small organic molecules in organic solvents, it is difficult to introduce long-range, non-covalent interactions such as those between the conserved tyrosine and water molecules and their associated hydrogen bonding networks, which have been shown to be important for HCO function.

As an alternative to studying native enzymes or purely synthetic molecules, we chose to use a small, stable, easy to produce and well-characterized protein to design an oxygen reduction enzyme that could mimic HCOs[2]. Myoglobin (Mb) is an ideal choice, as it is much smaller than HCOs, (17kDa) and easier to prepare and crystallize than both native HCOs and their synthetic model complexes. As a heme protein without other metal-binding sites, Mb has been a model heme protein for many spectroscopic studies and thus has often been used to calibrate spectroscopic signatures of heme proteins.

2.1.2 Review of myoglobin and selected Cu_BMb oxygen chemistry

Sperm whale Myoglobin (swMb) has been extensively studied for many decades[29]. Under reducing conditions at or near physiological pH, swMb has been observed to undergo

autoxidation, i.e. the conversion of ferrous oxygen bound myoglobin (OxyMb) to the water coordinated ferric iron myoglobin (MetMb) form with the release of superoxide[30]. This rate increases as the pH is decreased from pH 8 to pH 6 due to an increase in protonation of the bound oxygen which is released as superoxide. The rate of autoxidation can also be enhanced by the presence of copper[31]. The introduction of two histidine residues into the heme pocket of myoglobin at positions 29 and 43 (L29H and F43H) resulted in the formation of a copper binding site in myoglobin ligated by the two introduced histidines and the naturally occurring distal histidine (His 64), forming a Cu_B site similar to that in Cytochome *c* Oxidase C*c*O[32], a type of HCO (Figure 2.1). This myoglobin mutant, called Cu_BMb, displays copper dependent degradation of the heme cofactor into verdoheme (heme oxygenase activity), which is not observed in wild-type swMb[32,33]. This result is noteworthy in that C*c*O oxidase activity, the active site chemistry that we are modeling, shares some intermediates with heme oxygenase activity.

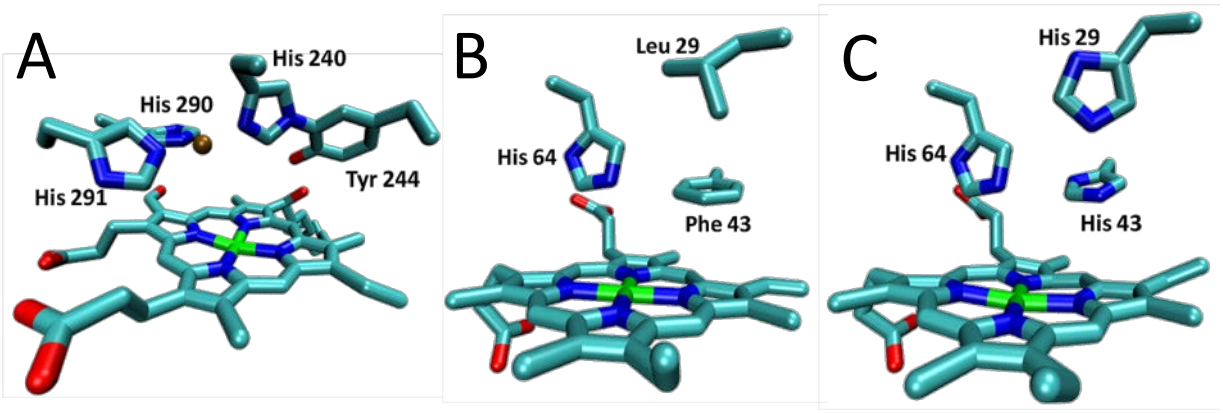

Figure 2.1 Comparison of (A) bovine C*c*O heme-Cu_B site (PDB 1V54), (B) Heme pocket of WTswMb (PDB 1JP6) and (C) Heme pocket of Cu_BMb.

2.2 Materials and methods

All chemicals, unless otherwise specified, were obtained from Sigma (St. Louis, MO) or Fisher Scientific (Hampton, NH).

2.2.1 Purification of proteins

The F33Y and G65Y mutations were introduced as previously described[32] and confirmed by DNA sequencing at the Biotechnology Center of the University of Illinois. F33Y Cu_BMb and G65Y Cu_BMb were purified using a protocol previously described[11] from inclusion bodies with a yield of ~20 mg/L with the following changes: R/Z (an estimate of protein purity with higher R/Z representing a purer protein preparation) was calculated using A_{408}/A_{280} for F33Y Cu_BMb, and A_{410}/A_{280} for G65Y Cu_BMb. Proteins with R/Z values of 3.5 or greater for G65Y Cu_BMb and 4 or greater for Cu_BMb and F33Y Cu_BMb were used in these studies. Cu_BMb was purified as previously described[32] using a modified protocol for WTswMb.

2.2.2 Crystallization of F33Y Cu_BMb

F33Y Cu_BMb (1.0 mM) in 100 mM Tris base pH 8, (pH adjusted H_2SO_4), was mixed 1:3 with well buffer (0.1 M sodium cacodylate, 0.2 M sodium acetate trihydrate and 30% w/v polyethylene glycol 8000) using the hanging drop method with 300 µL well buffer in the well of the crystallization tray.

2.2.3 Diffraction data collection

The crystals were first soaked briefly in cryoprotectant (30 % polyethylene glycol 400) and were flash frozen in liquid nitrogen. The diffraction data sets summarized in Table S1 were collected at the National Synchrotron Light Source beamline X12C (Upton, NY) and were processed with HKL2000 software[34].

2.2.4 Crystal structure determination

The crystal structure was solved by the molecular replacement method using MOLREP in the CCP4 Package[35]. Refinement was performed using X-plor[36] and SHELX'97[37]. For the crystal structure of Cu_BMb, the positions of H43 and H29 were rebuilt using the program O[38]. For the structure of F33Y Cu_BMb, the position of Y33 was rebuilt using the program O [38]. All crystal structure determinations were performed by Mr. Yi-Gui Gao, of the George L. Clark X-Ray Facility and 3M Materials Laboratory, University of Illinois at Urbana-Champaign, as part of a collaboration.

2.2.5 Computer modeling of proteins

Computer models for F33Y Cu_BMb and G65Y Cu_BMb were created using Visual Molecular Dynamics[39] (VMD) and NAMD[40] (Molecular Dynamics Simulator) as described previously[11] with the following changes: the Cu_BMb structure was used as the starting structure upon which computer modeling simulations were performed on and the non-heme metals were not introduced into the simulation.

2.2.6 ^{17}O Nuclear magnetic resonance (NMR) spectroscopy

^{1}H Decoupled ^{17}O NMR spectra were collected at 81.3 MHz on a Varian UNITY INOVA spectrometer with a 5 mm AutoTuneX probe. Temperature was held constant at 25 °C by an FTS Systems unit. Gradient shimming was performed and the water signal was referenced to 0 ppm. Samples were placed inside an Omni-Fit NMR tube from Wilmad LabGlass (Vineland, NJ). ^{17}O labeled (phenol-^{17}O 35 %) L-tyrosine (~ 380 mM in water) was sealed inside of a capillary and placed inside the Omni-Fit (gas tight) NMR tube, serving as an external standard against which the $H_2{}^{17}O$ signal could be monitored. An external standard was used instead of an internal

standard due to the high pH requirement for solubility as well as eliminating any possible interference in the reaction. The L-tyrosine concentration used allowed detection in a matter of minutes and overcame the small volume of the capillary as well as 35% labeling of L-tyrosine. *N,N,N′,N′*-Tetramethyl-*p*-phenylenediamine dihydrochloride (TMPD) and ascorbic acid were added to a protein solution of either F33Y Cu_BMb, G65Y Cu_BMb, or WtswMb resulting in a 500 µL volume sample at a concentration of 50 µM protein, 5 mM TMPD and 50 mM ascorbic acid in 50 mM potassium phosphate, pH 6. Immediately after TMPD and ascorbic acid addition, an initial spectrum collected over a period of ten minutes, followed by removal from the instrument, injection of 1 mL $^{17}O_2$ at roughly atmospheric pressure (Cambridge Isotope Laboratories, Inc., Andover, MA, 70.7 % oxygen-17 content) into the Omni-Fit NMR tube, sealing of the port, inversion for 15 seconds to aid in oxygen saturation of the solution, and subsequent data collection. During data collection the tube was spun at 10Hz to aid in mixing. Time points were collected as appropriate. In between each time point the tube was removed from the instrument, inverted for 15 seconds, and replaced. Data were analyzed using MestReNova (Mestrelab Research, Santiago de Compostela, Spain). The area of the tyrosine signal was set to 1 for all spectra and the area of the water signal was recorded in relation to this value. Collection of ^{17}O NMR spectra was performed with the assistance of Dr. Eric L. Null.

2.2.7 UV-visible spectroscopy

All UV-visible spectra were acquired with an Agilent 8453 spectrometer (Agilent Technologies, Santa Clara, CA) using the supplied Chemstation software and kinetics package. Ferric protein spectra were obtained by taking 2 mL of 6 µM protein as isolated. For deoxy protein spectra, excess sodium dithionite was added, for unambiguous assignment. For oxy protein spectra, the

protein was reduced using ascorbic acid (1000 eq) and TMPD (100 eq) and oxygen was bubbled into the solution to ensure a clean oxygen-bound spectrum.

For kinetic spectra monitoring of the reduced protein, the spectrum of the ferric (oxidized) form was collected first as a comparison using 2 mL of 6 µM protein in air-saturated 50 mM potassium phosphate pH 6 containing 2.2 µM catalase in a cuvette. The cuvette was sealed with a septum, wrapped with parafilm, and allowed to stir under an argon headspace. Then ascorbic acid (1000 eq) and TMPD (100 eq) were added to reduce the protein and spectra were collected over a period of 60 minutes.

For determination of heme degradation rate, 4 mL of 18 uM protein was reduced using ascorbic acid (1000 eq) and TMPD (100 eq) in 50 mM potassium phosphate pH 6 in the absence or presence of up to 2 eq $CuSO_4$ and with or without 2.2 µM catalase. After addition of reductant, the cuvette was capped to minimize oxygen from the air diffusing into solution. As both heme degradation and water production contributes to oxygen consumption, the rate of heme degradation was subtracted from the observed rates of oxygen consumption in the presence of copper to determine the total rate of water production (the activity that we are interested in modeling).

2.2.8 Oxygen consumption rate and turnover studies using an oxygen electrode

The reduction of myoglobin so that it may bing to oxygen requires a reductant to convert the oxidized metMb to a form able to bind oxygen. This is a required step in reduction of oxygen to water. Our reductant and mediator ascorbic acid (1000 eq) and TMPD (100 eq), respectively, were added to 500 µL of 18 µM protein in air saturated 50 mM potassium phosphate pH 6. We choose to study the protein at pH 6 because we found that the enzymatic activity is higher at

lower pH values, likely due to the greater availability of protons, which can play a significant role in O_2 reduction to water. Consumption of oxygen was monitored using either an oxygen electrode (Oxytherm System, Hansatech Instruments Ltd., Norfolk, England) with data collected every 0.1 seconds or a YSI Model 53 oxygen meter equipped with a water-jacketed and stirred-glass measuring vessel (1.8 mL volume) with data collected every 0.6 seconds. Oxygen consumption rates were calculated by taking the derivative of the oxygen concentration using a 30 s data window (300 points or 50 points). For data where catalase and SOD, (Superoxide Dismutase) (Enzo Life Sciences International, Inc., Plymouth Meeting, PA), were used, 2.2 µM and 250 units (as defined by manufacturer) were added, respectively, before addition of reductant. The reaction of catalase and SOD with hydrogen peroxide and superoxide, respectively should produce one equivalent of oxygen per two equivalents of the respective ROS[41,42] This is important as the production of ROS and water both consume oxygen. By being able to determine how much ROS are produced we can use that rate to calculate the amount of water, if any produced. The maximum initial rate of oxygen consumption measured was reported after subtraction of a background rate of oxygen consumption caused from added reductant and mediator alone reacting with oxygen.

Studies to determine the maximal number of turnovers related to oxygen consumption the model protein can perform, i.e. multiple turnover studies were performed with the same starting conditions as the rate oxygen consumption rate studies above, except that the starting oxygen concentration was ~500 µM (~28 eq). Reductant was added and oxygen consumption was monitored until all oxygen was consumed. After the consumption of all oxygen, approximately 500 µM oxygen in solution was reestablished by was introduced oxygen gas into the head space of sealed chamber. This process was repeated until no more turnovers were observed. Turnovers

performed during oxygen addition were not used in the calculation of overall activity. After every 4 cycles, ascorbic acid (~330 eq) and TMPD (~33 eq) was added to compensate for consumed reductant.

2.2.9 ICP-MS studies

ICP-MS samples for WTswMb, Cu_BMb, F33Y Cu_BMb, and G65Y Cu_BMb were prepared by exchanging, the as purified the protein into 50 mM Bis-Tris pH 7 and diluting to a concentration of 100 µM. Samples were assayed by the microanalysis facility at the University of Illinois for the presence of Fe, S, Zn, Ag, Cu.

2.3 Results and discussion

2.3.1 Design of tyrosine containing Cu_BMb mutants

In an attempt to more closely model the active site of native C*c*O, a tyrosine was introduced in proximity of the Cu_B site of Cu_BMb to mimic the His-Tyr crosslink in the native system and to study the effects of introducing a tyrosine into the model system (see Chapter 4 for efforts in introducing the His-Tyr crosslink).

In designing F33Y Cu_BMb, the sequences of A and B type C*c*Os were considered. In these C*c*Os, the crosslinked His-Tyr are four residues apart, i.e. His 240 is linked to Tyr 244 in an alpha helical structure. The corresponding locations in Cu_BMb for a tyrosine are residues 25 and 33 for linkage to His 29, residues 39 and 47 for linkage to His 43, and residues 60 and 68 for linkage to His 64. Many of these locations are too far from the heme iron to be viable locations based on the Cu_BMb crystal structure (e.g. residues 25, 60, 47) or may potentially interfere with heme binding or oxygen chemistry, residues 39 (based on computer simulations). Therefore, residue 33 was considered the best location. With regard to steric considerations, the mutation of

the native phenylalanine at position 33 to a histidine should be fairly conservative. See Figure 2.2 for an overlay of the computer model and crystal structure of F33Y Cu_BMb. The high level of agreement between the model and structure provides confirmation of our modeling techniques. For reference, an overlay of bovine C*c*O and F33Y Cu_BMb has also been included. Although the Cu_BMb His residues overlay well with the bovine C*c*O structure[43] (PDB: 1V54) the positioning of the tyrosines do not overlay well.

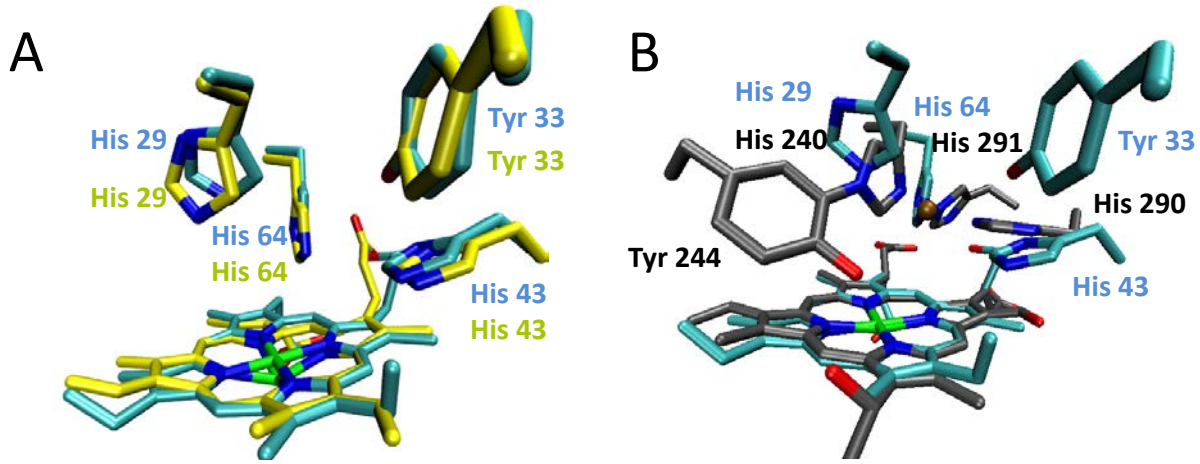

Figure 2.2 Comparision of a 1.9 angstrom Met F33Y Cu_BMb crystal structure (cyan) with (A) F33Y Cu_BMb computer model (yellow) and (B) Crystal structure of bovine C*c*O (1V54) (grey). Note: the waters in the F33Y Cu_BMb structure have been omitted for clarity.

The design of G65Y Cu_BMb was influenced by two factors. First, the three dimensional structure of bovine C*c*O was used as a basis for positioning of the Tyr-OH–heme Fe distance. Secondly, because all the possible His-Tyr positions based on A- and B-type C*c*Os had been considered in the design of F33Y Cu_BMb, a design that more closely mimicked the C-type C*c*Os was attempted[44]. C-type C*c*Os have crosslinked His-Tyr residues on separate alpha helicies. This allowed for other locations not previously considered to be evaluated. Based on energy minimized molecular dynamics simulations, the G65Y Cu_BMb Tyr-OH is positioned approximately 5.6 angstoms from the Fe atom of the heme which is nearly identical to the distance in Bovine C*c*O[43,45]. The relative positioning of the Tyr-OH is also supported by the first

reported structure of a C-type C*c*O[46], which was published after G65Y Cu_BMb was designed. An overlay of the computer model of G65Y Cu_BMb and *Pseudomonas stutzeri* C*c*O (Ps C*c*O) can be seen in Figure 2.3. The positioning of tyrosine hydroxyl in the model and the *Pseudomonas stutzeri* C*c*O relative to the heme is in good agreement.

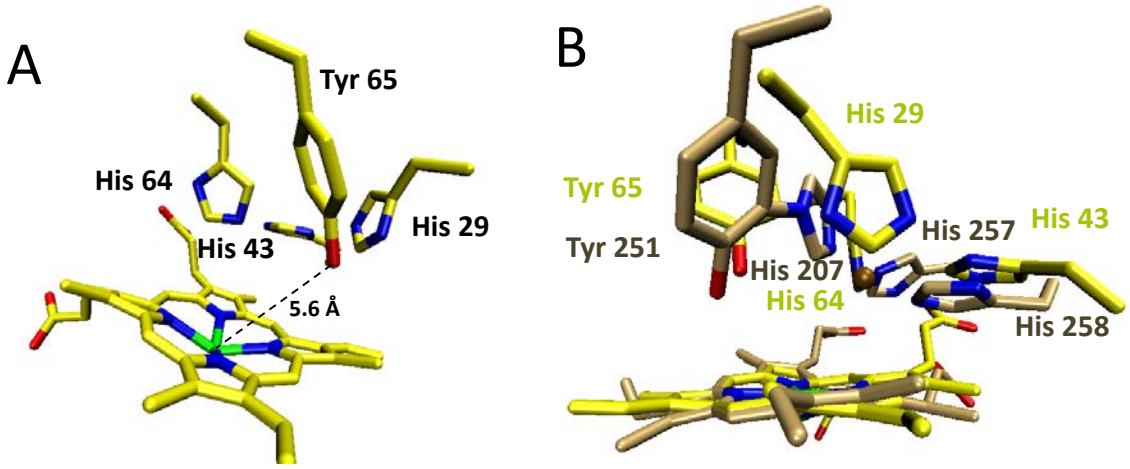

Figure 2.3 (A) Energy minimized computer model of G65Y Cu_BMb and (B) Overlay of the crystal structure of *cbb*$_3$ HCO from *Pseudomonas stutzeri* (tan) and G65Y Cu_BMb computer model (yellow).

2.3.2 Myoglobin, Cu_BMb, F33Y Cu_BMb, and G65Y Cu_BMb oxygen chemistry at pH 6

It should be noted that the Cu_BMb proteins are purified do not contain a metal in the Cu_B site as confirmed by ICP-MS (see Table 2.1). The work described in this section is without metal added.

2.3.2.1 UV-visible spectroscopy

Myoglobin is well studied and the oxidized (MetMb), reduced (DeoxyMb), and oxygen bound (OxyMb) states are well known[29]. Figure 2.4 contains reference UV-visible spectra of WTswMb, F33Y Cu_BMb, and G65Y Cu_BMb. The oxidized form of G65Y Cu_BMb has a significant bis-His ligated population, where the distal His64 is ligated to heme iron. Interestingly, the oxygen bound forms of the Cu_BMb tyrosine derivatives have blue-shifted Soret

bands at ~411 nm, versus a Soret band of ~418 nm for WTswMb, suggesting that the introduction of a tyrosine residue perturbs the environment of the heme pocket.

Comparing the UV-visible traces of the three proteins under reducing conditions, WtswMb quickly forms OxyMb as expected and displays a fairly stable OxyMb spectrum even after reaction for one hour. Both tyrosine containing mutants also quickly formed OxyMb. However, unlike WtswMb, a population of DeoxyMb was also detected for the tyrosine mutants, which increased as the reaction proceeded. This suggests that enough oxygen is being consumed by the proteins to preclude oxygen binding, leading to the formation of DeoxyMb. Cu_BMb also displays this activity but it is much slower than the tyrosine mutants. This activity is different than what was observed by Sigman et al.[32] where the OxyMb Soret at 418 nm was fairly stable without metal added.

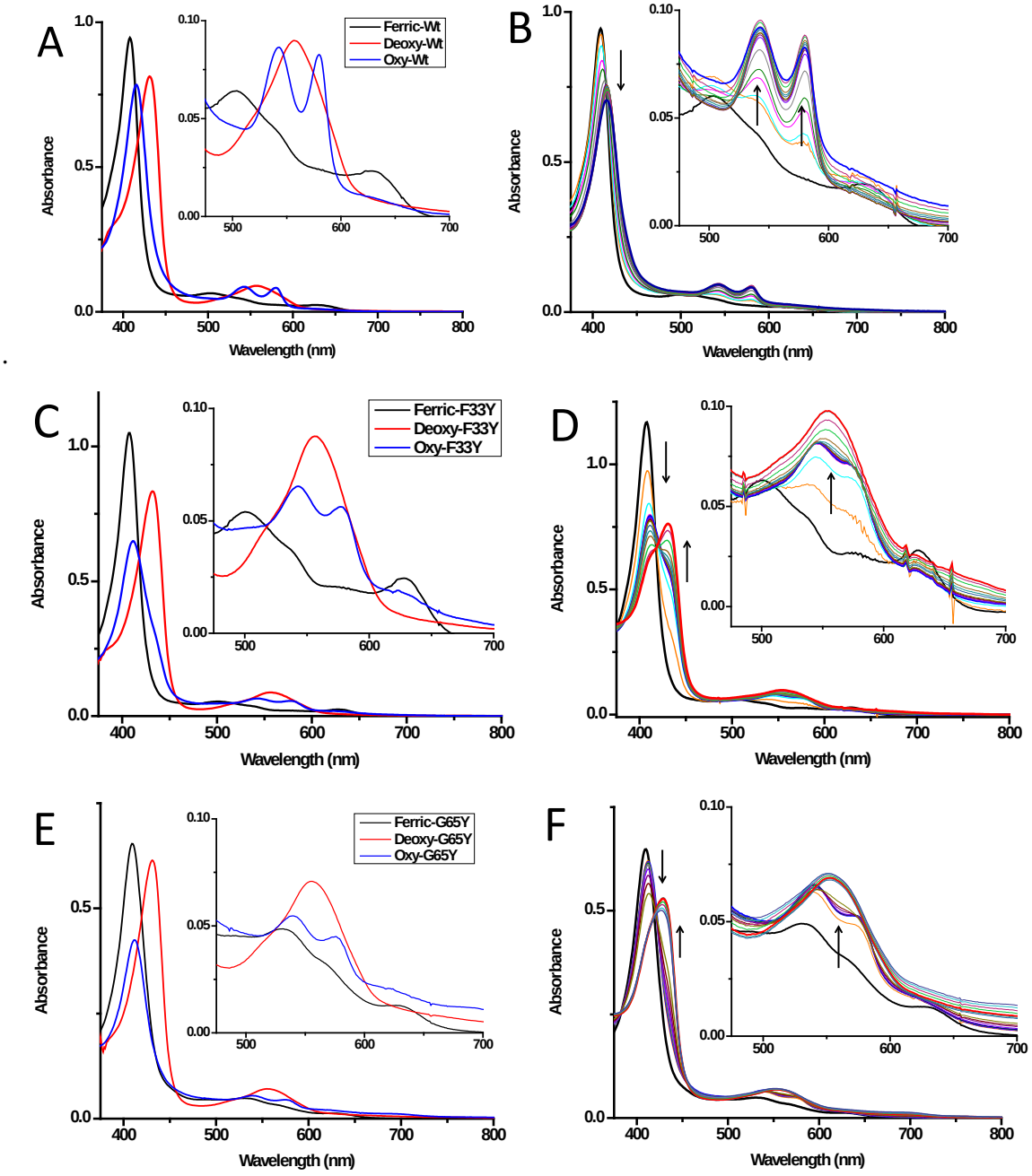

Figure 2.4 Reference UV-visible spectra and time-dependent spectra, respectively of the reaction of 6 µM of WTswMb (A-B), F33Y Cu_BMb (C-D), and G65Y Cu_BMb (E-F) under reducing conditions at pH6. Reactions were monitored for one hour to ensure that the reaction was complete. Note: 'Ferric' is used in the reference as G65Y Cu_BMb contains a population of bis-His myoglobin in the oxidized state.

2.3.2.2 Oxygen electrode studies

Oxygen electrode studies were performed to assay both the product and relative rates of protein oxygen consumption. In these studies, we observed a rate of oxygen consumption for all

four proteins (Figure 2.5). The activity observed for WTswMb is surprising given that UV-vis studies show only oxygen binding capability. However, differences in the amount of protein used and difficulty in completely preventing leaking of air into the cuvette during the UV-visible studies could explain lack of observed activity by UV-visible work. In fact WtswMb is expected to have an increased rate of autoxidation[30], i.e. the release of superoxide from OxyMb and the formation of MetMb, under mildly acidic conditions. This increase is caused by a higher rate of protonation of the bound oxygen compared to more basic conditions. This expected autoxidation rate explains the activity (i.e. oxygen consumption) observed with WTswMb in the sealed chamber of the oxygen electrode. The main products of WTswMb oxygen consumption in the oxygen electrode are reactive oxygen species, based on control studies where the rate of apparent oxygen consumption by WTswMb slows in the presence catalase. Similar results were also obtained in the presence of both SOD and catalase. Therefore based on the activity of catalase and SOD to convert reactive oxygen species back to oxygen, which caused the apparent slower rate, the product is a ROS. The similarity between the conditions with catalase only and with both SOD and catalase results, indicates hydrogen peroxide is the ROS produced. The source of the species in solution, hydrogen peroxide, is autoxidation. The product of autoxidation, superoxide, is unstable under the slightly acidic (i.e. pH 6) and reductive conditions of the assay[47] and forms hydrogen peroxide. The amount of rate change caused by the addition of catalase and SOD can be used to calculate the rate of water production as half of the ROS is converted by these enzymes back to oxygen. The maximal decrease in observed oxygen consumption rate possible by SOD and catalase, if no other processes are occurring, and all the product is ROS is half the oxygen consumption rate observed in the absence of SOD and catalase. Therefore, if the apparent oxygen consumption rate in the presence of SOD and catalase

is greater than half the oxygen consumption rate in the absence of SOD and catalasesome water must be formed assuming no other processes are interfering, such as verdoheme formation.

Cu_BMb has a slower overall rate of oxygen consumption than WTswMb but the percentage of water produced, as opposed to ROS species, is greater based on a smaller percentage change in the apparent oxygen consumption rate in the presence of catalase and SOD for Cu_BMb compared to WtswMb, (See Figure 2.5C). This is probably because the reduction of oxygen to water has many more steps than the release of a partially reduced intermediate. It should be noted that the calculated rate of water production in Cu_BMb is approximately equal to that of WTswMb. Therefore, Cu_BMb is either lacking the hydrogen bonding network to deliver protons to the bound oxygen or the ability to reduce the oxygen effectively. Considering the reactions are carried out with excess reductant, there should be enough electrons or reducing equivalents available for the complete reduction of oxygen to water. If instead, Cu_BMb was unable to provide an environment where the initial reduction of the oxygen was more favorable than WtswMb, results similar to WTswMb would be expected because protonation of the bound oxygen, the alternative under these conditions, would cause autoxidation because the protonated oxygen leaves a neutral superoxide[30].

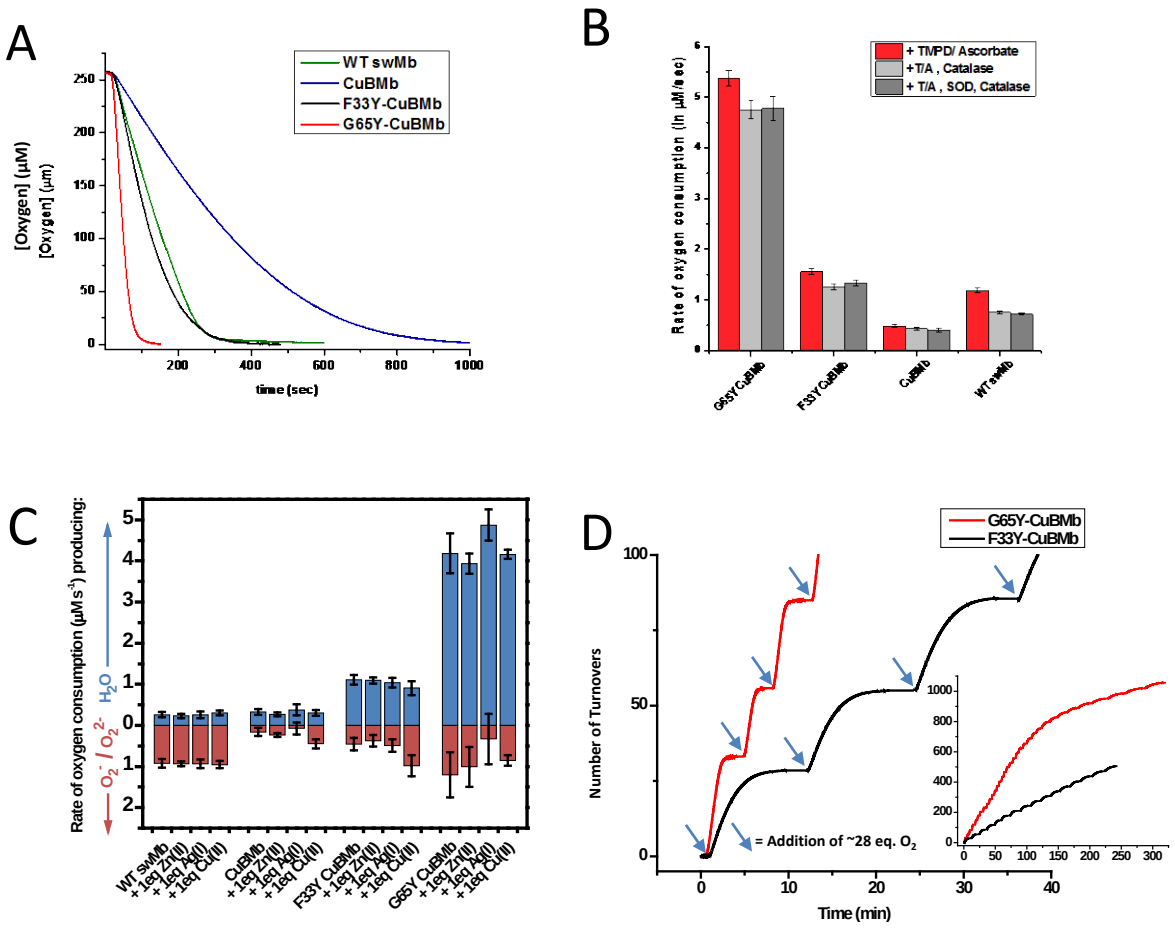

Figure 2.5 – Oxygen consumption data for WtswMb, Cu_BMb, F33Y Cu_BMb, and G65Y Cu_BMb at pH 6. (A) Representative oxygen consumption traces in the absence of SOD and catalase. (B) Oxygen consumption rates in the presence or absence of catalase or catalase/SOD. (C) Calculated rates of water and peroxide/superoxide production in the presence or absence of 1eq Zn, Ag, or Cu and absence of catalase or catalase/SOD. (D) Multiple turnover data for G65Y Cu_BMb and F33Y Cu_BMb.

The substitution of a tyrosine at position 33 in F33Y Cu_BMb results in an approximately 3-fold increase in rate of oxygen consumption over that of Cu_BMb, with a comparable ratio of water to ROS produced based on the comparable percentage rate decrease in the presence of catalase and SOD. The rate of oxygen consumption of F33Y Cu_BMb is about 1.5 times faster than that of WTswMb with a considerably higher percentage of water production in F33Y Cu_BMb compared to WtswMb (see Figure 2.5C). This is based on the lower percent change of apparent oxygen consumption rate in F33Y CuBMb change with catalase and SOD (see Figure

2.5B), compared to WTswMb. The increase in the rate of water production, compared to Cu_BMb (see Figure 2.5C), could be due to a better hydrogen bonding network in F33Y Cu_BMb since the hydroxyl group on the tyrosine which is not present in Cu_BMb could potentially stabilize a bound water molecule. With a Tyr-OH to heme iron distance of ~8Å, it is unlikely that Tyr33 is directly interacting with the bound oxygen directly and must be communicating through a water molecule. The Met F33Y Cu_BMb structure does not contain a water (see Figure 2.6B) within hydrogen bonding distance for F33Y Cu_BMb to interact through. However, a reorganization of the water molecules present in the structure, is possible once a ligand binds. Crystal structures of WTswMb in the Met[48] and Oxy[49] forms, PDB 1JP6 and 1MBO, respectively (see Figure 2.6), suggest that such a rearrangement is possible. A potential location for stabilization of a water molecule is near Tyr33 and His43 is possible due to potential hydrogen bonding partners. In addition, a crystal structure of F33Y Cu_BMb with a side-on bound, putatively assigned as peroxo species, bound to the heme iron has been obtained, as discussed later in Chapter 5, this structure has a different positioning of water molecules in the heme pocket, and this distribution of waters contains one which is within hydrogen bonding distance of Tyr33.

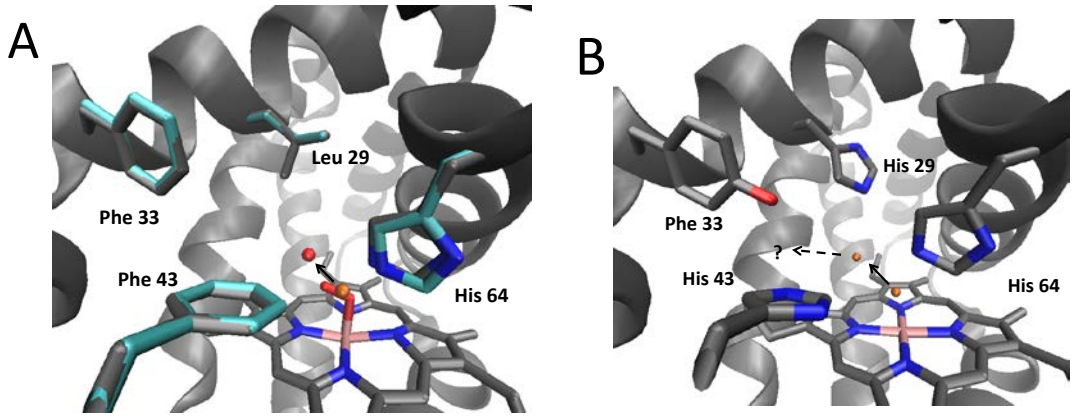

Figure 2.6 Potential rearrangement of waters after ligand binding. (A) Crystal structures of WtswMb in the Met (grey) and Oxy forms (Cyan) and (B) Suggested rearrangement for F33Y-Cu_BMb based on Met structure.

G65Y Cu_BMb has a faster rate of oxygen consumption compared to Cu_BMb and F33Y Cu_BMb by 9- and 3-fold, respectively (see Figure 2.5B). Along with the increase in oxygen consumption there is a comparable ratio of water to ROS production (see Figure 2.5C). The relative position of the tyrosine in G65Y Cu_BMb may be more favorable for creating a hydrogen bonding network that promotes the reduction of oxygen to water. Considering that Tyr65 was designed to more closely mimic the position of the native C*c*O His-Tyr crosslink with respect to the position of the heme (Figure 2.3), this explanation seems reasonable. Since an actual His-Tyr crosslink is not present in the G65Y Cu_BMb system, it is unlikely that Tyr65 could aid in oxygen reduction by donating a proton to the reaction, as the pKa of Tyr (without a cross-link) is around 10. To confirm that the heme was involved in the observed activity, oxygen consumption reactions for G65Y Cu_BMb and F33Y Cu_BMb were repeated in the presence of 18 mM cyanide, as an inhibitor of oxygen chemistry at the heme iron, with significantly decreased oxygen consumption activity (see Figure 2.7).

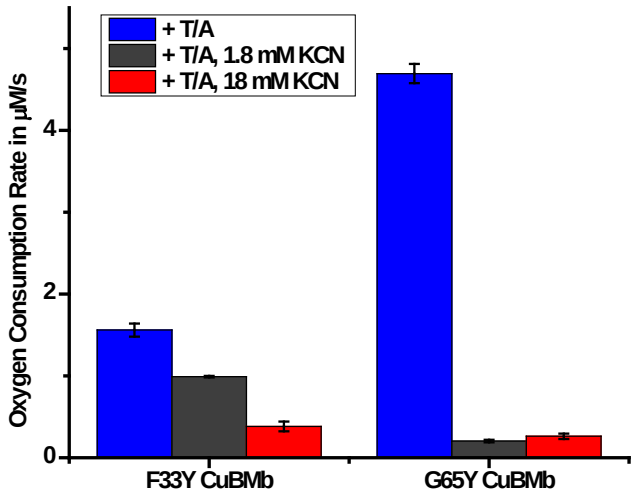

Figure 2. 7 Effect of cyanide addition on oxygen consumption rate for F33Y Cu_BMb and G65Y Cu_BMb.

To test the limits of the designed proteins, we performed multiple turnover reactions, i.e. reactions where the protein was allowed to consume oxygen until it was depleted, as above, and

then, additional oxygen was added until the oxygen consumption activity of the enzyme had slowed greatly. To a solution containing F33Y Cu_BMb or G65Y Cu_BMb and excess reductant, ~500 μM or ~28 equivalents O_2 was added, and oxygen reduction was monitored using an oxygen electrode until all oxygen was consumed. After complete consumption, a further addition of ~28 equivalents of O_2 was carried out and oxygen reduction was measured again until all the oxygen was reduced. These stepwise additions resulted in the multiple plateaus observed in the traces for both proteins (Figure 2.5) with F33Y Cu_BMb reaching 505 turnovers and G65YCu_BMb achieving 1056 turnovers (Figure 2.5D, inset). The number of turnovers reported here is an underestimate since the extra turnovers occurring during oxygen addition were not included in the calculation. These results demonstrate that the designed proteins are capable of hundreds of turnovers; with G65Y Cu_BMb exhibiting more than 1000 turnovers.

2.3.2.3 ^{17}O NMR characterization

To confirm that F33Y Cu_BMb and G65Y Cu_BMb are indeed reducing oxygen to water as designed, a more direct assay than oxygen consumption (via oxygen electrode studies) is required. Therefore, ^{17}O NMR was used to identify the product of oxygen consumption by these proteins. By injecting $^{17}O_2$ into the headspace of an NMR tube containing WTswMb, F33Y Cu_BMb or G65Y Cu_BMb, the production of $H_2{}^{17}O$ above the natural abundance of $H_2{}^{17}O$ in water, as produced by protein oxygen reduction, could be monitored. A typical ^{17}O NMR spectrum, shown in Figure 2.8, consists of a peak assignable to $H_2{}^{17}O$ (referenced to 0 ppm) and a second small peak at 150 ppm assignable to ^{17}O-labeled Tyr, which was added as an external standard to assist quantification. The normalized ratio of the $H_2{}^{17}O$ peak area and that of the ^{17}O-Tyr peak at 30, 60, 90, and 120 min are shown in Figure 2.7B. Consistent with UV-vis studies, the normalized ratio of WTswMb remains the same as that of the natural abundance of $H_2{}^{17}O$ in

water, suggesting that the protein did not produce any new $H_2{}^{17}O$. In contrast, F33Y Cu_BMb and G65Y Cu_BMb produced up to 10 mM $H_2{}^{17}O$ at 120 min, as indicated by an increase in the normalized ratio between $H_2{}^{17}O$ and ^{17}O Tyr to 1.5. These results confirm that water is indeed a product of F33Y Cu_BMb and G65Y Cu_BMb oxygen reduction, moreover, the designed protein is performing HCO-like chemistry.

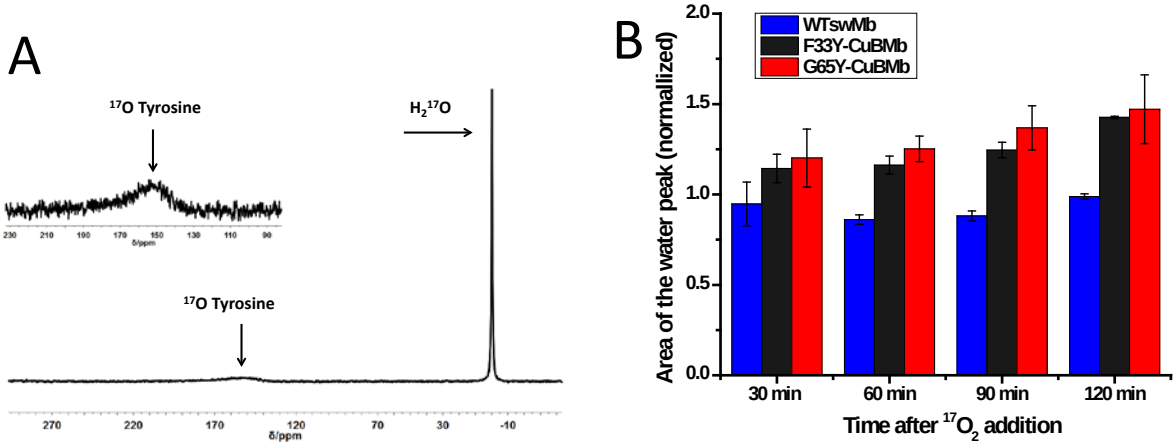

Figure 2. 8 ^{17}O NMR spectroscopy. (A) Typical background spectrum observed. (B) Normalized change in the ratio of the ^{17}O labeled Tyrosine and ^{17}O water peak areas over time.

2.3.3 Effect of different metal ions on activity

Cu_BMb and the tyrosine containing variants were purified from *E. coli* cells using a protocol that includes dialysis against buffer with 30 mM EDTA[11,32] intended to remove metals that may have bound to the Cu_B site during purification. The effectiveness of this metal removal can be seen by the ICP-MS data of purified Cu_BMb, F33Y Cu_BMb, and G65YCu_BMb (Table 2.1). This means that the oxygen reduction activity described above is in the absence of metal in the designed metal binding site (i.e. Cu_B site of Cu_BMb and its variants). These results are significant since the HCOs are purified with a Cu loaded in the Cu_B site. It should be made clear that HCOs with Cu_B site mutations or copper chaperone knock out mutants have much lower activity, indicating the importance of the metal in the Cu_B site to C*c*O activity *in vivo*. In the Cu_BMb proteins metal

must be added after purification otherwise the site is occupied by a water molecule. See Figure 2.6B for F33Y Cu_BMb with water in the Cu_B site. Therefore to observe the effect of metal ions in the site they must be added.

Table 2.1 ICP-MS results for levels of Ag, Cu, Fe, S, and Zn in as purified protein

Sample	ppm Cu	ppm Fe	ppm S	ppm Ag	ppm Zn	Ratio Cu:Fe	Ratio Ag:Fe	Ratio Zn:Fe
CuBMb	0.00	5.60	8.67	0.01	0.04	0.00	0.00	0.01
F33Y CuBMb	0.00	5.60	10.76	0.00	0.04	0.00	0.00	0.01
G65Y CuBMb	0.00	5.60	9.37	0.00	0.03	0.00	0.00	0.00

Note: All samples were normalized to 5.60 ppm Fe for clearer comparison

As seen in Figure 2.5C, addition of 1 eq of Ag(I) or Zn(II) has no effect on the activity (within error for any of the proteins assayed). This is not completely unexpected as Ag(I) and Zn(II) are redox inactive and cannot donate an electron to the bound oxygen. The addition of 1 eq of Cu(II) under reductive conditions yields an interesting but unexpected result. The addition of copper to Cu_BMb and F33YCu_BMb results in an increase in the rate of oxygen consumption, which can be seen with larger length of the red and blue bars together, as these two rates sum to the overall rate (Figure 2.5C). However, after further experiments in the presence of catalase and superoxide dismutase, the rate increase appears to be from increased reactive oxygen species formation and not increased water production (red bars in Figure 2.5C). For G65Y Cu_BMb, the rate oxygen consumption actually slows slightly upon copper addition. This result suggests that the protein is becoming deactivated or not binding copper. To confirm that the tyrosine-containing mutants could bind copper, metal binding titrations to determine dissociation constants, K_d, values for copper were performed (Figure 2.9). For F33Y Cu_BMb and G65Y Cu_BMb, the Kd was determined to be 2 μM and 100 μM, respectively. As a result, we performed studies with up to 2 eq of copper for Cu_BMb and its tyrosine variants to increase the percentage of Cu_B sites occupied. As seen in Figure 2.9C, the rate of oxygen consumption does increase

with increasing copper concentration for Cu_BMb and F33Y Cu_BMb. However, in the presence of SOD, catalase and copper, the rate of oxygen consumption observed is slow, suggesting a high level of hydrogen peroxide formation either by the enzyme or by free copper. G65Y Cu_BMb showed a decrease in the rate of oxygen consumption with copper compared to rates with no metal. This result is possibly due to increased copper-dependent heme oxygenase activity, which would inactivate G65Y Cu_BMb, was observed for Cu_BMb in a previous studies[33,50], as the presence of 2 eq of Cu resulted in a visibly greenish solution, consistent with the formation of verdoheme, the product of heme oxygenase activity. To adjust for this activity an UV-vis based assay was performed by adapting an assay performed in previous work[50] on Cu_BMb for copper-dependent verdoheme formation. A UV-Vis based assay was performed using the pH 6 reaction conditions and verdoheme rates were measured (see Table 2.2). The addition of Cu(II) under reaction conditions induces formation of verdoheme in all three proteins. The raw oxygen consumption rate data was then corrected using the rate of verdoheme formation obtained for the assay to reflect this information (see Figure 2.9D). The resulting corrected oxygen consumption rates obtained in the presence and absence of catalase and SOD still corresponded to high levels of hydrogen peroxide formation. Unfortunately, no copper containing assay condition attempted improved water production. However the observation of copper dependent verdoheme formation does suggest that copper is indeed binding.

Table 2.2 Verdoheme formation rates (s^{-1}) in the absence or presence of catalase and SOD

Reagents Added	CuBMb			F33Y CuBMb			G65Y CuBMb		
+ 1 eq Cu	8.47E-03	+/-	3.79E-04	3.77E-03	+/-	1.30E-04	8.83E-03	+/-	1.00E-03
+ 2 eq Cu	1.90E-02	+/-	8.12E-04	7.91E-03	+/-	4.54E-04	1.95E-02	+/-	7.90E-04
+ 1eq Cu, Catalase, SOD	3.38E-03	+/-	4.09E-04	2.07E-03	+/-	8.69E-05	1.98E-03	+/-	1.17E-04
+ 2eq Cu, Catalase, SOD	8.67E-03	+/-	1.24E-03	5.78E-03	+/-	4.91E-04	2.58E-03	+/-	3.22E-04

Rates of verdoheme formation per second for Cu_BMb, F33Y Cu_BMb and G65Y Cu_BMb. Error indicated is Standard Deviation from the mean.

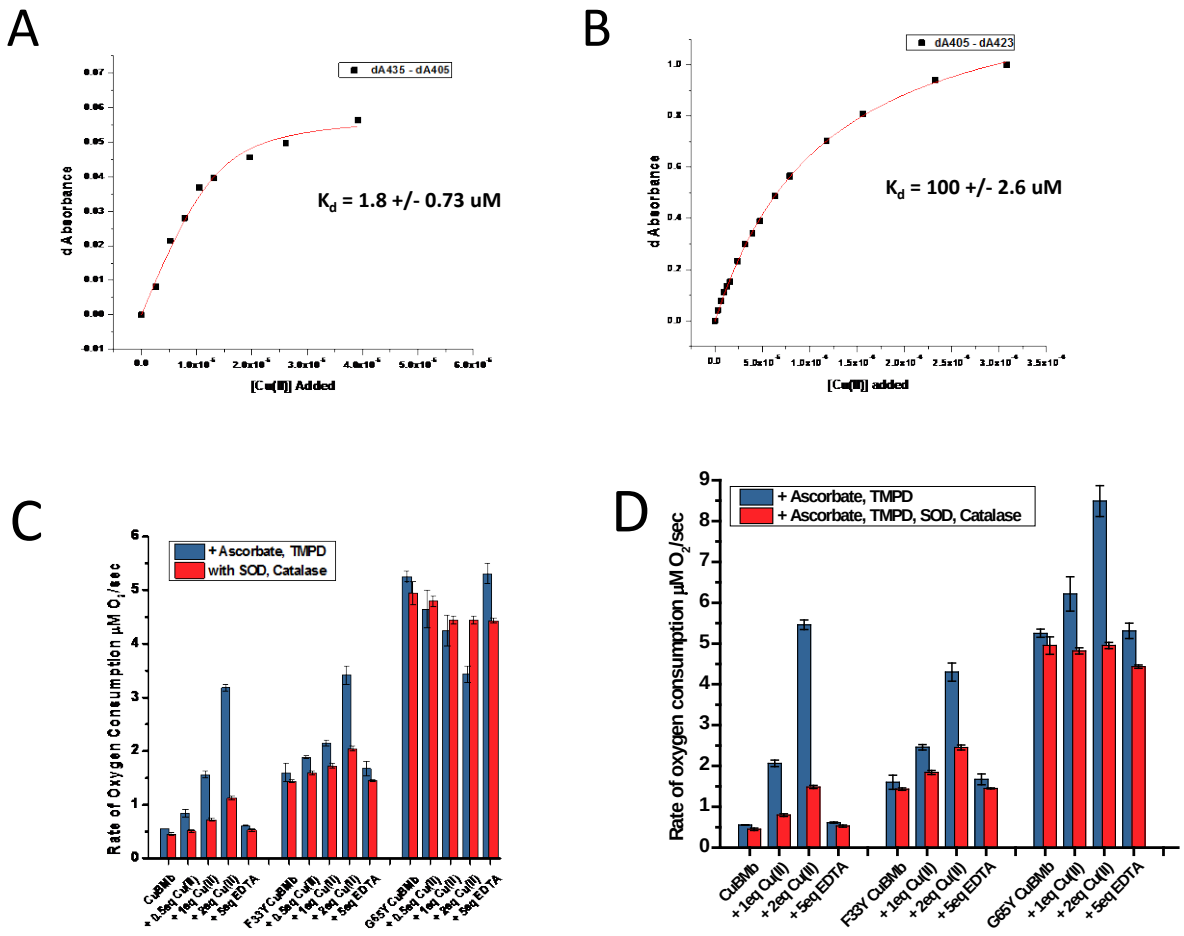

Figure 2. 9 Determination of copper affinity and effect of copper dependent verdoheme formation.. Copper Kd determination for oxidized (A) F33Y Cu_BMb and (B) G65Y Cu_BMb in bis-Tris HCl pH 7. Observed oxygen consumption rates with up to 2 eq Cu for Cu_BMb, F33Y Cu_BMb, and G65Y Cu_BMb (C) with and (D) without correction for verdoheme formation.

2.4 Summary and Conclusions

Cu_BMb and its tyrosine containing variants perform HCO like chemistry, even in the absence of copper in the engineered Cu_B site. This result is unexpected as HCOs are generally isolated with copper in the Cu_B site and are inactive if mutations are made that interfere with Cu binding. This suggests that copper is not required for this type of chemistry to occur and that the role of the copper in the Cu_B site in HCOs may only be to increase the activity of the native system up to physiologically required levels, as we have shown that our system can perform the

required chemistry without the copper but a levels much lower than HCOs. Electrons used by our proteins are supplied via the addition of excess reductant that either reduces the heme and/or ligand to the heme. The Cu_BMb system appears to be unable to fully utilize copper for C*c*O chemistry as demonstrated by the observed verdoheme activity and the lack of an increase in HCO-like activity upon binding of copper to Cu_BMb and its tyrosine containing variants. Despite this shortcoming, the oxygen consumption rate of G65Y Cu_BMb is only 300-fold below that of some HCOs. As copper has been shown to provide an electron to reduce bound oxygen in C*c*Os, there are two likely causes of the proteins described here to produce water at a higher rate with copper. The first possibility is our system is unable to utilize the copper due to being unable to transfer electrons in and out of the Cu_B copper. This may be plausible as antiferromagnetic coupling of the copper in the Cu_B site and heme iron in our system requires a ligand bound to the heme iron such as cyanide to be observed as shown previously[32]. The absence of antiferromagnetic coupling without a ligand implys poor communication between the sites, and as a result the copper may not be becoming reduced before the oxygen binds and therefore does not have an electron to donate to the reduction of oxygen to water. An alternate possibility is that proton delivery is limiting, and that without efficient delivery of protons the enzyme has a rate limiting step of proton delivery that prevents rapid rate increase with copper. Such a proton delivery problem may be indicated the observed copper-dependent heme oxygenase activity, which is a result of a presumably increased population of the ferric hydroperoxo species (cpd 0) that is common to both HCO and heme oxygenase chemistries without the formation of cpd I, which would have resulted from efficient proton delivery to cpd 0 . To resolve this a more extensive hydrogen bonding network or an efficient source of protons analogous to proton channels of HCOs might be required. The resolution of these issues will make the Cu_BMb

system more efficient and more specific (less ROS production), making the system more ideally suited for practical applications. As described here, as a first generation model, this system could potentially be used in practical applications if one can prevent catalyst deactivation (likely due to catalyst poisoning by ROS production) after ~1000 turnovers. Described in the following chapter are early attempts at resolving these issues by using native HCOs and knowledge gained from previous studies with our system as a guide.

2.5 References

1 Das, R. & Baker, D. Macromolecular modeling with Rosetta. *Annu. Rev. Biochem.* 77, 363 (2008).

2 Lu, Y., Yeung, N., Sieracki, N. & Marshall, N. M. Design of functional metalloproteins. *Nature* 460, 855 (2009).

3 Calhoun, J. R. *et al.* Artificial diiron proteins: From structure to function. *Biopolymers* 80, 264 (2005).

4 Regan, L. & DeGrado, W. F. Characterization of a helical protein designed from first principles. *Science* 241, 976 (1988).

5 Bolon, D. N. & Mayo, S. L. Enzyme-like proteins by computational design. *Proc. Natl. Acad. Sci. U.S.A.* 98, 14274 (2001).

6 Robertson, D. E. *et al.* Design and synthesis of multi-heme proteins. *Nature* 368, 425 (1994).

7 Kuhlman, B. *et al.* Design of a novel globular protein fold with atomic-level accuracy. *Science* 302, 1364 (2003).

8 Korendovych, I. V. *et al.* De Novo Design and Molecular Assembly of a Transmembrane Diporphyrin-Binding Protein Complex. *J. Am. Chem. Soc.* 132, 15516 (2010).

9 Koder, R. L. *et al.* Design and engineering of an O-2 transport protein. *Nature* 458, 305 (2009).

10 Thyme, S. B. *et al.* Exploitation of binding energy for catalysis and design. *Nature* 461, 1300 (2009).

11 Yeung, N. *et al.* Rational design of a structural and functional nitric oxide reductase. *Nature* 462, 1079 (2009).

12 Jiang, L. *et al.* De novo computational design of retro-aldol enzymes. *Science* 319, 1387 (2008).

13 Watanabe, Y. & Hayashi, T. Functionalization of myoglobin. *Prog. Inorg. Chem.* 54, 449 (2005).

14 Ghosh, D. & Pecoraro, V. L. Probing metal-protein interactions using a de novo design approach. *Curr. Opin. Chem. Biol.* 9, 97 (2005).

15 Namslauer, A. & Brzezinski, P. Structural elements involved in electron-coupled proton transfer in cytochrome c oxidase. *FEBS Lett.* 567, 103 (2004).

16 Babcock, G. T. & Wikstrom, M. Oxygen Activation and the Conservation Of Energy In Cell Respiration. *Nature* 356, 301 (1992).

17 Ferguson-Miller, S. & Babcock, G. T. Heme/Copper Terminal Oxidases. *Chem. Rev.* 96, 2889 (1996).

18 Che, C. M., Chiang, H. J., Margalit, R. & Gray, H. B. Preparation and properties of osmoglobins. Oxidation-reduction catalytic activity of ruthenated osmoglobin. *Catal. Lett.* 1, 51 (1988).

19 Kim, E., Chufan, E. E., Kamaraj, K. & Karlin, K. D. Synthetic Models for Heme-Copper Oxidases. *Chem. Rev.* 104, 1077 (2004).

20 Collman, J. P. *et al.* A Cytochrome c Oxidase Model Catalyzes Oxygen to Water Reduction Under Rate-Limiting Electron Flux. *Science* 315, 1565 (2007).

21 Collman, J. P. & Decreau, R. A. Functional biomimetic models for the active site in the respiratory enzyme cytochrome c oxidase. *Chem. Commun.*, 5065 (2008).

22 Bashyam, R. & Zelenay, P. A class of non-precious metal composite catalysts for fuel cells. *Nature* 443, 63 (2006).

23 Lefevre, M., Proietti, E., Jaouen, F. & Dodelet, J.-P. Iron-Based Catalysts with Improved Oxygen Reduction Activity in Polymer Electrolyte Fuel Cells. *Science* 324, 71 (2009).

24 Brzezinski, P. & Gennis, R. B. Cytochrome c oxidase: exciting progress and remaining mysteries. *J. Bioenerg. Biomembr.* 40, 521 (2008).

25 Koepke, J. *et al.* High resolution crystal structure of Paracoccus denitrificans cytochrome c oxidase: New insights into the active site and the proton transfer pathways. *Biochim. Biophys. Acta* 1787, 635 (2009).

26 Aoyama, H. *et al.* A peroxide bridge between Fe and Cu ions in the O2 reduction site of fully oxidized cytochrome c oxidase could suppress the proton pump. *Proc. Natl. Acad. Sci. U.S.A.* 106, 2165 (2009).

27 Egawa, T., Lee, H. J., Gennis, R. B., Yeh, S.-R. & Rousseau, D. L. Critical structural role of R481 in cytochrome c oxidase from Rhodobacter sphaeroides. *Biochim. Biophys. Acta* 1787, 1272 (2009).

28 Collman, J. P. & Ghosh, S. Recent Applications of a Synthetic Model of Cytochrome c Oxidase: Beyond Functional Modeling. *Inorg. Chem.* 49, 5798.

29 Antonini, E., Brunori, M., Neuberger, A. & Tatum, E. L. *Hemoglobin and Myoglobin in their Reactions with Ligands*. Vol. 21 (Elsevier New York N. Y, 1971).

30 Brantley, R. E., Jr., Smerdon, S. J., Wilkinson, A. J., Singleton, E. W. & Olson, J. S. The mechanism of autooxidation of myoglobin. *J. Biol. Chem.* 268, 6995 (1993).

31 Van Dyke, B. R. *et al.* Site-directed mutagenesis of histidine residues involved in copper(II) binding and reduction by sperm whale myoglobin. *Proc. Natl. Acad. Sci. U.S.A.* 89, 8016 (1992).

32 Sigman, J. A., Kwok, B. C. & Lu, Y. From Myoglobin to Heme-Copper Oxidase: Design and Engineering of a CuB Center into Sperm Whale Myoglobin. *J. Am. Chem. Soc.* 122, 8192 (2000).

33 Wang, N., Zhao, X. & Lu, Y. Role of Heme Types in Heme-Copper Oxidases: Effects of Replacing a Heme b with a Heme o Mimic in an Engineered Heme-Copper Center in Myoglobin. *J. Am. Chem. Soc.* 127, 16541 (2005).

34 Otwinowski, Z. & Minor, W. Processing of x-ray diffraction data collected in oscillation mode. *Methods Enzymol.* 276, 307 (1997).

35 Vagin, A. & Teplyakov, A. MOLREP: an automated program for molecular replacement. *J.Appl.Crystallogr.* 30, 1022 (1997).

36 Brunger, A. T. *et al.* Crystallography & NMR System: a new software suite for macromolecular structure determination. *Acta Crystallogr.* D54, 905 (1998).

37 Sheldrick, G. M. & Schneider, T. R. SHELXL: high-resolution refinement. *Methods Enzymol.* 277, 319 (1997).

38 Jones, T. A., Zou, J. Y., Cowan, S. W. & Kjeldgaard, M. Improved methods for building protein models in electron density maps and the location of errors in these models. *Acta Crystallogr.* A47, 110 (1991).

39 Humphrey, W., Dalke, A. & Schulten, K. VMD: Visual molecular dynamics. *J. Mol. Graphics* 14, 33 (1996).

40 Phillips, J. C. *et al.* Scalable molecular dynamics with NAMD. *J. Comput. Chem.* 26, 1781 (2005).

41 McCord, J. M. & Fridovich, I. Superoxide dismutase. Enzymic function for erythrocuprein (hemocuprein). *J. Biol. Chem.* 244, 6049 (1969).

42 Murthy, M. R. N., Reid, T. J., III, Sicignano, A., Tanaka, N. & Rossmann, M. G. Structure of beef liver catalase. *J. Mol. Biol.* 152, 465 (1981).

43 Tsukihara, T. *et al.* The low-spin heme of cytochrome c oxidase as the driving element of the proton-pumping process. *Proc. Natl. Acad. Sci. U.S.A.* 100, 15304 (2003).

44 Hemp, J. *et al.* Evolutionary Migration of a Post-Translationally Modified Active-Site Residue in the Proton-Pumping Heme-Copper Oxygen Reductases. *Biochemistry* 45, 15405, doi:10.1021/bi062026u [doi] (2006).

45 Tsukihara, T. *et al.* The whole structure of the 13-subunit oxidized cytochrome c oxidase at 2.8 Angstrom. *Science* 272, 1136 (1996).

46 Buschmann, S. *et al.* The structure of cbb3 cytochrome oxidase provides insights into proton pumping. *Science* 329, 327 (2010).

47 Marklund, S. Spectrophotometric study of spontaneous disproportionation of superoxide anion radical and sensitive direct assay for superoxide dismutase. *J. Biol. Chem.* 251, 7504 (1976).

48 Urayama, P., Phillips, G. N. & Gruner, S. M. Probing substates in sperm whale myoglobin using high-pressure crystallography. *Structure (Cambridge, MA, U.S.); Structure (Cambridge, MA, United States)* 10, 51 (2002).

49 Phillips, S. E. V. Structure and refinement of oxymyoglobin at 1.6 .ANG. resolution. *J. Mol. Biol.* 142, 531 (1980).

50 Sigman, J. A., Kim, H. K., Zhao, X., Carey, J. R. & Lu, Y. The role of copper and protons in heme-copper oxidases: Kinetic study of an engineered heme-copper center in myoglobin. *Proc. Natl. Acad. Sci. U.S.A.* 100, 3629 (2003).

CHAPTER 3

EFFECT OF ADJUSTING HYDROGEN BONDING NETWORKS ON OBSERVED OXYGEN CHEMISTRY

3.1 Introduction

3.1.1 Role of hydrogen bonding networks

The secondary coordination environments of proteins can have a significant effect on activity in a given active site. For instance, hydrogen bonding networks can modulate the activity of proteins by affecting the pKa values of amino acid side chains or allowing transfer of protons to substrates In heme proteins it has been postulated that one of the key differences between heme oxygenases[1,2], that use oxygen to degrade heme, and heme proteins that cleave the dioxygen bond, such as heme copper oxidases (HCOs)[3,4] that convert oxygen to water is the extensiveness of the hydrogen bonding network around the bound oxygen[5] and thus the ability to donate protons to it. The delivery of protons to the heme-Cu_B site in HCOs must be efficient in order to maintain the proton gradient[6,7] used to produce ATP and to sustain efficient reduction of oxygen to water. The transfer of protons in HCOs is mediated by proton channels[3,8], namely the so called D and K channels, which supply protons to the Heme-Cu_B site for reduction of oxygen to water, as well as for translocation across the membrane, in the case of the D-channel. Many studies have been devoted to elucidating the function of these proton channels[9-11]. The water molecules in K-channel hydrogen bond to the hydroxyl group of the a/o-type heme in the heme-Cu_B site and to the hydroxyl of the His-Tyr crosslinked residues[4,12].

The Cu_BMb and F33Y Cu_BMb and G65Y Cu_BMb work presented in Chapter 2 showed that the tyrosine-containing mutants of Cu_BMb could produce water from molecular oxygen and

that the rate varied with positioning of the introduced tyrosine. The fastest mutant described, G65Y Cu_BMb, had a rate of oxygen consumption that is approximately 300-fold slower than some HCOs. However, in the work above there were no proton channels designed to deliver protons to the Heme-Cu_B site, nor was there a heme that contained a hydroxyl group analogous to the hydroxyl group of hydroxyfarnesyl substituent of the a/o-type hemes. In an effort to study the effects of these features in Cu_BMb and its tyrosine containing mutants, a non-natural heme cofactor and a hydrophilic channel were introduced, separately into each mutant.

3.1.2 Advantages of introducing a proton channel over further reduced pH

Considering that lowering the pH from 8 to 6 allowed for discovery of the oxygen activity of this system, it might be expected that a further lowering of the pH of the bulk solution might further improve the activity observed. While this suggestion is logical, the stability of myoglobin in acidic conditions is limited as pH decreases[13,14]. Also, further decrease of pH will likely increase the rate of autoxidation that produces ROS[15], and with His residues being our likely proton source, the probability of significantly increasing population of protonated His is low. Therefore, further introduction of mutations to mimic proton channels to increase proton access to the site is a more attractive but technically more difficult alternative. If achieved it would make our model system more like HCOs. However, the locations need to be chosen carefully, as a high number of mutations or highly destabilizing mutations may be as problematic as lowering the pH.

3.1.3 Summary of previous work with Cu_BMb containing a mimic of heme o

Our other proposed route to improve the activity of Cu_BMb and tyrosine-containing variants, introducing a non-natural heme cofactor with a hydroxyl group analogous to the

hydroxyl of a hydroxyfarnesyl group of a/o type hemes, has been performed previously for Cu_BMb[16]. In the previous study, the effect of incorporating Fe(III)-2,4-(4,2)-hydroxyethyl-vinyldeuterioporphyrin IX (referred to as heme o mimic) on copper dependent verdroheme formation the Cu_BMb system was investigated. 2,4-(4,2)-Hydroxyethyl-vinyldeuterioporphyrin IX is a compound nearly identical to protoporphyrin IX (heme b) with one vinyl group replaced with a hydroxyethyl group (see Figure 3.1). The replacement of the native heme b of myoglobinwith heme o mimic in Cu_BMb, denoted Cu_BMb(o), was achieved by unfolding Cu_BMb purified with heme b (denoted Cu_BMb(b)) and replacing with the heme o mimic. In a later obtained crystal structure, a crystallographic water was observed within hydrogen bonding distance of the hydroxyl group of the heme o mimic in V68T Cu_BMb, which is not observed in Cu_BMb with the native heme b[17] (see Figure 3.3 below).

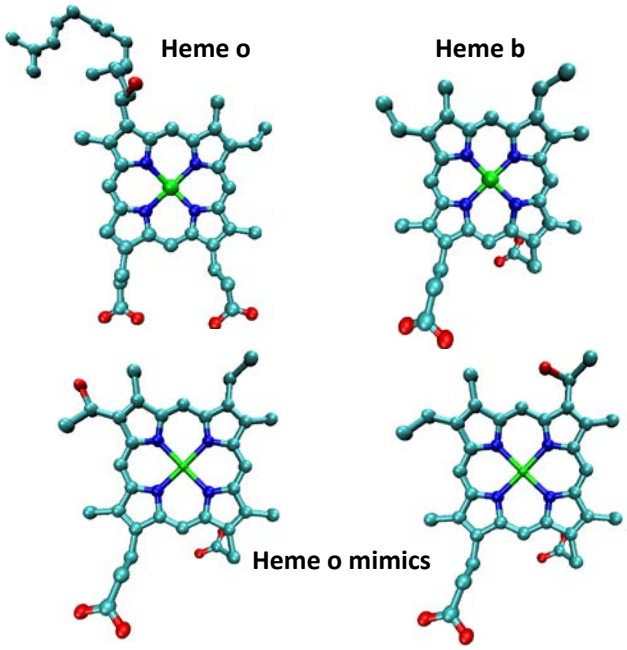

Figure 3.1 Comparision of heme types

At pH 8 Cu_BMb displays a copper dependent heme oxygenase activity as shown by Sigman et al.[18] To form verdoheme, an intermediate in heme oxygenase chemistry, an Fe (III)-

hydroperoxo intermediate, also known as compound 0 (cpd 0), is formed. This subsequently reacts with the alpha-meso carbon[5] and begins the pathway toward verdoheme/biliverdin formation. However, protonation of this intermediate would result in scission of the oxygen-oxygen bond, forming compound I (cpd I) and releasing a molecule of water. The incorporation of the heme o mimic leads to a 19-fold reduction in the rate of the copper dependent verdoheme formation at pH 8[16]. This effect was not seen with the mesoheme cofactor that replaces the vinyl of heme b with an ethyl. This reduction in observed verdoheme rate can be explained by at least two possible effects; either the formation of the Fe (III)-hydroperoxo, (cpd 0), was slowed, thus inhibiting the formation of the intermediate required to form both HCO or heme oxygenase chemistry or the other possibility is that the rate of HCO-like activity was increased by the improved hydrogen bonding network and the Fe (III)-hydroperoxo intermediate became protonated more efficiently. In the process of performing the work in Chapter 2 we developed an assay for testing HCO-like activity in the Cu_BMb system. The results of the assay were confirmed using ^{17}O NMR and we therefore have confidence in its accuracy. This assay should allow us to begin to answer the question of how the heme o mimic slows verdoheme formation by assaying its effect on HCO-like activity. Therefore, the goals of the work below is to investigate the effects of altering the hydrogen bonding network in Cu_BMb, F33Y Cu_BMb, and G65Y Cu_BMb on HCO-like activity by two methods: First, incorporate the heme o mimic into the Cu_BMb and its tyrosine variants. Second, make multiple point mutations to design hydrophilic channels to attempt to mimic the proton channels found in HCOs. The aim of this approach is to provide better proton access to the heme pocket and possibly improve chemistry performed in the Cu_BMb system by increasing the rate oxygen consumption and/or ratio of water to ROS produced.

3.2 Materials and methods

3.2.1 Protein purification

The mutations were introduced using site directed mutagenesis using a protocol previously described[19] and confirmed by DNA sequencing at the Biotechnology Center of the University of Illinois. All proteins except Cu_BMb were purified from inclusion bodies using a protocol previously described[20] with a yield of ~20 mg/L. For F33Y Cu_BMb and variants R/Z was calculated using A_{408}/A_{280}, and for G65Y Cu_BMb and variants using A_{410}/A_{280}; for G65Y-Cu_BMb, protein with an R/Z value of 3.5 was used. Cu_BMb was purified as previously described[19] using a modified protocol for WTswMb.

3.2.2 Heme o mimic preparation and incorporation into protein

2,4-(4,2)-hydroxyethyl-vinyldeuterioporphyrin IX was obtained from Frontier Scientific. Iron was incorporated as previously described[16]. The mass of the product was confirmed via ESI-MS. Product with less than 20% signal intensity corresponding to b-type heme or Fe-HVD-acetate ester was used for incorporation. The yield of Fe(III)-2,4-(4,2)-hydroxyethyl-vinyldeuterioporphyrin IX obtained was assayed by UV-Visible spectroscopy, by dissolving in 0.066M NaOH and was diluting into acetonitrile. Yield was estimated using an ε_{395} of 12.4 mM^{-1}. Apo-protein was prepared by extracting the heme using 2-butanone as was described previously[16]. Apo-protein concentrations were determined spectroscopically using an ε_{280} of 30 mM^{-1}. Protein was diluted to ~10 µM, and typically buffered with ~10 mM potassium phosphate pH 7, which seemed to increase the incorporation yield. Protein was slowly incorporated with heme o mimic by addition of 1/6 equivalent every 15-20 min, with the protein solution on ice with stirring and wrapped in foil. After 1 eq had been added, a second was added by 1/3 eq additions every hour. Incorporation was allowed to proceed overnight. R/Z ratios and protein

concentrations were measured using the Soret absorbances at 404 nm for Cu_BMb(o), F33Y Cu_BMb(o), and 405 nm for G65Y Cu_BMb(o). Soret extinction coefficients of heme b variants were used as estimates for the heme o forms. Please note that as G65Y Cu_BMb met form has not been characterized, therefore met F33Y Cu_BMb extinction coefficient was used as many Cu_BMb mutants have a similar coefficient.

3.2.3 Computer models for hydrophilic channels

Energy minimized computer models for H36S/F106S F33Y Cu_BMb (2S_F33Y Cu_BMb) and V21S/V68S/F36S G65Y Cu_BMb (PCM_G65Y Cu_BMb) were performed using Visual Molecular Dynamics (VMD) [21] and Scalable Molecular Dynamics (NAMD) [22] as mentioned in Chapter 2,with the following changes - the starting structure for 2S_F33Y Cu_BMb was V68T Cu_BMb(o) with the heme o mimic replaced with heme b and Thr68 reverted back to Val68. All necessary mutations were made in addition to these. For PCM_G65Y Cu_BMb, the starting structure was the last time point of a G65Y Cu_BMb molecular dynamics equilibration of 10 ps. Because the goal of this simulation was to see positioning of water in the heme pocket and designed hydrophilic channels, molecular dynamics simulations were carried out for a longer duration (50 ps), than those described in Chapter 2.

3.2.4 Oxygen electrode studies

Oxygen electrode studies were performed as described in section 2.2.8 of chapter 2. Extinction coefficients ε_{408} of 135 mM^{-1} and 109 mM^{-1} were determined for 2S_F33Y Cu_BMb and 2S_G65Y Cu_BMb, respectively, using a hemachromagen assay. It should be noted that the water and ROS calculations assume that all rate reductions are purely from activity of catalase and/or SOD. Other factors such as copper dependent verdoheme formation may need to be corrected for separately.

3.3 Results and discussion

3.3.1 UV-Visible characterization of heme o mimic incorporated proteins

Consistent with previous studies[16], the incorporation of the heme o mimic into Cu_BMb, denoted $Cu_BMb(o)$, causes a blue shift of the metMb Soret band to 404 nm confirming that $Cu_BMb(o)$ is formed (Figure 3.2). F33Y Cu_BMb and G65Y Cu_BMb displayed a similarly shifted Soret band after incorporation with heme o mimic. In the case of G65Y $Cu_BMb(o)$ the Soret band at 405 nm was unexpected, as G65Y Cu_BMb with native heme b, as purified has a significant bis-his population, with a Soret at ~410 nm and R/Z ratio of ~3.5. G65Y $Cu_BMb(o)$ refolded with an R/Z of ~4 which is consistent with larger population of metMb. An extinction coefficient of 175 $mM^{-1}cm^{-1}$ was used to estimate concentrations, as many Cu_BMb mutants have approximately this value for metMb. It should be noted, refolding of G65Y Cu_BMb to obtain a higher population of met could be useful for crystallization, as no conditions have been found for crystallizing G65Y Cu_BMb as purified.

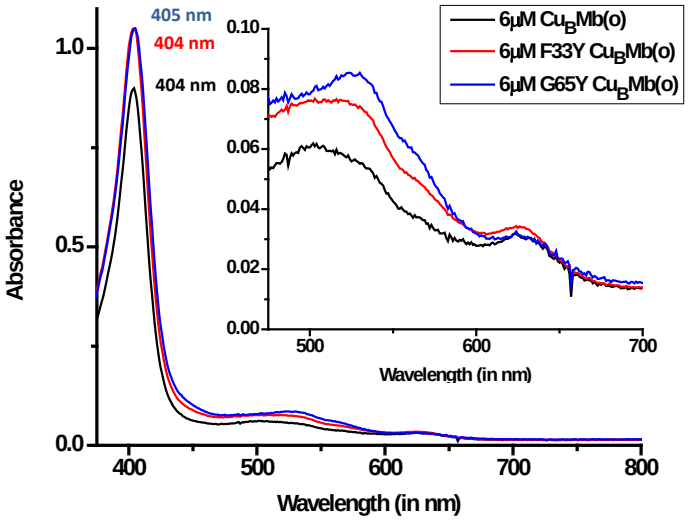

Figure 3.2 UV-Visible spectra of 6uM CuBMb(o) (black), F33Y CuBMb(o)(red) and G65Y CuBMb(o) (blue).

3.3.2 Effect of heme o mimic on Cu_BMb activity

The rationale for expecting a difference in activity using the heme o mimic stems from the reduction on copper-dependent verdoheme formation previously observed and the observation of an additional an unpublished crystal structure where V68T Cu_BMb(o) displayed a crystallographic water not observed in the Cu_BMb structure with heme b (see Figure 3.3A). This extra water appears to be within hydrogen bonding distance of both the water observed in the Cu_B site and the hydroxyl of the heme o mimic. A stabilized water in this position may help form a better hydrogen bonding network for activity. The presence of heme o mimic in Cu_BMb results in an increase of the rate of oxygen consumption of approximately 50% compared to Cu_BMb (see Figure 3.3B). Interestingly Cu_BMb(o) relative ratio of water to ROS is approximately the same as Cu_BMb, meaning that the heme o mimic enhanced the activity. The addition of Zn(II) and Ag(I) as redox inactive mimics has no effect on the rate of Cu_BMb(o) similar to equivalent data for Cu_BMb. In the case of Zn(II)-Cu_BMb(o) the ratio water to ROS produced is lower however, this result is nearly within error. Addition of Cu(II) causes an increase in observed rate that is likely due to an increase in ROS produced, but is also nearly within error. These results suggest that the metal in the site, even a redox inactive metal, is disrupting the chemistry observed in Cu_BMb(o). It is possible that the metal is disrupting an interaction of His43 with a water stabilized by the additional hydroxyl group, by binding to the Cu_B site and affecting the hydrogen bonding network.

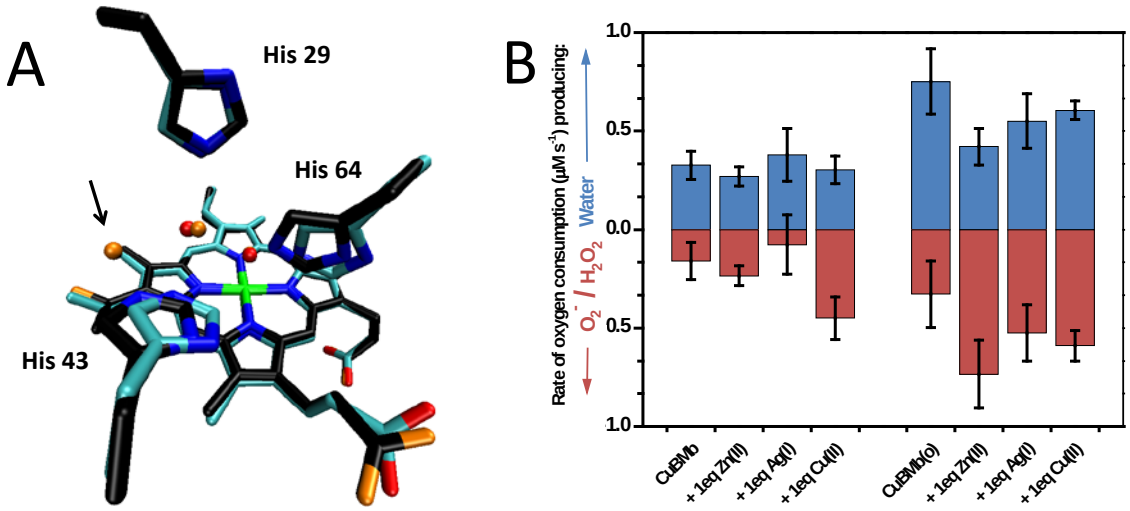

Figure 3.3 (A) Overlay of Cu_BMb (cyan) and V68T Cu_BMb(o) (black) structures Orange spheres are water in the V68T CuBMb(o) structure. Arrow indicates the additional water observed. (B) Rates of water (blue) and ROS production in CuBMb and CuBMb(o). Arrow indicates the additional water observed.

3.3.3 Effect of heme o mimic on F33Y Cu_BMb

When compared to Cu_BMb, F33Y Cu_BMb displays a 3-fold higher rate with the native heme b in the heme pocket. Based on the increase just discussed with Cu_BMb(o), it would be reasonable to expect that F33Y Cu_BMb(o) would have a rate between those of F33Y Cu_BMb and G65Y Cu_BMb. The rate increase in the latter case is approximately 20%, much less than the Cu_BMb case and the ratio of water to ROS is comparable to the results obtained with F33Y Cu_BMb with the native heme b. The calculated rates of water and ROS production are within error. Even in the presence of metal the rates and ratios are essentially the same. It seems that there is little effect from heme o mimic aside from the slight rate increase. This may be rationalized by the suggestion of reorganized waters in the pocket with a ligand bound as discussed in the conclusions of Chapter 2. If the tyrosine hydroxyl is stabilizing a water molecule within hydrogen bonding distance of His43 as suggested with a ligand bound the heme o mimic hydroxyl may be hydrogen bonding to a water that exists in the heme b version of F33Y Cu_BMb.

Considering the position in the heme pocket of the hydroxyl of the structure, there may be no proton for the additional network to transfer and thus only a mild effect on activity.

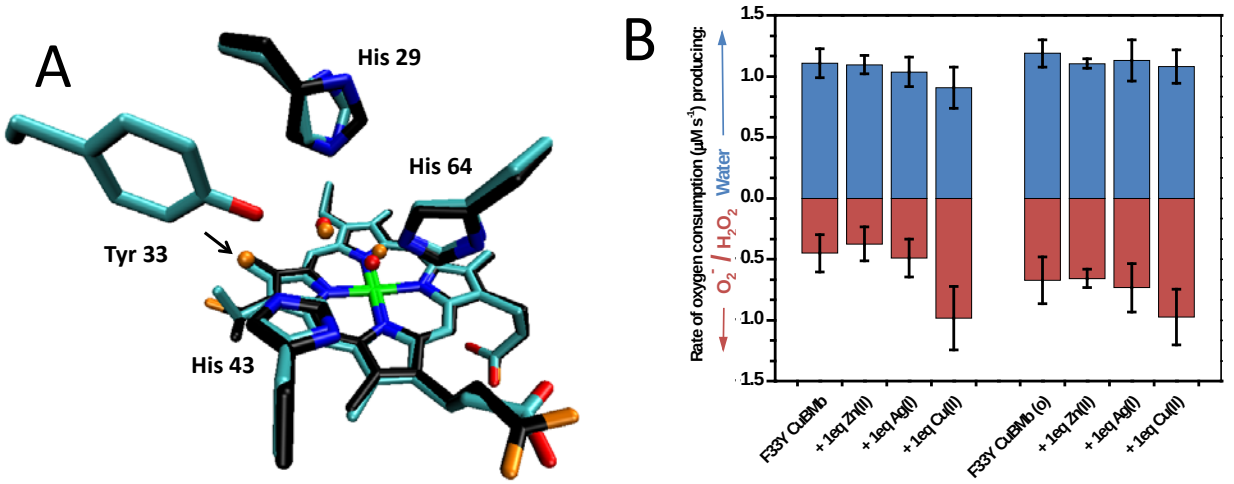

Figure 3.4 (A) Overlay of F33Y Cu_BMb (cyan) and V68T Cu_BMb(o) (black) structures (B) Rates of water (blue) and ROS production in with and without heme o mimic(o). Arrow indicates addition water observed.

3.3.4 Effect of heme o mimic on G65Y Cu_BMb

For G65Y Cu_BMb, the effect of the heme o mimic is hard to predict as the location of the tyrosine based on the computer model of G65Y Cu_BMb is relatively distant from the heme o hydroxyl, unlike in HCOs, and may have little effect. However, the likelihood of stabilizing a water near His43 could be similar to that of Cu_BMb and following the logic and results of the argument for the lack of activity increase for F33Y Cu_BMb, an increase like that observed in Cu_BMb might be expected in G65Y Cu_BMb. The rate of oxygen consumption for G65Y Cu_BMb(o) is within error of the rate for its heme b counterpart, both approximately 5.4 μM/s. The ratio of water to ROS is close but G65Y Cu_BMb(o) appears to produce more ROS compared with the native heme incorporated, in the presence or absence of metal, although the individual water and ROS production rates are very close to the level of error for most metals. For G65Y Cu_BMb with native heme b, verdoheme production in the presence of copper slows the apparent

rate, as described in Chapter 2. In G65Y Cu_BMb(o), the apparent oxygen consumption rate is faster in the presence of copper. The observed rates are 5.4 µM/s without copper and with 5.9 µM/s respectively which is beyond error. The percentages of water produced is ~65% in both cases. This would suggest that copper enhances the rate slightly but not the product formed. As G65Y Cu_BMb(o) produces more ROS in general, this copper-enhanced rate with no effect on product is a step in the right direction; but excitement is tempered by the general effect of heme o mimic in G65Y Cu_BMb increasing ROS.

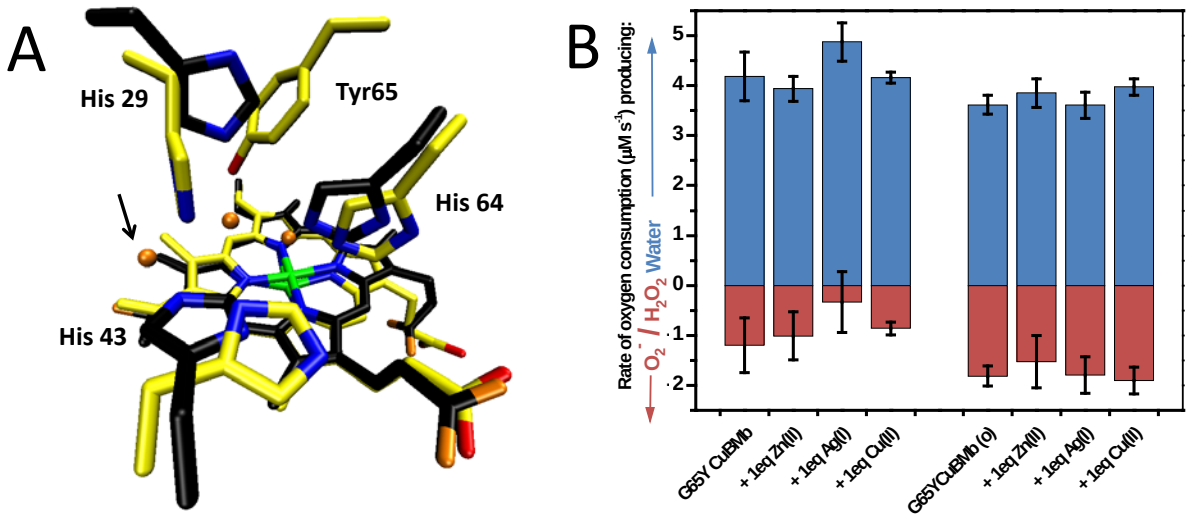

Figure 3.5 - (A) Overlay of G65Y Cu_BMb model and V68T Cu_BMb(o) structure (B) Rates of water (blue) and ROS production in with and without heme o mimic. Arrow indicates addition water observed.

3.3.5 Rationale and Design of F33Y Cu_BMb Channel Mutant

In CcOs the K-channel ends near the location of the His-Tyr crosslink. The hydroxyl group of the hydroxyfarnesyl group of o and a type hemes is suggested to be hydrogen bonded to the water in the K-channel[4,23]. With this in mind a design for a simple hydrophilic channel that ended near the location of both the hydroxyethyl group of heme o mimic incorporated Cu_BMb variants based on the V68T Cu_BMb(o) structure, and Tyr33 in F33Y Cu_BMb was attempted. The

shortest route to bulk solvent would be by making a hole in the heme pocket wall formed by BC loop region and the G-helix. The closest residue to the location of the hydroxyl of the heme o mimic that points into the heme pocket is Thr39. Because this residue is already suitable for hydrogen bonding, all that may be needed are mutations to make space for water to enter into the back of heme pocket. Mutations introducing potential hydrogen bonding partners to stabilize water in the proposed channel were introduced, namely F106S and H36S. F106S was selected as alternative to mutations in literature that are known to destabilize myoglobin[24], specifically Y103X, while still making space in the desired region of the protein. H36S was selected becuase it is surface exposed and might potentially interact with Glu38, which could block our channel. Simulations were performed to test this design before attempting to express the designed protein. To simulate potential extra water in the heme pocket of myoglobin as a result of the new channel, the above crystal structure of V68T Cu_BMb with heme o mimic was used because it has three crystallographic waters compared to the two of F33Y Cu_BMb. To this starting structure the T68V/F33Y mutations were made in addition to the hydrophilic channel mutations. The resulting molecular dynamics equilibrated model can be seen in Figure 3.6. Interestingly the serine hydroxyl groups appear to hydrogen bonding to a water from the bulk solvent occupying part of the space generated by the F106S mutation. This simulation also suggested that methyl group of Thr39 might be blocking access of water to the heme pocket. Therefore two mutants of F33Y Cu_BMb were made, H36S/F106S/F33Y Cu_BMb and H36S/T39S/F106S Cu_BMb (referred to as 2S_F33Y Cu_BMb 3S_F33Y Cu_BMb respectively).

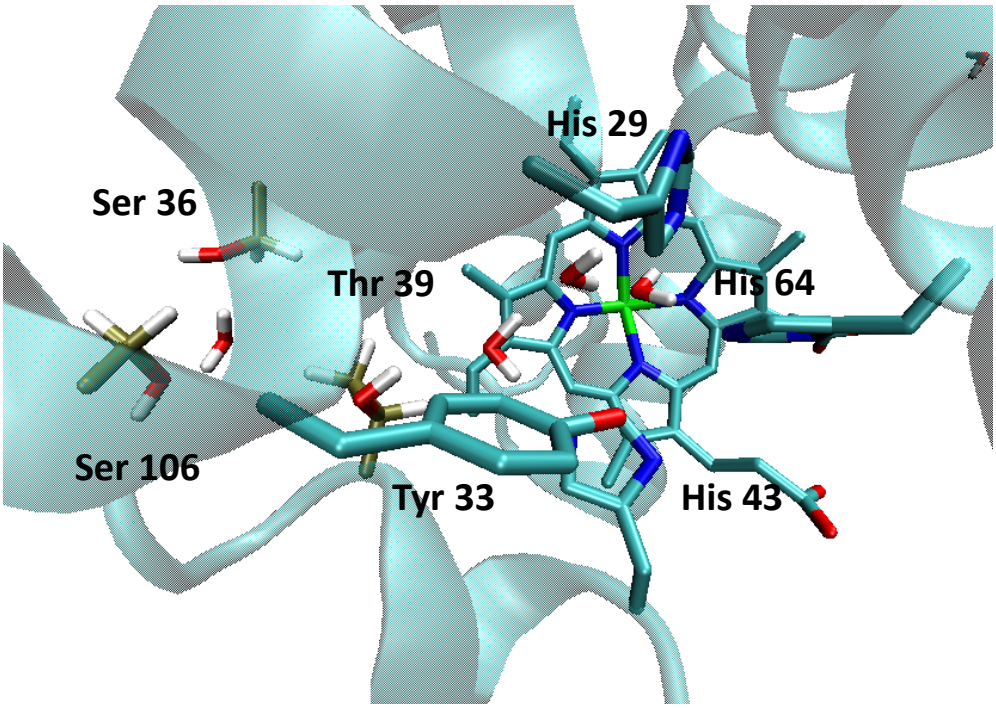

Figure 3.6 Molecular Dynamics simulation results for 2S_F33Y Cu_BMb. Proposed channel residues are shown in Tan.

3.3.6 Effect of hydrophilic channel mutations on F33Y Cu_BMb

Both 2S_F33Y Cu_BMb and 3S_F33Y Cu_BMb mutants were able to reduce oxygen using TMPD and ascorbate similar to F33Y Cu_BMb. The observed oxygen consumption rates of these new mutants were approximately twice that of F33Y Cu_BMb, with approximately the same ratio of water to ROS produced (see Figure 3.7A). The 2S_F33Y Cu_BMb mutant was found to be more stable than 3S_F33Y Cu_BMb and was obtained at a higher yield, and was therefore used for more thorough characterization of the channel. The addition of metals to 2S_F33Y Cu_BMb had a similar effect to what was observed in F33Y Cu_BMb (See figure 3.7B). This would suggest that the introduction of mutations designed to allow bulk solvent better access for the purpose of enhancing the existing hydrogen bonding network was a success.

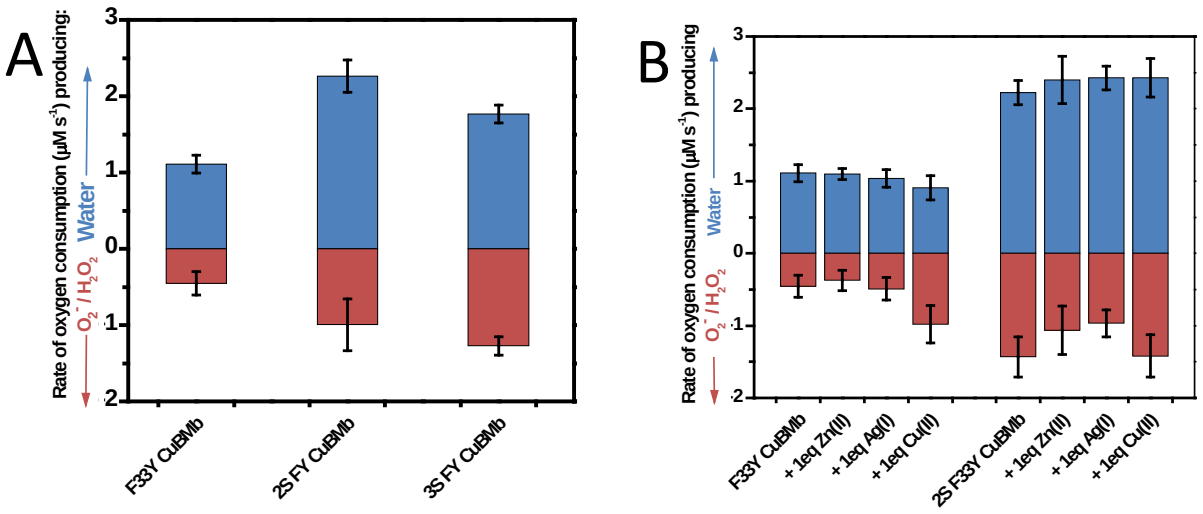

Figure 3.7 – Rates of water and ROS production for (A) F33Y Cu_BMb and the 2S and 3S variants and (B) F33Y Cu_BMb and 2S_F33Y Cu_BMb in the presence and absence of 1eq Zn, Ag, and Cu.

3.3.7 Rationale and Design of G65Y Cu_BMb Channel Mutants

In designing a proton channel mutant for G65Y Cu_BMb to deliver protons near the introduced tyrosine, we chose not to immediately use the above mutations designed for F33Y CuBMb, because Tyr65 is located on the opposite side of the heme pocket from residue 33. We also decided against simply making a hole in the nearest wall, as it was likely that the exposed heme edge would become larger or that the interaction between the porphryin and hydrophobic residues would be disrupted by mutation to hydrophilic residues. These effects could make interpretation difficult. We therefore decided to engineer a channel into the hydrophobic core of myoglobin that would emerge into the heme pocket near Tyr65. This channel design consisted of 3 mutations to G65Y Cu_BMb. Val 21, Val68, and Leu69 were mutated to serine residues. Computer simulation of this mutant was performed using the G65Y Cu_BMb simulation results as a starting point and then introducing the 3 mutations (See Figure 3.8). Val21 is surface exposed and should pose minimal problems. Val68 has been mutated to both Thr and Ser in the literature and myoglobin was able to fold. Leu69 is the residue most likely to pose a problem to folding as

it is in the myoglobin core and is surrounded by hydrophobic residues. However, the space generated by this mutation could allow for a water to be trapped and hopefully stabilized by hydrogen bonds to the introduced serines or the backbones of nearby residues. Also, as further investigation of the effect of the H36S/F106S mutations introduced into F33Y Cu_BMb. These mutations were introduced into G65Y Cu_BMb for comparison (referred to as 2S_G65Y Cu_BMb).

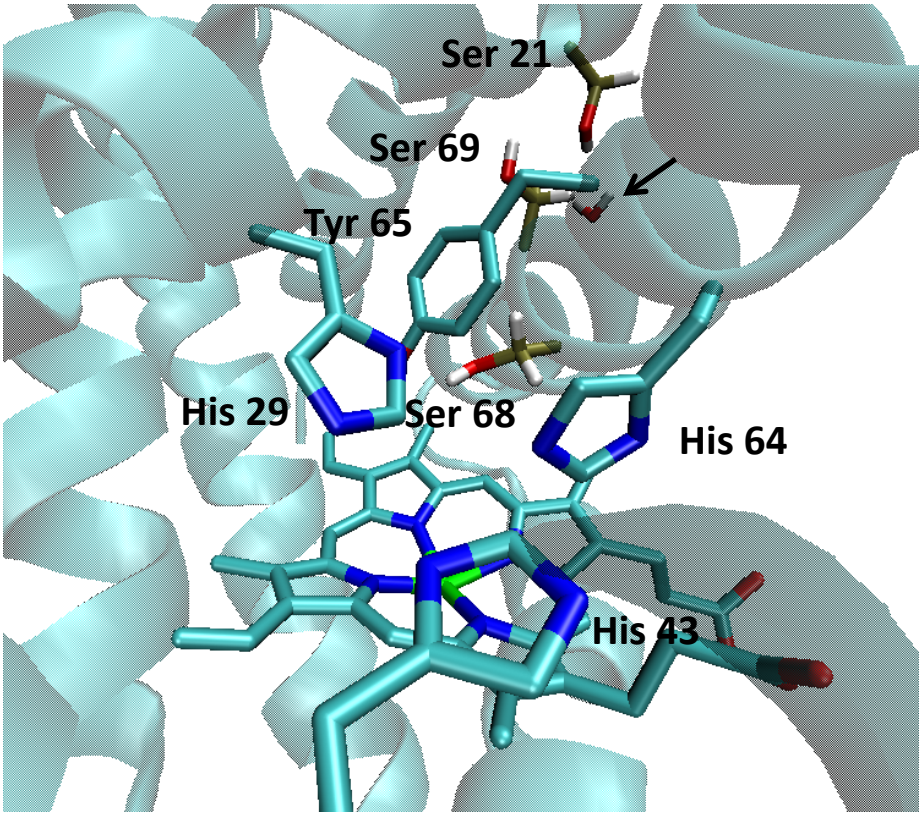

Figure 3.8 Molecular Dynamics simulation results for PCM_G65Y Cu_BMb. Proposed channel residues are shown in Tan.

3.3.8 Effect of Channel Mutations on G65Y Cu_BMb

The effect of the introduction of the three serine residues designed to create PCM_G65Y Cu_BMb on activity is still yet to be determined, as the protein as isolated had low yield due to protein instability. The portion that was recovered was folded into a bis-His state that would not

readily reduce with TMPD and ascorbate. However, heme extraction and refolding of this mutant may yield more of a metMb-like population, as was observed for G65Y Cu_BMb with heme o mimic, and potentially avoid this issue. These difficulties lead to characterization of 2S_G65Y Cu_BMb to see the general effect of these mutations.

The results of the introducing the F106/H36S mutations into G65Y Cu_BMb (2S_G65Y Cu_BMb) is different than that of 2S_F33Y Cu_BMb. This is not completely unexpected becuase the mutations are on the other side of the heme pocket from Tyr65. Instead of increasing the rate of oxygen consumption as in 2S_F33Y Cu_BMb, 2S_G65Y Cu_BMb actually has an approximately 30% slower rate, compared to G65Y Cu_BMb. While initially this would seem like a setback, reactions in the presence of catalase and SOD had nearly no effect on the oxygen consumption rate observed. This would suggest that the product formed in 2S_G65Y Cu_BMb is exclusively water, within error of our methodology (see Figure 3.9). The rates of oxygen consumption toward water are comparable for both G65Y Cu_BMb and 2S_G65Y Cu_BMb. This may be because the hydrogen bonding network in 2S_G65Y Cu_BMb could be hydrogen bonding from multiple sides of the bound oxygen or the introduced hydrogen bonding could adjusting the pKa of His43 allow it to transfer protons more effectively. Either of these could alter the rate of proton donation to the bound oxygen and allowing for a more rapid transfer to the bound oxygen. The introduction of redox inactive metals into the site had little effect on the oxygen consumption rate but the apparent level of ROS production is higher. In the case of copper the observed rate is slower without catalase and therefore our assumptions in calculation of water and ROS fail (see red bar in the water direction in Figure 3.8) this would suggest that ROS are being consumed which is not the case. This failure is likely the result of copper-induced

verdoheme formation. As rates of verdoheme formation have not been determined for this mutant, G65Y's rates were used as an estimate to obtain an estimate of water to ROS ratios.

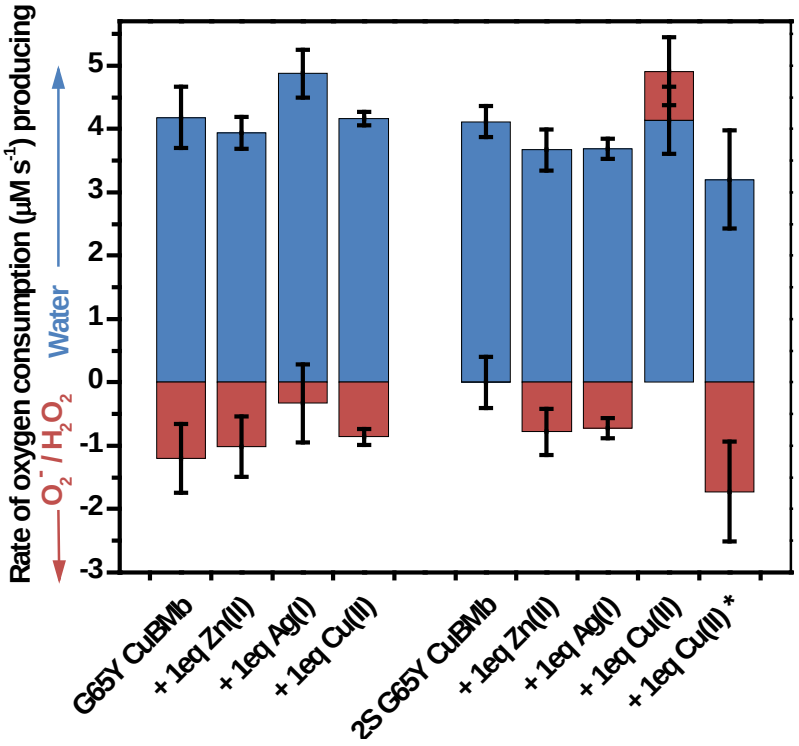

Figure 3.9 – Water (blue) and ROS (red) production rates for G65Y Cu_BMb and 2S_G65Y Cu_BMb in the absence and presence of 1eq of Zn, Ag, and Cu. The red bar in the water side of graph suggesting ROS consumption is breakdown of our assumptions. Asterisk indicates correction using G65Y Cu_BMb verdoheme rates

3.4 Summary and Conclusions

The effects of trying to alter the hydrogen bonding network in Cu_BMb and its tyrosine variants shown to perform HCO like chemistry are interesting. The incorporation of heme o mimic into the Cu_BMb, F33Y Cu_BMb and G65Y Cu_BMb had a different result in each mutant. For Cu_BMb the overall rate increased by 50% without metal and the ratio of products was essentially unchanged. With metal the percent ROS increased slightly. For F33Y Cu_BMb there was essentially no change, which seems to be consistent with the hypothesis that a water may be stabilized by Tyr33 in the oxygen bound state which would likely not allow heme o mimic enough space to have another water molecule. For G65Y Cu_BMb the inclusion of the cofactor

caused a small general increase in the percent ROS formed. However, copper-loaded G65Y Cu_BMb(o) kept the same product ratio and slightly increased overall rate. This is in contrast to G65Y Cu_BMb with native heme b which is slowed by Cu addition, likely from verdoheme formation. The addition of hydrophilic channels with the goal of increasing the access of protons into heme pocket has been shown to have two different effects; the first effect is a rate increase if the channel added is from the same side of the heme pocket as the tyrosine as in 2S_F33Y Cu_BMb, but little change in the ratio of products formed. This effect might an indication of better flow of protons into the same hydrogen bonding network. The other observed effect is potentially both more important and more interesting. This second effect occurs when the channel introduced is on the opposite side of the pocket from the introduced tyrosine residue as in 2S_G65Y Cu_BMb. The rate of the oxygen consumption decreases but the products formed have a higher percentage of water, in the case of metal free 2S_G65Y Cu_BMb nearly 100% conversion to water from oxygen. This cleaner catalyst should be more robust in terms of total turnovers, as the production of ROS is believed to be the downfall of G65Y Cu_BMb causing a significant slowing after about 850 turnovers. Design of a proton channel on the same side as the introduce tyrosine G65Y Cu_BMb was performed, in the PCM_G65Y-CuBMb mutant, but the resulting protein was difficult to purify and characterize. The combination of the heme o mimic and 2S hydrophilic channel in G65Y Cu_BMb has the potential be a very interesting protein. The resulting 2S_G65Y Cu_BMb(o) could potentially be very clean and not be degraded as quickly in the presence of copper. The heme o hydroxyl would be well positioned to interact with both the hydrophilic channel and waters in the heme pocket, potentially improving the effect of the channel further.

3.5 References

1 Ortiz de Montellano, P. R. Heme Oxygenase Mechanism: Evidence for an Electrophilic, Ferric Peroxide Species. *Acc. Chem. Res.* 31, 543 (1998).

2 Ortiz de Montellano, P. R. & Wilks, A. Heme oxygenase structure and mechanism. *Adv.Inorg.Chem.* 51, 359 (2001).

3 Kaila, V. R. I., Verkhovsky, M. I. & Wikstrom, M. Proton-Coupled Electron Transfer in Cytochrome Oxidase. *Chem. Rev.* 110, 7062 (2010).

4 Blomberg, M. R. A., Siegbahn, P. E. M. & Wikstroem, M. Metal-Bridging Mechanism for O-O Bond Cleavage in Cytochrome c Oxidase. *Inorg. Chem.* 42, 5231 (2003).

5 Fujii, H., Zhang, X., Tomita, T., Ikeda-Saito, M. & Yoshida, T. A role for highly conserved carboxylate, aspartate-140, in oxygen activation and heme degradation by heme oxygenase-1. *J. Am. Chem. Soc.* 123, 6475 (2001).

6 Babcock, G. T. How oxygen is activated and reduced in respiration. *Proc. Natl. Acad. Sci. U.S.A.* 96, 12971 (1999).

7 Babcock, G. T. & Wikstrom, M. Oxygen Activation and the Conservation Of Energy In Cell Respiration. *Nature* 356, 301 (1992).

8 Namslauer, A. & Brzezinski, P. Structural elements involved in electron-coupled proton transfer in cytochrome c oxidase. *FEBS Lett.* 567, 103 (2004).

9 Zhu, J., Han, H., Pawate, A. & Gennis, R. B. Decoupling Mutations in the D-Channel of the aa3-Type Cytochrome c Oxidase from Rhodobacter sphaeroides Suggest That a Continuous Hydrogen-Bonded Chain of Waters Is Essential for Proton Pumping. *Biochemistry* 49, 4476 (2010).

10 Pawate, A. S. *et al.* A Mutation in Subunit I of Cytochrome Oxidase from Rhodobacter sphaeroides Results in an Increase in Steady-State Activity but Completely Eliminates Proton Pumping. *Biochemistry* 41, 13417 (2002).

11 Koepke, J. *et al.* High resolution crystal structure of Paracoccus denitrificans cytochrome c oxidase: New insights into the active site and the proton transfer pathways. *Biochim. Biophys. Acta* 1787, 635 (2009).

12 Buschmann, S. *et al.* The structure of cbb3 cytochrome oxidase provides insights into proton pumping. *Science* 329, 327 (2010).

13 Palaniappan, V. & Bocian, D. F. Acid-induced transformations of myoglobin. Characterization of a new equilibrium heme-pocket intermediate. *Biochemistry* 33, 14264 (1994).

14 Yang, A.-S. & Honig, B. Structural origins of pH and ionic strength effects on protein stability. Acid denaturation of sperm whale apomyoglobin. *J. Mol. Biol.* 237, 602 (1994).

15 Brantley, R. E., Jr., Smerdon, S. J., Wilkinson, A. J., Singleton, E. W. & Olson, J. S. The mechanism of autooxidation of myoglobin. *J. Biol. Chem.* 268, 6995 (1993).

16 Wang, N., Zhao, X. & Lu, Y. Role of Heme Types in Heme-Copper Oxidases: Effects of Replacing a Heme b with a Heme o Mimic in an Engineered Heme-Copper Center in Myoglobin. *J. Am. Chem. Soc.* 127, 16541 (2005).

17 Wang, N. *Exploring the Roles of Heme Type and Histidine-Tyrosine Cross-Link in Heme-Copper Oxidases Using a Myoglobin Model* Ph. D. thesis, University of Illinois, (2007).

18 Sigman, J. A., Kim, H. K., Zhao, X., Carey, J. R. & Lu, Y. The role of copper and protons in heme-copper oxidases: Kinetic study of an engineered heme-copper center in myoglobin. *Proc. Natl. Acad. Sci. U.S.A.* 100, 3629 (2003).

19 Sigman, J. A., Kwok, B. C. & Lu, Y. From Myoglobin to Heme-Copper Oxidase: Design and Engineering of a CuB Center into Sperm Whale Myoglobin. *J. Am. Chem. Soc.* 122, 8192 (2000).

20 Yeung, N. *et al.* Rational design of a structural and functional nitric oxide reductase. *Nature* 462, 1079 (2009).

21 Humphrey, W., Dalke, A. & Schulten, K. VMD: Visual molecular dynamics. *J. Mol. Graphics* 14, 33 (1996).

22 Phillips, J. C. *et al.* Scalable molecular dynamics with NAMD. *J. Comput. Chem.* 26, 1781 (2005).

23 Uchida, T., Mogi, T., Nakamura, H. & Kitagawa, T. Role of Tyr-288 at the Dioxygen Reduction Site of Cytochrome bo Studied by Stable Isotope Labeling and Resonance Raman Spectroscopy. *J. Biol. Chem.* 279, 53613 (2004).

24 Rao, S. I., Wilks, A. & Ortiz de Montellano, P. R. The Roles of His-64, Tyr-103, Tyr-146, and Tyr-151 in the Epoxidation of Styrene and Beta-Methylstyrene by Recombinant Sperm Whale Myoglobin. *J. Biol. Chem.* 268, 803 (1993).

CHAPTER 4

PROGRESS TOWARD HIS-TYR CROSSLINK FORMATION IN CU_BMB MUTANTS WITH TYROSINE

4.1 Introduction

The purpose of the work described herein is to improve the Cu_BMb[1,2] model of heme copper oxidases (HCOs) by introducing a His-Tyr crosslink and then comparing the activity of uncrosslinked tyrosine-containing Cu_BMb with that of the crosslinked version, in a fashion similar to the work described in the preceding chapters. Such a study would allow for a direct comparison of the crosslinked His-Tyr with the same His and Tyr uncrosslinked in the same protein environment. Such work has yet to be reported in HCOs.

4.1.1 Brief overview of crosslinked posttranslational modifications

Posttranslational modifications such as phosphorylation, glycosylation, and ubiquination are common is living systems[3]. These modifications can extend the functionality of proteins beyond that of the 20 amino acids or hold two sections of a protein in close proximity by covalent linkage[4]. Modifications can range in size from a linkage of 2 amino acids, e.g. disulfide bonds, to addition of sugars, to the attachment of whole proteins such as ubiquination[3]. The function of these modifications can also vary: Some are structural in nature and lock the protein into a given conformation, others are involved in signaling; for example ubiquination is well known to signal for degradation. Many enzymes in the cell either modify other enzymes or are modified themselves by other enzymes; e.g. the kinases involved in signaling pathways. Some amino acid linkages are proposed to be mediated by nearby metal cofactors, such as the recently reported Phe-Val crosslink in protein [4]. This result in particular is interesting because it is

relatively difficult to form radicals at both of the involved amino acid side chains. The novel His-Tyr crosslink of HCOs is also thought to result from the early turnovers at the heme-Cu_B site[5].

4.1.2 Summary of His-Tyr Crosslink features and proposed roles

The His-Tyr crosslink is a unique structural feature found in all HCOs. This structural feature was first identified using X-ray crystallography[6,7] and was confirmed via Mass Spectrometry and Edman Degradation[5]. Mutation of the crosslinked Tyr residue to Phe[8] causes loss of copper in the Cu_B site and abolishes enzyme function. Unfortunately, HCOs have not been isolated lacking the His-Tyr crosslink unless mutation of the crosslinked residues had been performed. This makes study of function in the native system difficult, as changes needed to remove the crosslink change more than the crosslink itself. Small molecule analogs of the crosslinked His-Tyr amino acids have been made to study the effects of this covalent bond on the properties compared to His and Tyr[9-11]. Similar analogs have been incorporated into synthetic models of HCOs[12-14]. The proposed function of the crosslink ranges from merely structural[15] to the donation of a proton and/or an electron to the reduction of oxygen to water[16]. The pKa of the hydroxyl of the crosslinked His-Tyr was ~3 pKa units below that of Tyr. This would make the pKa of the His-Tyr linkage ~7. Under physiological conditions such a residue should be able to donate a proton and therefore could be expected to be a source of protons for the reduction of oxygen to water.

4.1.3 Rationale for inclusion in Cu_BMb system and unique benefits

As part of the process of constructing a functional bottom-up model of CcO from myoglobin an effort has been made to incorporate this unique and important feature. How the His-Tyr crosslink is formed in HCOs is unknown but it is believed to be formed during the early

turnovers of the enzyme[5]. Therefore, our experiments, if successful, may provide new insight into the mechanism of formation of this feature in the native enzyme and what relative positioning of the two components relative to each other may be required. The experimental design involves reaction of the Tyr-containing Cu_BMb mutant with either oxidant (such as H_2O_2), copper alone, reductant alone, or copper with reductant. Ideally, we would prefer formation via reductant or reductant with copper for a more physiologically relevant result. The sections below summarize the progress made toward incorporating a His-Tyr crosslink into the CuBMb system and note observed side reactions.

4.2 Materials and methods

4.2.1 Protein purification

All tyrosine containing mutants and variants described in this chapter are purified from inclusion bodies using a previously described protocol.[17] Typical yields from the inclusion body protocol are ~20 mg/L. I28Y and F33Y Cu_BMbs and variants purify in the metMb form and the purified protein is evaluated for quality by taking the ratio of A_{408}/A_{280} and if the R/Z value is 4 or greater the protein is consider usable. For G65Y Cu_BMb the ratio of A_{410}/A_{280} is used and the protein with a value of ~3.5 is used. The lower cutoff is a result of a population of bis-His ligated protein that is present in this mutant; as bis-His has a lower extinction coefficient than the met form. As discussed in Chapter 2 this purification protocol results in protein that does not contain metal in the Cu_BMb site based on Inductively Coupled Plasma-Mass Spectrometry (ICP-MS) results.

4.2.2 Crosslinking experiments

Unless otherwise noted all buffer solutions were treated with Chelex 100 beads (Sigma) to remove divalent metal ions.

To check for crosslinking under reaction conditions 1 mL of 50 µM protein was reacted in a 1.5 mL eppendorf tube with stirring and with the appropriate reagents for 30 minutes at room temperature. Reactions at pH 8 and pH 6 used 20 mM tris-HCl and 100 mM potassium phosphate , respectively. In reactions with catalase, enzyme was added in levels consistent with work by Sigman *et al.*[2] Reactions were stopped by running the reaction mixture down a PD-10 column equilibrated with either water or 20 mM Tris-HCl, pH 8. Colored eluent was collected.

Two different methods were used to remove the heme cofactor before digestion with the appropriate protease. The first method used was analytical High Pressure Liquid Chromatography (HPLC) using a C18 column after concentrating the reaction products to a volume of ~100 µL. This instrument used was a Waters Delta 600 with Waters 600 controller and Waters 2487 Dual λ detector. The reaction was injected onto a pre-equilibrated Vydac 218TP54 C18 column. The column was equilibrated using 84% solvent A and 16% solvent B where solvent A is 0.05% TFA in distilled H_2O (dH_2O) and solvent B is60 % acetonitrile (ACN), 0.05 % trifluoroacetic acid (TFA) in dH_2O. The percentage of Buffer B was ramped up to 83% over the first 20 minutes then ramped up to 100% over the next 2 minutes, and then held for eight minutes to clean the column (30 minutes overall). Over the next 2 minutes buffer B was lowered to 16% (84% A) and then held for the remainder of the run (13 minutes) to equilibrate the column. The whole procedure lasted 45 min per sample. Absorbances at A_{280} and A_{380} were used to monitor protein and free heme respectively. Any heme signal associated with the protein was presumed to be covalently attached. The protein containing fractions were pooled, flash

frozen, and lyophilized overnight. The lyophilized protein was resuspended in the buffer needed for the protease used.

The second method used was extraction of the heme using 2-butanone. For this method the protein was exchanged in to water. The protein was then unfolded using 1% v/v of 2 M HCl and to this an equal volume of ice cold water saturated with 2-butanone was added and then the mixture was mixed by inversion. The butanone layer (top) should be red from free heme. The bottom layer should be colorless, if not additional HCl was added and mixed again. If still colored then there is likely covalently attached heme. In reaction conditions known to form verdoheme, a greenish color was observed. The top layer was removed by Pasteur pipet and replaced with fresh 2-butanone until top layer was colorless. To remove the 2-butanone dialysis against water was performed until 2 exchanges after the 2-butanone was no longer smelt, typically 5 to 6 dialysis steps. The final exchange was against the buffer used for protease digest.

4.2.3 Digestion of proteins with proteases after removal of the heme

The heme-free protein was digested by either 20 µL of 1 µg/µL Salt Free α-Chymotrypsin (Sigma) in 100 mM Tris-HCl, pH 7.8 for I28Y Cu_BMb or by 20 µL of 1 µg/µL Proteomics Grade Trypsin (Sigma) in 1 mM HCl added to protein in 230 µL of 100 mM ammonium bicarbonate, pH 8.5 for all others. Crude digest mixtures were then either analyzed using MALDI-MS or injected onto an HPLC column for further purification.

4.2.4 Isolation of crosslinked peptide by HPLC

After digestion of protein the resulting crude digestion mixture was purified by HPLC to isolate the potentially crosslinked fragment. Crude digestion mixture in the amount of 100 µL was injected onto a pre-equilibrated Vydac 218TP54 C18 column. The column was equilibrated

90% solvent A and 10% solvent B where solvent A was 0.05% TFA in dH_2O and solvent B was 100% ACN, 0.05% TFA in dH_2O. The method was run at 1 mL/min and starting conditions of 10% B were held for 10 minutes. The percentage of Buffer B was ramped up to 60% over the first 120 minutes and then ramped up to 100% to wash the column for 30 minutes, and then re-equilibrated over 40 minutes. Absorbances at A_{225} and A_{315} were monitored (A_{225} for peptide backbone and A_{315} for possible crosslink specific signal) The resulting peaks were then run on MALDI-MS (Matrix Assisted Laser Desorption Ionization Mass Spectometery) to determine the mass of the peptide(s) in the peak.

4.2.5 UV-Vis characterization of isolated peptide

Specrta were collected using a Cary 3E spectrophotometer (Varian). The isolated potentially crosslinked fragment was dissolved in modified universal buffer (50 mM sodium acetate, 40 mM MES, 40 mM MOPS, 40 mM Tris, 40 mM CAPS, 100 mM potassium phosphate). The 100 mM sodium nitrate normally used was replaced with 100 mM potassium chloride to avoid absorbance from the nitrate interfering with the monitoring of changes in the UV region. To adjust the pH 2 M HCl was added. The pH values listed were measured by adding a given amount of HCl to buffer before adding the peptide fragment. The same amount was added to buffer containing either isolated potentially crosslinked peptide or a control peptide ordered with the appropriate sequence based on MALDI-MS results.

4.2.6 MALDI-MS

MALDI-MS , using a Voyager DE, as performed on either the crude digestion product or fractions collected after HPLC using a C18 column. The matrix used was α-cyano-4-hydroxycinnamic acid. The accelerating voltage was 20000 V, the mass range was 400 – 4000

Da, and the low mass gate was set to 400 Da. Laser intensity varied from 1800 – 2200 depending on sample. An insulin/angiotensin mixture was used as a standard for calibration. Crude digest samples could typically be seen with usable intensity with a 1:10 ratio of sample-to-matrix solution. HPLC purified peptide samples could be seen typically with a 1:5 dilution. All expected values were based on the use of the Protein Prospector tool (prospector.ucsf.edu).

4.2.7 LC-ESI-MS/MS

Crude digest samples were also submitted for LC-ESI-MS/MS (Liquid Chromatography – Electrospray tandem Mass Spectometry and the liquid chromatography step was performed using the same protocol and column used for the HPLC purification for consistent peak elution times for comparison purposes. The LC-MS/MS samples were run by the Mass Spectrometry facility at the University of Illinois at Urbana-Champaign.

4.3 Results and Discussion

Please note that all observed crosslinking masses obtained using MALDI-MS are hydrogen peroxide-dependent unless stated.

4.3.1 I28Y Cu_BMb

Considering the positioning of the three His residues that form the Cu_B site in Cu_BMb, covalent attachment between Tyr28 and His29 seems the most reasonable based on 3-dimensional location (see Figure 4.1). For I28Y, Cu_BMb chymotrypsin protease was used. Chymotrypsin cleaves primarily after Trp, Tyr, Phe, and Leu (with lower frequency) residues. Based on the sequence of I28Y Cu_BMb this should produce a His containing peptide with a mass of 686 Da and a Tyr containing peptide of mass 1460 Da and crosslinking of the two would give

a mass of 2142 Da. See Figure 4.2 for the I28Y sequence with potential cleavage points noted by arrows and Table 4.1 for a list of expected and observed masses by MALDI-MS.

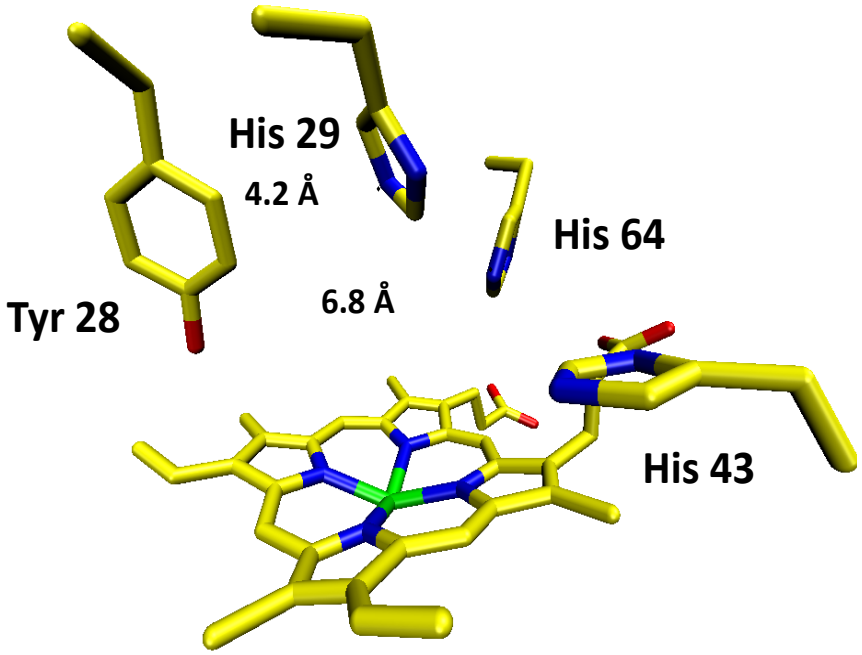

Figure 4. 1 Molecular dynamics simulation results for I28Y Cu_BMb.

I28Y Cu_BMb did not display a mass corresponding to the crosslinked peptides of interest. This result is not unexpected as residues to be crosslinked are adjacent residues in an alpha helix. The distance between the His nitrogen and the nearest Tyr carbon that would give the appropriate crosslink are 4.2 angstroms based on computer modeling results. However, there is a peak with a mass that is 4 Da less than the expected crosslinking mass and that is hydrogen peroxide dependent (See Table 4.1).

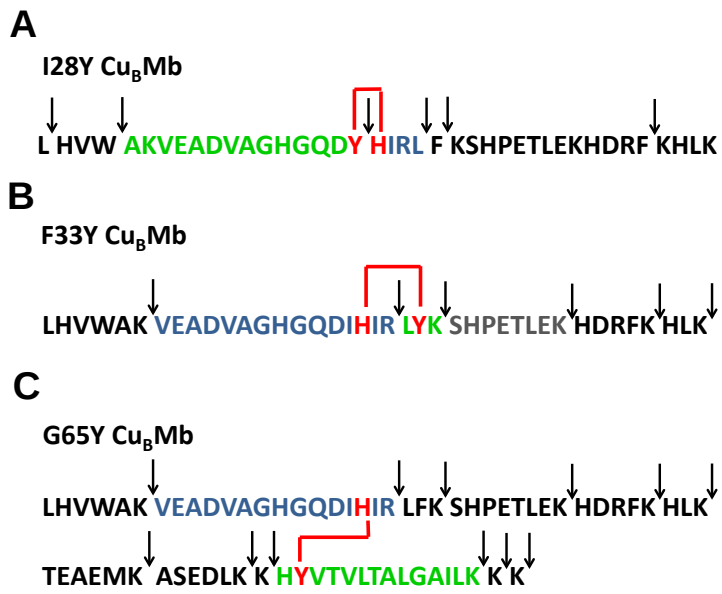

Figure 4.2 Potential cleavage sites for A) chymotryptic digest of I28Y Cu_BMb, tryptic digest of B) F33Y Cu_BMb, and C) G65Y Cu_BMb. Intended His and Tyr for crosslinking are colored red. The smallest possible Tyr containing peptide is shown in green. For F33Y Cu_BMb grey sequence is Tyr containing peptide if Lys34 cleavage is missed The smallest possible His containing peptide is shown in blue.

4.3.2 F33Y Cu_BMb

The protease used for F33Y Cu_BMb was trypsin. Trypsin cleaves after Arg and Lys residues. As seen in Figure 4.2 the F33Y Sequence has a cleavage site in between the His and Tyr and shortly after the Tyr. Based on the sequence of F33Y Cu_BMb this should produce a His containing peptide with a mass of 1617 Da, Tyr containing peptides of masses 423 Da and 1345 Da (depending on cleavage after Lys 34), and crosslinking of the two peptides would give masses of 2040 Da and 2961 Da. See Figure 4.2 for F33Y Cu_BMb sequence with potential cleavage points noted by arrows and Table 4.1 for other masses of interest.

Table 4.1 Expected and observed digested protein fragments for His 29 Tyr 33 crosslinking

Protein	Residues	Sequence	Expected Mass	Observed Mass
His containing peptide				
I28Y Cu_BMb	29 - 33	**H**IRLF	685	686
All non-I28Y Cu_BMb	17 - 31	VEADVAGHGQDI**H**IR	1617.7	1618
Tyr containing peptide				
I28Y Cu_BMb	15 - 28	AKVEADVAGHGQD**Y**	1460	1459
F33Y Cu_BMb	32 - 42	L**Y**KSHPETLEK	1345.5	N. A.
L32V/F33Y Cu_BMb	32 - 42	V**Y**KSHPETLEK	1331.5	N. A
L32V/F33Y/T39A	32 - 42	V**Y**KSHPEALEK	1301.5	N. A.
L32V/F33Y/L40A	32 - 42	V**Y**KSHPETAEK	1289.5	N. A.
G65Y Cu_BMb	64 - 78	H**Y**VTVLGAILK	1499.8	1500
Crosslinked peptide				
I28Y Cu_BMb	15 - 28 XL	AKVEADVAGHGQD**Y + H**IRLF	2142	2138
F33Y Cu_BMb	17- 42 XL	VEADVAGHGQDI**H**IR + L**Y**KSHPETLEK	2961.2	2963
L32V/F33Y CuBMb	17- 42 XL	VEADVAGHGQDI**H**IR + V**Y**KSHPETLEK	2947.2	2964
L32V/F33Y/T39A CuBMb	17- 42 XL	VEADVAGHGQDI**H**IR + V**Y**KSHPEALEK	2917.2	2936
L32V/F33Y/L40A	17- 42 XL	VEADVAGHGQDI**H**IR + V**Y**KSHPETAEK	2905.2	2923
G65Y CuBMb	17 - 31 , 64 - 78 XL	VEADVAGHGQDI**H**IR + H**Y**VTVLGAILK	3115.5	N.A.

4.3.2.1 Studying the isolated crosslinked peptide

F33Y Cu_BMb, like I28Y Cu_BMb, forms a new mass upon reaction with hydrogen peroxide. The mass observed by MALDI-MS is 1-2 Da more than calculated which is within error of the MALDI-MS. The mass observed would require amino acids 17-42 to be present in the crosslinked peptide (see Table 4.1). The most plausible interpretation would be that a covalent bond involving Tyr 33 is formed that prevents the cleavage of the peptide backbone after Arg 31 or Lys34. The peptide of interest was isolated by HPLC from a crude trypsin digest mixture. See Figure 4.3 for an overlay of the HPLC traces of the tryptic digests for F33Y Cu_BMb + H_2O_2 and unreacted F33Y Cu_BMb and the corresponding MALDI-MS spectra. In the inset of

Figure 4.3A a small peak in the H_2O_2 reacted sample can be seen; this peak has a mass of 2963 Da when isolated and MALDI-MS is performed (see Figure 4.4).

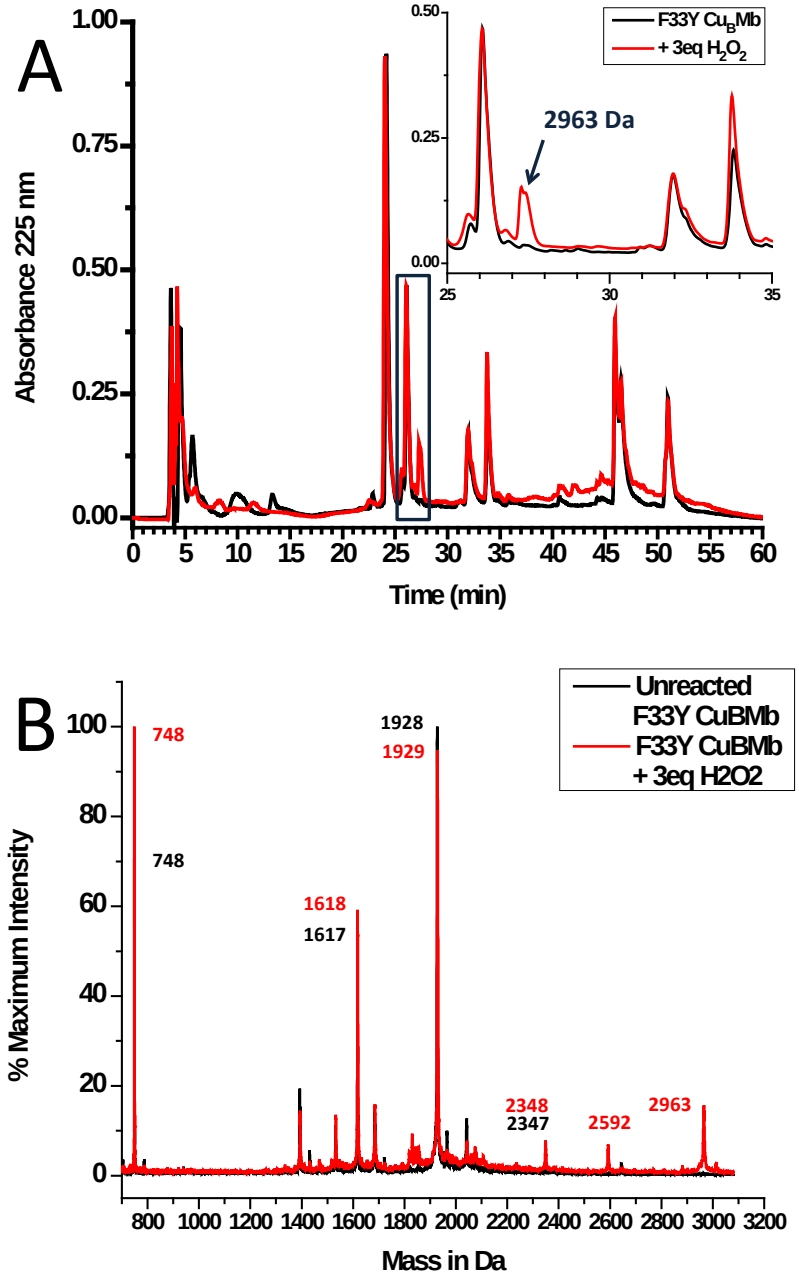

Figure 4.3 Overlay of (A) HPLC traces and (B) MALDI-MS spectra of tryptic digests of F33Y Cu_BMb with (red) and without reaction with H_2O_2 (black). Boxed region indicates region in the inset of (A). Crosslinked peak indicated by arrow with observed mass by MALDI-MS. Masses listed in (B) in are colored with respect to spectrum referred to. Only masses of interest or masses at 100% intensity for both spectra are labelled.

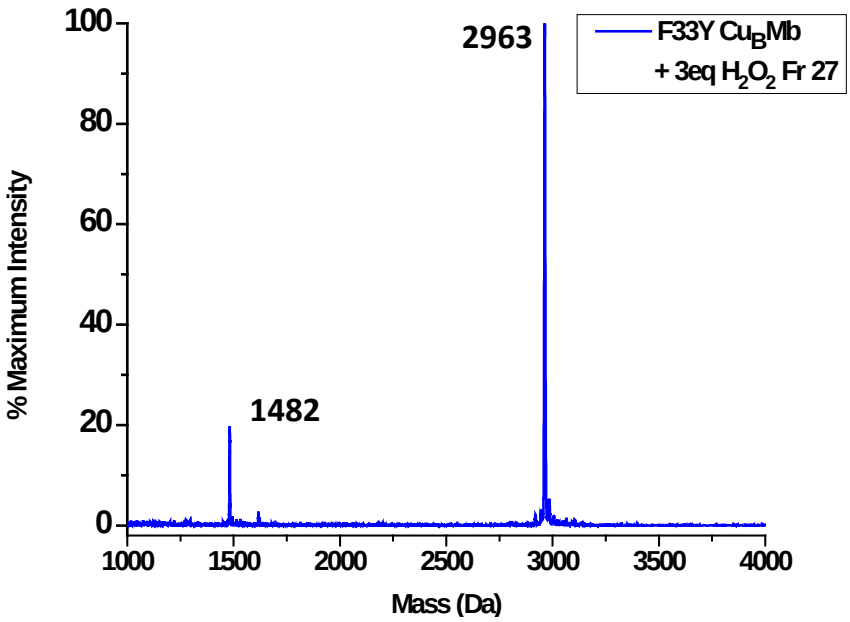

Figure 4. 4 MALDI-MS spectrum of Isolated F33Y "Crosslinked" peptide The peaks observed correspond to the +1 and +2 charged states of the peptide.

Peptide sequencing using Edman Degradation on the isolated peptide resulted in the readout shown in Figure 4.5. This sequence reads as if there are two N-termini similar to observations with unreduced disulfide linked peptides[18]. Based on the MALDI-MS spectrum of the isolated peptide where neither of the masses corresponding to the individual peptides are observed, the only plausible interpretation is a covalent bond between a residue before Lys 34 and a residue after Lys34. The backbone must be cleaved after Lys34 otherwise there would be no "2nd N-terminus". The presence of the residues after Lys34 in the sequence requires the covalent bond otherwise the MALDI-MS results would not show one species. This interpretation suggests that the introduced tyrosine could be forming a covalent bond with a sidechain or backbone atom with a residue between 35 and 42 (Figure 4.5). In addition, there is no evidence for cleavage of the backbone at Arg 21, otherwise the first cycle of Edman Degradation would have indicated V, S, and L indicating a 3rd N-terminus. Therefore there is interference with trypsin cleavage at this site.

Cycle #	AA identified
1	V, S
2	-
3	E , H
4	A , P
5	D , E
6	V , T
7	A , L
8	G , E
9	H , K
10	G , k
11	Q , d
12	D
13	i
14	-
15	-
16	-
17	-
18	-

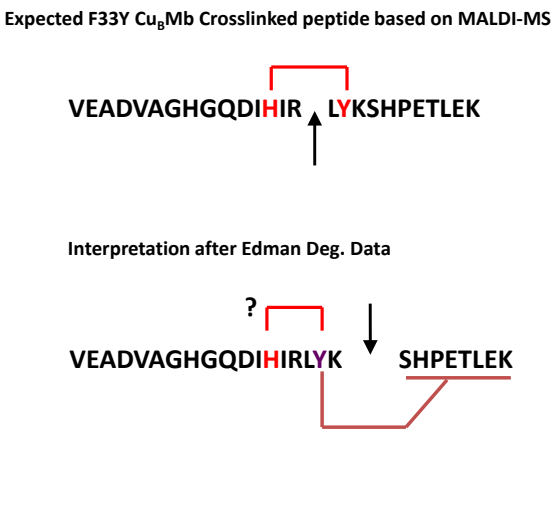

Figure 4.5 Edman degradation results and the effect on the expected peptide. The red line in the table represents the expected missed signal. Arrows represent trypsin cleavage.

UV-Visible data on the isolated peptide showed a pH-dependent shift in the UV-Visible region peak (Figure 4.6) similar to those observed with crosslinked synthetic His-Tyr model compounds[10]. Based on controls using a synthesized peptide with the same primary sequence this shift was not observed. These results taken together suggest that there is indeed a covalent attachment formed by Tyr33 and another location in F33Y however it seems unlikely the attachment is with His29 as intended.

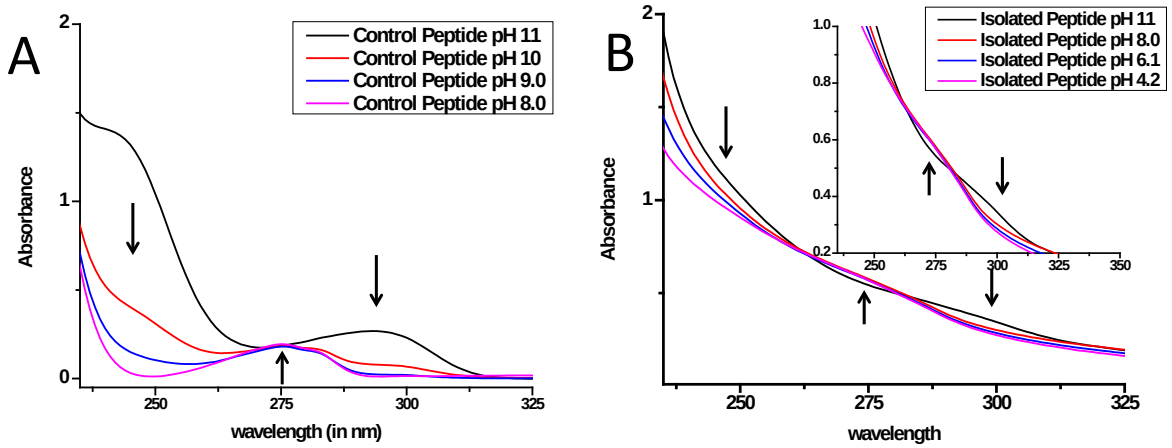

Figure 4.6 UV-Visible changes with (A) control and (B) "crosslinked" peptide with pH change. Note: selected pH values displayed for B for clarity

4.3.2.2 Work done using mutants of F33Y Cu_BMb

Mutations were made to F33Y Cu_BMb for two reasons. The first was to attempt to increase the likelihood of a His-Tyr crosslink as the best conditions using hydrogen peroxide gave a ~15% yield based on peak area of the HPLC traces. The second reason was to discern the location of the covalent bond formation between Tyr33 and the peptide containing residues 35 to 42 as based on Edman degradation UV-Vis studies on the peptide. Mutations aimed at increasing crosslink formation include L32V/F33Y Cu_BMb and Y146F/Y151F/F33Y Cu_BMb. An additional mutant, I30P/F33Y Cu_BMb, was purified from inclusion bodies and characterized. However, the protein was highly unstable and was unable to be reduced using ascorbate and TMPD. The L32V mutation would make Cu_BMb more like HCO in the region including His-Tyr as the conserved sequence is HPXVY in a and b type HCOs[5] and F33Y Cu_BMb in the corresponding sequence is HIRLY. Studies by Wikstrom and coworkers[19] observed that mutation of the corresponding Val to Ile caused a decrease in activity presumably from the more bulky residue affecting the water network in the pocket. Cu_BMb natively has an even more bulky Leu and this added bulk might interfere with crosslinking to His29. The HPLC traces of the two

mutants are highly similar as expected. However, the mass of the observed crosslinked peptide is 16 Da heavier than expected. This extra mass could be either some kind of oxidative damage on the peptide or potentially cleavage after Arg31 as well as after Lys34. However, this situation seems unlikely as the tyrosine would have to form two crosslinks to amino acids on different helicies for this proposed species to be observed. The HPLC traces showed no significant change in the relative yield. The Y146F/Y151F/F33Y mutations were made based on work by Ortiz de Montallano's group[20] showing myoglobin dimerization via a surface Tyr151. This naturally occurring radical pathway would funnel radicals away from Tyr33 crosslinking and lower efficiency. Unfortunately, this also did not improve yield.

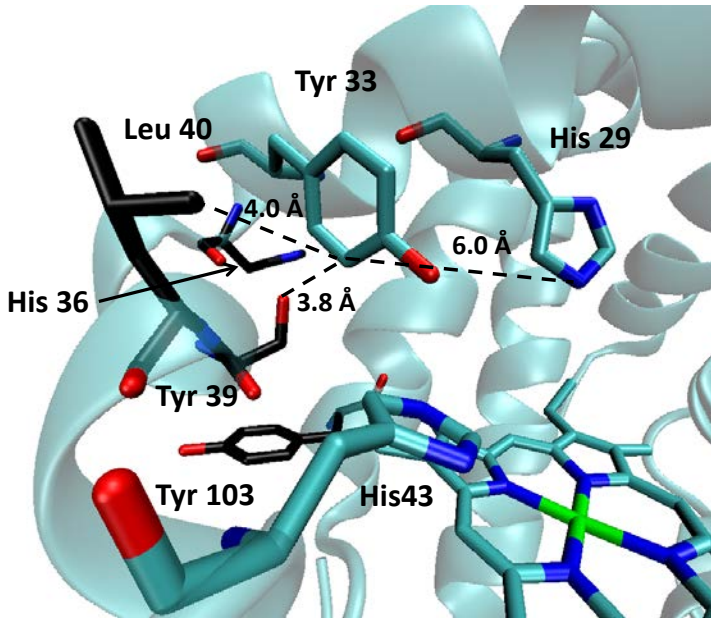

Figure 4.7 Relative positions of potential crosslink partners for Tyr 33

The second reason for introducing mutations was to discern the location of the covalent bond formation between Tyr 33 and the peptide containing residues 35 to 42 as based on Edman degradation UV-Vis studies on the peptide. If the identity of the amino acid Tyr is crosslinked to was known, we could potentially mutate it to a less reactive amino acid to avoid undesired

crosslinking. Point mutations replacing Thr39 and Leu40 with either Ala or Pro were made as these residues were closest to Tyr33 based on the crystal structure of F33Y Cu_BMb (see Figure 4.7). These mutations were made in L32V/F33Y Cu_BMb. For our purposes the elimination of the linkage should theoretically be the same for F33Y Cu_BMb. The intent of the Ala mutations was to disrupt potential crosslinks formed to a sidechain and the proline mutations where intended minimize the reactivity of the backbone amine at these positions. Based on MALDI-MS results, summarized in Table 4.1, these point mutations did not eliminate the crosslinked peptide as the mass in all cases shifted as expected with respect to the L32V/F33Y background. Mutation of His36 to Ala was also performed in order to remove the residue most likely to crosslink based on chemical properties of the sidechains, His36 is the only aromatic side chain aside from Phe 42 which is too far away from Tyr33. In addition to the shifted crosslinked mass, some mutations displayed a new species not previously observed, with a mass corresponding to a linkage between Tyr33 and Tyr103, a known radical site in wild type Mb. Table 4.2 has the calculated masses for Tyr33 and Tyr103 linkage and the observed masses. This result is interesting in that we are indeed forming a radical at Tyr33 if a dityrosine linkage is formed. However, it indicates a low likelihood of success of obtaining a His-Tyr crosslink as desired, as both the crosslink between residues 35 and 42 and the dityrosine crosslink suggest that Tyr33 moves away from His29 instead of toward it.

Table 4.2 Peptide masses for observed alternate crosslinks

Protein	Residues	Sequence	Expected Mass	Observed Mass
Tyr33 containing peptide				
F33Y Cu_BMb	33-35	L**Y**K	423.5	N. A.
L32V/F33Y Cu_BMb	33-35	V**Y**K	407.5	N. A
L32V/F33Y/T39A	33-35	V**Y**K	407.5	N. A.
L32V/F33Y/L40A	33-35	V**Y**K	407.5	N. A.
Y103 Containing Peptide				
All Mutants	103-118	**Y**LEFISEAIIHVLHSR	1928	1927/1928
Potential Y33-Y103 Crosslinked peptides				
F33Y Cu_BMb	33-35, 103-118 XL	**Y**LEFISEAIIHVLHSR + L**Y**K	2334	N/A
L32V/F33Y CuBMb	33-35, 103-118 XL	**Y**LEFISEAIIHVLHSR + V**Y**K	2318	N/A
L32V/F33Y/T39A CuBMb	33-35, 103-118 XL	**Y**LEFISEAIIHVLHSR + V**Y**K	2318	2336
L32V/F33Y/L40A			2318	2336

4.3.3 G65Y Cu_BMb

In an attempt to avoid the undesired covalent attachments observed in F33Y Cu_BMb, G65Y Cu_BMb was developed. The G65Y mutation was selected based on overlays of bovine CcO and Cu_BMb crystal structures. Computer minimization confirmed that the heme iron and Tyr-OH distance is ~5 angstoms. The distance based on computer modeling between Tyr65 and His29 is ~3.3 angstoms. (see Figure 4.8). This distance is closer than the equivalent distances in F33Y Cu_BMb. Reactions with G65Y Cu_BMb were performed in a similar manner to that of F33Y Cu_BMb. The expected His containing fragment is 1617 Da as in F33Y Cu_BMb. The expected Tyr containing fragment is 1500 Da. Therefore the expected crosslink mass is 3115 Da. It should be noted that the 1617 Da peptide mass has been observed reproducibly in F33Y Cu_BMb. For G65Y Cu_BMb the smallest digested fragment is flanked on both sides by at least one additional Lys residue. The crosslinking were to interfere with backbone cleavage by trypsin at the predicted locations, these flanking Lys residues would minimize the increase in the number of unexpected amino acids but providing additional locations to cleave the backbone.

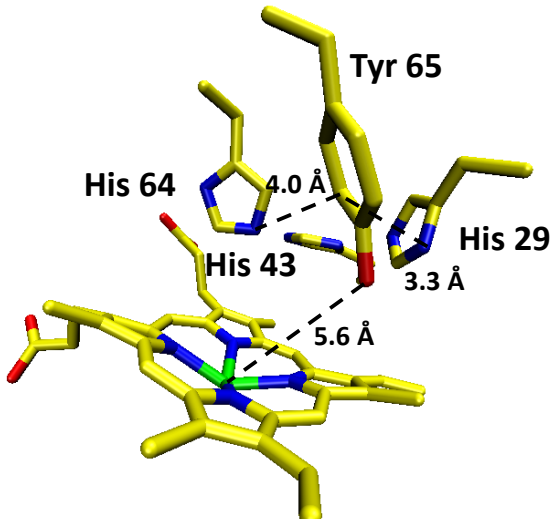

Figure 4.8 Energy minimized model of G65Y Cu_BMb with closest His nitrogen to Tyr carbon distances labeled

4.3.3.1 Observed MALDI-MS and LC-ESI-MS/MS

Reactions with H_2O_2 or copper with reductant did not yield any expected crosslinking fragments nor did MALDI-MS reproducibly give fragments corresponding to as His29-Tyr65 crosslink. The only condition that showed a mass close to that expected was G65Y Cu_BMb + 2 eq. Cu with 1000 eq. TMPD and ascorbate. This observation required a higher intensity than normally used on the MALDI-MS which produced a very small peak that could arguably be noise. To independently check for the crosslinked mass, sample was submitted for LC-ESI-MS/MS. The same column and conditions used for HPLC peptide isolation for F33Y Cu_BMb was performed to confirm that digestion was proceeding properly and to identify the Tyr containing fragment and its elution time off the HPLC column. Compared to the control sample where only buffer was added during reaction there was significantly less of the fully digested Tyr containing peptide in the Cu + reductant reaction. This is interesting in that copper with reductant is inducing a major change to the tyrosine peptide. Unfortunately, no new Tyr containing fragment was observed via MS and no obvious sharp new peak was observed via LC. This may

be explained by the observation that crosslinked His29-Tyr65 would have a mass above 2000 m/z and thus be outside the range of ESI-MS/MS. The peptide would have to be at least doubly charged to be observed. This however assumes complete digestion. If there is a missed cleavage, especially on the His29 peptide, the mass could be higher and require a triply charged peptide to be observed. However, a missed cleavage event requiring a triply charge peptide to be observed is less likely on the G65Y peptide as it is flanked on both sides by at least one additional Lys residue that could be cleaved.

4.4 Summary, conclusions, and future experiments

In summary, reactions of I28Y Cu_BMb and F33Y Cu_BMb formed unique peptides after reaction with H_2O_2. Based on Edman degradation and MALDI-MS, the isolated peptide for F33Y Cu_BMb does contain the portion of the protein with the His and Tyr residues for crosslinking. In addition, there is further support based on mutations to that portion of F33Y Cu_BMb causing the appropriate mass shifts as observed by MALDI-MS. The peptide does not appear to contain a His-Tyr crosslink based on Edman degradation results. However, based on UV-Visible studies where the pH of the solution containing the peptide isolated was adjusted from pH 11 to pH 3 there is a shift in the UV region similar to those observed for His-Tyr crosslink small molecule analogs. It is likely that this species is composed of Tyr crosslinked to either an amino acid side chain or backbone atom of the residues between Ser34 and Lys42. Based on distances from crystal structures, the most likely residues are Thr39 and Leu40 if the linkage is to the sidechain. This is not as unreasonable as it may seem in light of a recently reported Phe-Val crosslink mediated by a metal site[4]. However, Edman degradation should have given either no signal or an unknown signal for one of the residues[5] if the linkage was via sidechain (unless the linkage was broken by the edman reaction). However, it may be more

likely that the linkage is to the backbone, which would not be altered by mutagenesis and would be more likely to be broken by the edman reaction.

For G65Y Cu_BMb there was no reproducibly observed crosslinked mass using H_2O_2 or reductant in the presence or absence of copper. However, ESI-MS/MS shows significant differences between unreacted and protein reacted with copper and reductant. The unreacted trace shows a Tyr containing peak. The copper and reductant treated sample does not, nor does it show any new peaks that contain components of the peptide containing Tyr65. This absence is possibly due to poor cleavage induced by a covalent attachment and the resulting less digested peptide that has an m/z ratio of greater than 2000, and thus is less likely to be observed. In other words, if the most digested version of the peptide is produced, with a mass of 3115 Da it would require a charge of +2 to have an m/z less than 2000 and be observed. If a less digested peptide product has a mass over 4000 Da then a +3 charge would be needed, which would require a ~900 Da mass increase. A potential source for this mass increase may be a covalent linkage to the heme cofactor as it has a mass of 616 Da and due to size might interfere with complete digestion. If the mass is less than 4000 Da such a linkage would also strongly alter the elution of the peptide off of the C18 column, as such a column separates by hydrophobicity and heme is very hydrophobic.

To resolve these potential issues in G65Y Cu_BMb there are multiple routes including making point mutations to increase the positive charged residues that are not cleavable by trypsin. A related strategy is to add additional Lys or Arg residues to create smaller digest fragments, so that a lesser charge is needed to observe the peptide of interest. As for the covalent linkage with heme, a separate purification step separating the peptide peaks from the heme containing peaks (similar to the HPLC protocol described for heme extraction as was described

in the methods section) could isolate such a linkage. Subsequent direct injection into a MS instrument may yield confirmation of this idea.

In the case of F33Y Cu_BMb, based on computer modeling of G65Y Cu_BMb, adding bulk at position 65 causes His29 to move toward Phe33. If a Phe65 mutation was made it might be possible to compete with the undesired linkage. However, based on K_d studies for G65Y Cu_BMb the copper binding, described in chapter 2, in this situation the likelihood of copper mediated linkage would be greatly reduced due to less copper binding at a given concentration of metal. True confirmation of any crosslinking analogous to that of HCOs will eventually require either Edman Degradation or crystallization to confirm any linkage. Edman Degradation was shown not to disrupt the linkage in HCOs by Buse *et al.*[5] Therefore our crosslink should be able to withstand Edman degradation if it is the correct linkage. Crystallization would be the best way to confirm proper connectivity.

4. 5 References

1 Sigman, J. A., Kim, H. K., Zhao, X., Carey, J. R. & Lu, Y. The role of copper and protons in heme-copper oxidases: Kinetic study of an engineered heme-copper center in myoglobin. *Proc. Natl. Acad. Sci. U.S.A.* **100**, 3629 (2003).

2 Sigman, J. A., Kwok, B. C. & Lu, Y. From Myoglobin to Heme-Copper Oxidase: Design and Engineering of a CuB Center into Sperm Whale Myoglobin. *J. Am. Chem. Soc.* **122**, 8192 (2000).

3 Walsh, C. T., Garneau-Tsodikova, S. & Gatto, G. J., Jr. Protein posttranslational modifications: The chemistry of proteome diversifications. *Angew. Chem. Int. Ed.* **44**, 7342 (2005).

4 Cooley, R. B., Rhoads, T. W., Arp, D. J. & Karplus, P. A. A Diiron Protein Autogenerates a Valine-Phenylalanine Cross-Link. *Science* **332**, 929 (2011).

5 Buse, G., Soulimane, T., Dewor, M., Meyer, H. E. & Bluggel, M. Evidence for a copper-coordinated histidine-tyrosine crosslink in the active site of cytochrome oxidase. *Protein Sci.* **8**, 985 (1999).

6 Tsukihara, T. *et al.* Structures Of metal sites Of oxidized bovine heart cytochrome c oxidase at 2.8 Angstrom. *Science* **269**, 1069 (1995).

7 Ostermeier, C., Harrenga, A., Ermler, U. & Michel, H. Structure at 2.7 Å resolution of the Paracoccus denitrificans two-subunit cytochrome c oxidase complexed with an antibody Fv fragment. *Proc. Natl. Acad. Sci. U.S.A.* **94**, 10547 (1997).

8 Das, T. K., Pecoraro, C., Tomson, F. L., Gennis, R. B. & Rousseau, D. L. The Post-Translational Modification in Cytochrome c Oxidase Is Required To Establish a Functional Environment of the Catalytic Site. *Biochemistry* **37**, 14471 (1998).

9 Pesavento, R. P., Pratt, D. A., Jeffers, J. & van der Donk, W. A. Model studies of the CuB site of cytochrome c oxidase utilizing a Zn(II) complex containing an imidazole-phenol cross-linked ligand. *Dalton Transactions*, 3326 (2006).

10 Aki, M. *et al.* UV Resonance Raman Characterization of Model Compounds of Tyr244 of Bovine Cytochrome c Oxidase in Its Neutral, Deprotonated Anionic, and Deprotonated Neutral Radical Forms: Effects of Covalent Binding between Tyrosine and Histidine. *Journal of Physical Chemistry A* **106**, 3436 (2002).

11 McCauley, K. M., Vrtis, J. M., Dupont, J. & Van der Donk, W. A. Insights into the Functional Role of the Tyrosine-Histidine Linkage in Cytochrome c Oxidase. *J. Am. Chem. Soc.* **122**, 2403 (2000).

12 Collman, J. P. *et al.* A Cytochrome c Oxidase Model Catalyzes Oxygen to Water Reduction Under Rate-Limiting Electron Flux. *Science* **315**, 1565 (2007).

13 Liu, J.-G., Naruta, Y. & Tani, F. A functional model of the cytochrome c oxidase active site: Unique conversion of a heme-m-peroxo-CuII intermediate into heme-superoxo/CuI. *Angew. Chem. Int. Ed.* **44**, 1836 (2005).

14 Liu, J.-G., Naruta, Y. & Tani, F. Synthetic models of the active site of cytochrome c oxidase: influence of tridentate or tetradentate copper chelates bearing a His-Tyr linkage mimic on dioxygen adduct formation by heme/Cu complexes. *Chem. Eur. J.* **13**, 6365 (2007).

15 Hosler, J. P. *et al.* Insight into the active-site structure and function of cytochrome oxidase by analysis of site-directed mutants of bacterial cytochrome aa3 and cytochrome bo. *J. Bioenerg. Biomembr.* **25**, 121 (1993).

16 Gorbikova, E. A., Belevich, I., Wikström, M. & Verkhovsky, M. I. The proton donor for O O bond scission by cytochrome c oxidase. *Proceedings of the National Academy of Sciences* **105**, 10733, doi:10.1073/pnas.0802512105 (2008).

17 Yeung, N. *et al.* Rational design of a structural and functional nitric oxide reductase. *Nature* **462**, 1079 (2009).

18 Morris, H. R. & Pucci, P. A new method for rapid assignment of S-S bridges in proteins. *Biochem. Biophys. Res. Commun.* **126**, 1122 (1985).

19 Riistama, S., Puustinen, A., Verkhovsky, M. I., Morgan, J. E. & Wikstrom, M. Binding of O2 and Its Reduction Are Both Retarded by Replacement of Valine 279 by Isoleucine in Cytochrome c Oxidase from Paracoccus denitrificans. *Biochemistry* **39**, 6365 (2000).

20 Wilks, A. & Ortiz de Montellano, P. R. Intramolecular translocation of the protein radical formed in the reaction of recombinant sperm whale myoglobin with hydrogen peroxide. *J. Biol. Chem.* **267**, 8827 (1992).

CHAPTER 5

CHARACTERIZATION OF A NOVEL SIDE-ON BOUND OXYGEN SPECIES IN F33Y CU_BMB

5.1 Introduction

5.1.1 Side-on bound oxygen in biology

Since oxygen is diatomic, it can bind to protein in two ways: end-on, as in oxygen-bound myoglobin[1] (OxyMb) (Figure 5.1A) and hemerythin, or side-on, as in naphthalene dioxygenase[2] (Figure 5.1B) and homoprotocatechuate 2,3 dioxygenase[3]. In proteins, iron-bound, side-on oxygen species in proteins have been observed in non-heme iron sites. Side-on oxygen species bound to non-heme iron are reactive species. Karlsson *et al*. reported crystal structures for naphthalene dioxygenase with the side-on bound oxygen. They proposed that this species attacks the napthalene substrate and produces *cis*-1,2-dihydrodiol. Work by Lipscomb's lab[3] reported the structure of ferrous iron loaded homoprotocatechuate 2,3 dioxygenase with and oxygen side-on bound also suggest reaction with an aromatic substrate.

For heme proteins such as p450s, side-on bound intermediates have been proposed[4]; however, many p450s are believed to perform chemistry with the ferryl cation radical intermediate commonly referred to as compound I (cpdI)[5]. Computational work indicates that a side-on bound complex could not be activated to undergo dioxygen bond cleavage[6]. In some p450s, such as p450 aromatase[7,8] , however, the hydrogen-bonding network in the active site promotes the activation of the substrate, which may suggest that proton access to the ferric peroxo intermediate is limited. Thus, a side-on peroxo intermediate may be the active intermediate. Other in p450s, such as a p450 2B4[7,9] mutations of the active site proton donors

have demonstrated an enhancement of activity, i.e. the deformylation of cyclohexanecarboxaldehyde, that is thought to be performed by a side-on intermediate.

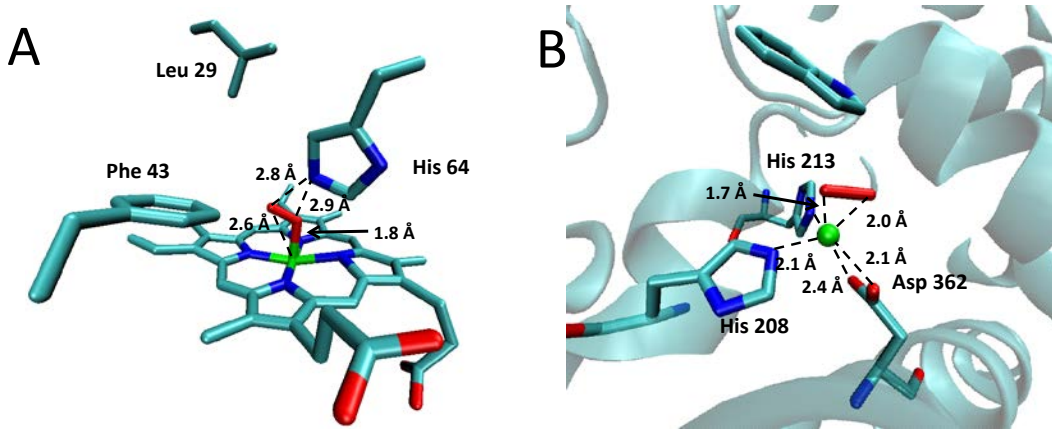

Figure 5. 1 Examples of side-on and end-on bound oxygen. (A) WtswMb (PDB 1MBO) and (B) Napthalene Dioxygenase (PDB 1O7M).

5.1.2 Side-on bound porphyrin complexes

Side-on bound oxygen species have also been observed in porphyrin-based organic complexes. Work by Valentine and coworkers have reported observations of side-on bound oxygen complexes with various metals[10,11], including iron[10,12,13]. The EPR spectra of these iron complexes have a signal at $g = 4.2$ that has been assigned to a side-on bound oxygen species. The side-on bound species observed were formed when porphryin complexes reacted with potassium superoxide in dry organic solvent. UV-visible studies for Valentine's iron complexes were described as having a low-energy Soret band, and the peaks in the visible region (between 500 nm and 700 nm) have shoulders similar to those of Ti complexes. The features of the reported complexes did not shift with changes in solvent or counter ion, suggesting that the complexes do not coordinate with them. As a result, these complexes are suggested to be six-coordinate. This leaves an open coordination site to the porphyrin as the oxygen is bound in a side-on fashion. These complexes are sensitive to moisture and air, and they decompose rapidly. As far as

reactivity, the complexes are generally not electrophilic, as they do not oxidize styrene or cyclohexene[12]. However, they have been shown to nucleophilically attack electron-poor olefins such as menadione to form menadione epoxide with an approximately 70% yield. The electrophilicity of the porphryin ring, however, does affect the ability of the complex to perform this chemistry. For protoporphyrin IX dimethylester (PPIXDME), an analog of the heme b in myoglobins, this activity does occur.

Work by Naruta and coworkers[14] in studies of porphyrin-complex-based models of HCOs has revealed a side-on bound peroxo species with a copper analogous to Cu_B in proximity. This complex was crystallized and will be discussed below (see Figure 5.2). Naruta and coworkers also recently described a seven-coordinate side-on complex that could be converted to an end-on ferric hydroperoxo species analogous to Cpd 0; it was produced upon protonation using methanol[15]. The additional seventh ligand, absent in side-on bound complexes mentioned above, was a histidine analog. The presence of this ligand was shown to be important in the conversion of the side-on complex to the end-on complex.

5.1.3 Relation to Cu_BMb studies

As described in the preceding chapters, Cu_BMb is a model system for the study of HCOs[16,17]. The formation of a ferric hydroperoxo intermediate is an important step in the reduction of oxygen to water. The hydroperoxo intermediate is protonated to form (cpd I): the ferryl species with a cation radical. As an alternate route to cpd I, hydrogen peroxide can be added to ferric heme proteins via a "peroxide shunt." A tyrosine-containing variant of Cu_BMb[17], F33Y Cu_BMb, was reacted with hydrogen peroxide for the purpose of inducing a His-Tyr crosslink (described in Chapter 4). After reacting F33Y Cu_BMb with hydrogen peroxide, a

covalent bond that is not yet fully characterized formed based on mass spectrometry. When hydrogen peroxide reacted F33Y Cu_BMb was crystallized in an attempt to determine the location of a newly formed covalent bond. Unexpectedly, we obtained a crystal structure with a side-on bound oxygen species. Contained in this chapter is the first, to our knowledge, structure of a side-on bound oxygen species heme iron in a protein system. Since this species is a proposed transient intermediate in some p450s[8] and is only observed as a relatively stable species in organic porphyrin complexes in dry organic solvent[12], there is much that could be learned by characterizing such a species.

5.2 Materials and methods

5.2.1 Purification of protein

The F33Y Cu_BMb used in this chapter was purified as described in Chapter 2. The cutoff ratio of A_{408}/A_{280} for useable protein was 4.

5.2.2 Crystallization of F33Y Cu_BMb

Side-on bound F33Y Cu_BMb crystals were obtained by taking 1.7mM as purified F33Y Cu_BMb (met form) in 20 mM Tris pH 8 (pH adjusted with H_2SO_4). To this protein, three eq. H_2O_2 were added and allowed to react for approximately 30 minutes. This protein was then concentrated using a centrifugal concentration device with a MWCO of 10 kDa. The reacted protein was then diluted to ~1.7 mM and mixed 2:2 with crystallization buffer (0.1 M sodium cacodylate, 0.2 M sodium acetate trihydrate with 30% w/v polyethylene glycol 8000) and stored over a well of 300 µL crystallization buffer using the hanging drop method. It should be noted that this method does not reproducibly result in crystals with the side-on bound oxygen species.

In fact, most F33Y Cu_BMb crystals obtained are of the met form. The resulting protein and well buffer solution has a pH of approximately 7.

Met-F33Y Cu_BMb crystals were also soaked with H_2O_2 in an attempt to reproduce the results of the solution crystallization described above. The crystallization of metMb has been described in the methods section of Chapter 2. However, the crystallization buffer used to produce these crystals contained 30% w/v PEG 10000 instead of 30% PEG 8000, as this was subsequently observed to form crystals more reliably. The crystal and mother liquor of metMb crystals had a volume of 4 µL. To this, 1 µL of well buffer and F33Y Cu_BMb in the same ratio (one volume 1mM F33Y Cu_BMb to three volumes well buffer) with 100 eq. H_2O_2. The hydrogen peroxide was added to the protein solution just prior to mixing with the well buffer. Mixing this solution 1:4 with the crystal drop would result in 20 eq. H_2O_2 compared to the total amount of protein in the drop. The higher amount of H_2O_2 compared to solution based crystallization was used to increase the probability of hydrogen peroxide reacting with the crystallized protein to form a side-on complex. Mr. Yi-Gui Gao aided in the reaction of crystals with H_2O_2 to ensure that the crystals were minimally damaged by the mixing procedure. The structure obtained by this procedure is more consistent with an end-on species not a side species.

5.2.3 Diffraction Data Collection

The crystals were first soaked briefly in cryoprotectant (30 % polyethylene glycol 400) and were flash frozen in liquid nitrogen. The diffraction data sets summarized in Table S1 were collected at the National Synchrotron Light Source beamline X12C (Upton, NY) and were processed with HKL2000 software[18].

5.2.4 Crystal Structure Determination

The crystal structure was solved by the molecular replacement method using MOLREP in the CCP4 Package[19]. Refinement was performed using X-plor[20] and SHELX'97[21]. For the crystal structure of Cu_BMb, the positions of H43 and H29 were rebuilt using the program O[22]. For the structure of F33Y Cu_BMb, the position of Y33 was rebuilt using the program O [22]. All crystal structure determination was performed by Mr. Yi-Gui Gao, of the George L. Clark X-Ray Facility and 3M Materials Laboratory, University of Illinois at Urbana-Champaign, as part of a collaboration.

5.2.5 EPR spectroscopy of H_2O_2-reacted F33Y Cu_BMb

EPR spectroscopy of H_2O_2-reacted F33Y Cu_BMb consisted of 300 µL of 500 µM protein reacting with three eq. H_2O_2 in 100 mM Tris-HCl (pH 8) while being stirred at room temperature. After the reaction, samples were mixed with 20% glycerol and flash-frozen in EPR tubes. EPR spectra were collected at 20K and 2mW power. The higher concentration of protein was used to maximize potential signals from any new species.

5.2.6 UV-visible spectroscopy of H_2O_2-reacted F33Y Cu_BMb

All UV-visible spectra were taken using an Agilent 8453 spectrometer (Agilent Technologies, Santa Clara, CA) using the supplied Chemstation software and kinetics package. 6 µM F33Y was reacted with three eq. H_2O_2 at pH 8 in 100 mM Tris-HCl and pH 6 in 100 mM potassium phosphate. The reaction was monitored for one hour.

5.3 Results and Discussion

5.3.1 Obtained crystal structures of H_2O_2-reacted F33Y Cu_BMb

As mentioned above, F33Y Cu_BMb was reacted with H_2O_2 for the purpose of inducing a His-Tyr crosslink analogous to that in HCOs. The 1.5 Å structure obtained after F33Y Cu_BMb reacted in solution did not contain any evidence of such a covalent bond. The structure did contain a side-on bound oxygen species; it is presumably a peroxo species, based on studies by Valentine and coworkers[12]. The structure obtained by Naruta and coworkers[14] is included for comparison as it is also a HCO model system. It should be noted that the Nartura structure is six-coordinate whereas the F33Y Cu_BMb structure is seven-coordinate. The two complexes contain a side-on bound oxygen species with an oxygen-oxygen bond distance that is too short to be two water molecules, and oxygen-iron distances too similar for both oxygen atoms for it to be an end-on species. Both structures have another molecule that interacts at least weakly with the bound peroxo species. This interaction was not required for the model complexes obtained by Valentine and coworkers[11] that were based on a Mn(II) side-on structure. For F33Y Cu_BMb, there is a water molecule within hydrogen-bonding distance to both oxygen atoms of the putative peroxo species, and His64 may be hydrogen bonding as well. An interesting feature of this structure not observed in the met F33Y structure is a water molecule within hydrogen-bonding distance of both His43 and Tyr33. This water molecule potentially allows Tyr33 and His43 to interact with the bound species via the hydrogen bonding network. The network of hydrogen bonds observed apparently stabilizes this intermediate and prevents the expected ferryl intermediates from forming.

Another structure of F33Y Cu_BMb reacted with hydrogen peroxide after crystallization. This structure was not side-on bound; the ligand appears to be end-on bound. As this structure was obtained by reaction in the crystal, it may be a trapped intermediate. There is a water molecule observed in the designed site is in the Cu_B site, formed by His29, His43, and His64, which is similar to what was observed in the met F33Y Cu_BMb structure in Chapter 2. The difference in the water distribution could indicate that the protein is unable to adopt a different conformation, or that there is a less occupancy of at water in this end-on structure at the location of the water observed in the side-on structure.

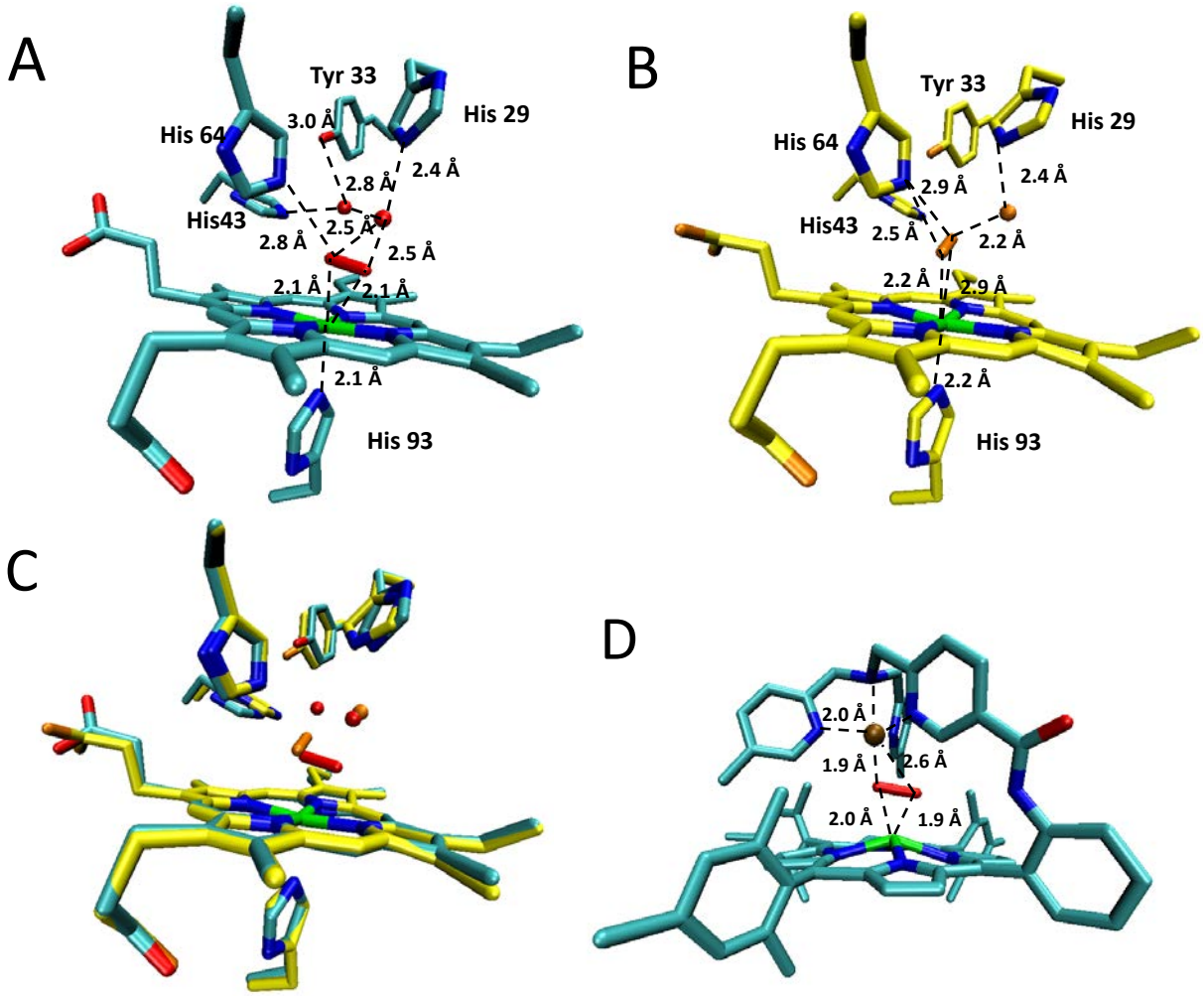

Figure 5.2 Comparison of F33Y Cu_BMb hydrogen peroxide structures, (A) The side-on bound F33Y Cu_BMb structure and (B) the F33Y Cu_BMb end-on structure, (C) Overlay of (A) and(B) and (D) (TMP)FeIII-(O2)-(5MeTPA)CuII obtained by Naruta and coworkers.

5.3.2 Reaction of F33Y Cu_BMb in solution with hydrogen peroxide

5.3.2.1 UV-visible spectroscopy

The reaction of F33Y Cu_BMb with H_2O_2 was characterized via UV-Vis using a diode array spectrometer. The reaction was initiated by adding three eq of H_2O_2 to met F33Y Cu_BMb. The addition of hydrogen peroxide cause the Soret band to decrease in intensity and shift to 411 nm. This is inconsistent with previously reported compound II spectra under these conditions in Cu_BMb[17]. As the reaction proceeded, a slight shoulder grew in at ~580 nm. When the reaction was repeated at pH 6, the reaction initially formed a species similar to that observed at pH 8. However, this species converted to a second species with a large shoulder at ~580 nm. This new species had a Soret band at ~412 nm, but as the observed spectra was a mixture, it might be more red-shifted. It would seem that both reactions starting out similarly, but at lower pH, the conversion to a second species was much more rapid. The visible region of the second species had a shape similar to the visible region of a side-on bound species reported by Valentine and coworkers in studies with PPIXDME (a heme b analog) and superoxide[12,13]. The Soret band, however, was blue-shifted by about 20 nm compared to the species reported with PPIXDME. This could be due to the additional ligand to the heme or a difference in the environment (a heme pocket of a protein versus organic solvent). The reduction of this species by TMPD and ascorbate did not produce a deoxyMb species or any significant spectral change, suggesting that the species formed under hydrogen peroxide-reacted conditions is not the same as the 411 nm oxyMb formed using reductant observed in work described in Chapter 2.

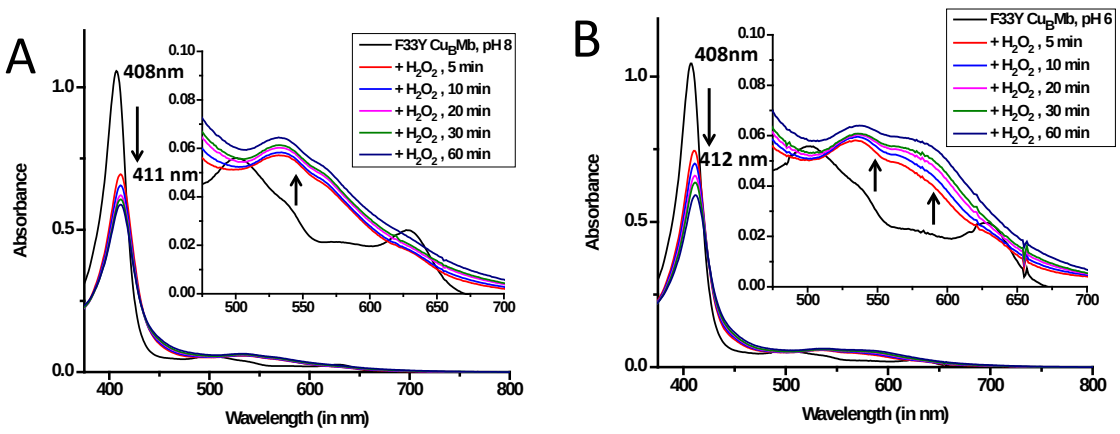

Figure 5. 3 UV-Visible spectra of F33Y Cu_BMb reaction with hydrogen peroxide. Reaction with three equivalents H2O2 at (A) pH 8 and (B) pH 6

5.3.2.2 EPR spectroscopy

To further characterize the reaction in solution with peroxide, EPR was performed with 500 uM F33Y Cu_BMb and three eq. H_2O_2 at pH 8. The reaction was monitored by taking aliquots at various time points, mixing the sample with 20% glycerol, and flash freezing. The reaction was monitored for one hour. EPR spectra were collected at 20K and 2mW power, conditions that are usually suitable for metMb. An initial sample of metMb was prepared as a control, and as a way to determine the signal due to the glycerol-induced conformational change in Mb to bis-his ligated, to avoid misinterpretation. As the reaction proceeded, the signal from metMb at g ~ 5.7 decreased as expected. At g ~ 2 and upon addition of H_2O_2, a peak formed that overlapped with a g ~ 2 peak from metMb. The peak at g = 2 that originated upon addition with H_2O_2 diminished with time. A small peak at g ~ 4.2 was observed that appeared constant after H_2O_2 was added, it did not diminish as the g ~2 peak did. It should be noted that peaks at this position have been assigned to free iron. Based on the UV-Vis work described above, there was no verdoheme formed, usually indicated by a small peak a 678 nm, which would be required

in order to degrade the heme and release the iron. Also, Valentine and coworkers[10] assigned a side-on peroxo species to a signal at this position. Therefore, this signal could be from a side-on peroxo, but EPR conditions should be adjusted as the signal intensity is very low.

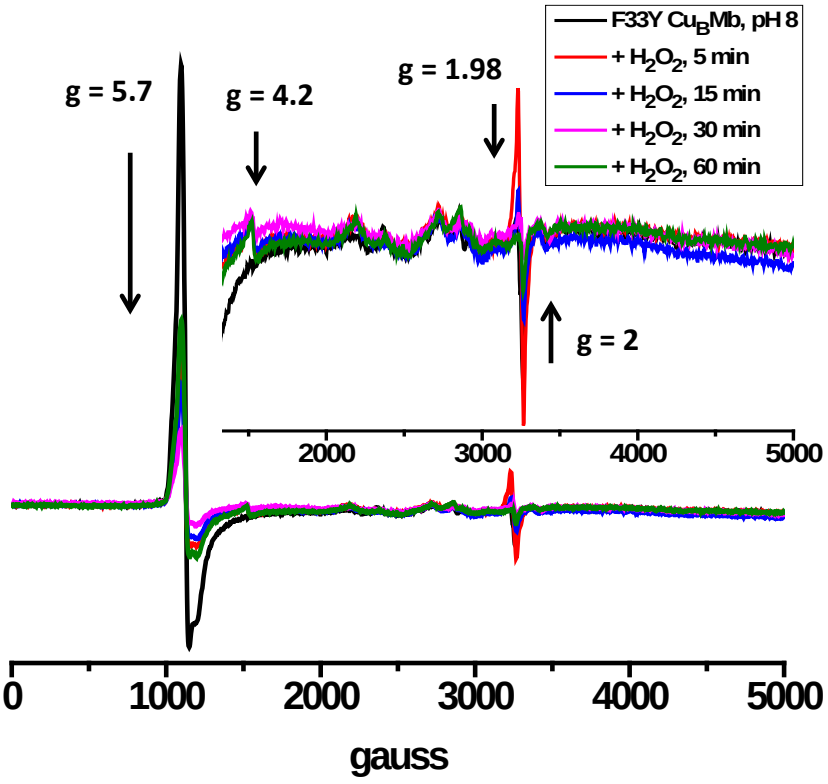

Figure 5.4 EPR spectroscopy of reaction between F33Y CuBMb and hydrogen peroxide pH 8

5.4 Summary and Conclusions

5.4.1 Relation of side-on oxygen species in F33Y Cu_BMb HCO-like chemistry

As mentioned above, the UV-visible spectra of the species formed after the reaction with hydrogen peroxide is different from the oxyMb species observed when TMPD and ascorbate were used (in Chapter 2); also, the addition of reductant does not cause spectra changes. This would suggest that the observed species is not able to reduced and cleave the dioxygen bond. This does not mean that oxygen chemistry is impossible under these conditions: there could

either be a small population that consumes oxygen slowly, or a population that is not active spectroscopically overlapping with any active species enough to preclude any observation of the relevant spectral changes. Based on Naruta's precedent of converting a seven-coordinate side-on species to an end-on species[15], protonation might convert our species to an intermediate found in HCO chemistry.

5.4.2 Future directions

The observed side-on species has yet to be spectroscopically characterized as a pure species. Efforts are underway to reproduce a side-on bound crystal using both ^{16}O- and ^{18}O-labeled hydrogen peroxide. If successful, UV-visible studies and resonance Raman studies of the crystals will provide reference spectra for a side-on bound oxygen in a protein environment, potentially providing a new route to confirm the existence of these suggested species in p450s. EPR studies at lower temperatures could yield a better signal at $g = 4.2$ so that these results could be more readily compared with studies by Valentine's lab[10]. Also, this side-on bound species could be better suited for reactions similar to olefin epoxidation reactions described by Valentine and coworkers[12]. If a substrate were able to enter the heme pocket of myoglobin, it is possible that interesting chemistry could be performed by the side-on species. Without mutations allowing such a substrate to enter the heme pocket, it may be difficult to observe such activity.

5.5 References

1 Phillips, S. E. V. Structure and refinement of oxymyoglobin at 1.6 .ANG. resolution. *J. Mol. Biol.* **142**, 531 (1980).

2 Karlsson, A. *et al.* Crystal Structure of Naphthalene Dioxygenase: Side-on Binding of Dioxygen to Iron. *Science* **299**, 1039 (2003).

3 Kovaleva, E. G. & Lipscomb, J. D. Crystal Structures of Fe2+ Dioxygenase Superoxo, Alkylperoxo, and Bound Product Intermediates. *Science* **316**, 453 (2007).

4 Akhtar, M., Calder, M. R., Corina, D. L. & Wright, J. N. Mechanistic studies on C-19 demethylation in estrogen biosynthesis. *Biochem. J.* **201**, 569 (1982).

5 Denisov, I. G., Makris, T. M., Sligar, S. G. & Schlichting, I. Structure and chemistry of cytochrome P 450. *Chem. Rev.* **105**, 2253 (2005).

6 Neese, F. Quantum chemical calculations of spectroscopic properties of metalloproteins and model compounds: EPR and Moessbauer properties. *Curr. Opin. Chem. Biol.* **7**, 125 (2003).

7 Wertz, D. L. & Valentine, J. S. Nucleophilicity of iron-peroxo porphyrin complexes. *Struct. Bonding (Berlin)* **97**, 37 (2000).

8 Graham-Lorence, S., Amarneh, B., White, R. E., Peterson, J. A. & Simpson, E. R. A three-dimensional model of aromatase cytochrome P450. *Protein Science* **4**, 1065 (1995).

9 Vaz, A. D. N., McGinnity, D. F. & Coon, M. J. Epoxidation of olefins by cytochrome P450: evidence from site-specific mutagenesis for hydroperoxo-iron as an electrophilic oxidant. *Proc. Natl. Acad. Sci. U.S.A.* **95**, 3555 (1998).

10 Burstyn, J. N. *et al.* Magnetic and spectroscopic characterization of an iron porphyrin peroxide complex. Peroxoferrioctaethylporphyrin(1-). *J. Am. Chem. Soc.* **110**, 1382 (1988).

11 VanAtta, R. B., Strouse, C. E., Hanson, L. K. & Valentine, J. S. Peroxo(tetraphenylporphinato)manganese(III) and chloro(tetraphenylporphinato)manganese(II) anions. Synthesis, crystal structures, and electronic structures. *J. Am. Chem. Soc.* **109**, 1425 (1987).

12 Selke, M., Sisemore, M. F., Y.N. Ho, R., Wertz, D. L. & Valentine, J. S. Dioxygen activation by iron complexes. The search for reactive intermediates. *J. Mol. Catal. A: Chem.* **117**, 71 (1997).

13 Selke, M., Sisemore, M. F. & Valentine, J. S. The Diverse Reactivity of Peroxy Ferric Porphyrin Complexes of Electron-Rich and Electron-Poor Porphyrins. *J. Am. Chem. Soc.* **118**, 2008 (1996).

14 Chishiro, T. *et al.* Isolation and crystal structure of a peroxo-bridged heme-copper complex. *Angew. Chem. Int. Ed.* **42**, 2788 (2003).

15 Liu, J.-G. *et al.* Spectroscopic Characterization of a Hydroperoxo-Heme Intermediate: Conversion of a Side-On Peroxo to an End-On Hydroperoxo Complex. *Angew. Chem. Int. Ed.* **48**, 9262 (2009).

16 Sigman, J. A., Kwok, B. C. & Lu, Y. From Myoglobin to Heme-Copper Oxidase: Design and Engineering of a CuB Center into Sperm Whale Myoglobin. *J. Am. Chem. Soc.* **122**, 8192 (2000).

17 Sigman, J. A., Kim, H. K., Zhao, X., Carey, J. R. & Lu, Y. The role of copper and protons in heme-copper oxidases: Kinetic study of an engineered heme-copper center in myoglobin. *Proc. Natl. Acad. Sci. U.S.A.* **100**, 3629 (2003).

18 Otwinowski, Z. & Minor, W. Processing of x-ray diffraction data collected in oscillation mode. *Methods Enzymol.* **276**, 307 (1997).

19 Vagin, A. & Teplyakov, A. MOLREP: an automated program for molecular replacement. *J.Appl.Crystallogr.* **30**, 1022 (1997).

20 Brunger, A. T. *et al.* Crystallography & NMR System: a new software suite for macromolecular structure determination. *Acta Crystallogr.* **D54**, 905 (1998).

21 Sheldrick, G. M. & Schneider, T. R. SHELXL: high-resolution refinement. *Methods Enzymol.* **277**, 319 (1997).

22 Jones, T. A., Zou, J. Y., Cowan, S. W. & Kjeldgaard, M. Improved methods for building protein models in electron density maps and the location of errors in these models. *Acta Crystallogr.* **A47**, 110 (1991).